UNIVERSIDADE ESTADUAL DE CAMPINAS

Pedro Henrique Pacheco de Almeida Schildknecht

O efeito tóxico do Al^{3+} em raízes de milho e em células V79 e a participação da parede celular na tolerância ao cátion

Este exemplar corresponde à redação final da tese defendida pelo(a) candidato (a) PEDRO HENRIQUE PACHECO DE ALMEIDA SCHILDKNECHT e aprovada pela Comissão Julgadora.

Tese apresentada ao Instituto de Biologia para obtenção do Título de Doutor em Biologia Celular e Estrutural na área de Biologia Celular.

Orientador: Prof.Dr.Benedicto Campos Vidal

1

Data da Defesa: 23/08/2002

Banca Examinadora

Prof.Dr. Benedicto Campos Vidal (Orientador)

_____
(Assinatura)

Profa. Dra. Maria Luiza Silveira Mello
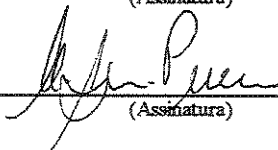
_____
(Assinatura)

Profa.Dra. Marília de Moraes Castro

_____
(Assinatura)

Prof.Dr. Marcelo dos Santos Guerra Filho

_____
(Assinatura)

Profa.Dra. Margarida Lopes Rodrigues de Aguiar Perecin

_____
(Assinatura)

Prof.Dr. Marcelo Menossi Teixeira

_____
(Assinatura)

Prof.Dr. Edson Rosa Pimentel

_____
(Assinatura)

3

À Patricia,
pela esposa e
química.

Campinas, 23 de agosto de 2002

AGRADECIMENTOS

- ✓ Ao **Prof. Dr. Benedicto Campos Vidal,** pela orientação, amizade e exemplo de vida.
- ✓ Aos meus pais, **Othmar** e **Marisílvia**, por terem sempre me apoiado.
- ✓ À Profa. Dra. Maria Luiza Silveira Mello, pelas valorosas discussões desde o início deste trabalho.
- ✓ À Profa. Dra. Marília Moraes de Castro, pelo auxílio em botânica.
- ✓ Aos professores: Dr. Edson Rosa Pimentel, Dra. Ione Salgado, Dr. Renato Atílio Jorge e Dr. Marcelo Menossi pela ajuda e pelas idéias.
- ✓ Ao Dr. Marco Antônio Guimarães, pelas sementes sem as quais este trabalho não poderia ter sido realizado.
- ✓ Ao Prof. Dr. Fernando Galembeck, pelo uso do microscópio de força atômica.
- ✓ Aos professores: Dra. Marcela Haun, pelo uso do laboratório de cultura celular, e Dr. Nelson Durán, pela violaceína.
- ✓ À mestre Patrícia Boscolo, pelas discussões químicas e pelas idéias.
- ✓ À doutoranda Sandra Gomes, pela ajuda nos experimentos.
- ✓ Ao Prof. Dr. Stephen Hyslop, por revisar gramaticalmente os manuscritos.
- ✓ À equipe do laboratório, pelos momentos únicos.
- ✓ À todas as pessoas do Departamento de Biologia Celular, especialmente à Liliam, pela colaboração nos grandes e pequenos detalhes deste trabalho.
- ✓ Aos Departamentos de Histologia e Embriologia, Fisiologia Vegetal, Botânica e Parasitologia, pelo uso de equipamentos.
- ✓ Aos amigos, que participaram dos momentos bons e ruins.
- ✓ Às agências FAPESP, CNPq e CAPES, pelo auxílio financeiro na forma de bolsas, reserva técnica e financiamento do projeto.

ÍNDICE

SUMÁRIO

O íon Al^{3+} é um agente tóxico relacionados com a baixa produtividade agrícola de cereais em solos ácidos e com doenças degenerativas em animais. O objetivo deste trabalho foi examinar os efeitos tóxicos do Al^{3+} em plantas de milho sensíveis e tolerantes ao Al^{3+} e também em células animais em cultura. Foi verificada a ligação do Al^{3+} com o DNA, causando neste uma perda de viscoelasticidade e a formação de precipitados cuja morfologia variou em consequência à quantidade de DNA e Al^{3+} disponíveis. Um modelo de interação Al-DNA foi proposto com base nos resultados obtidos neste trabalho. A análise das paredes celulares vegetais demonstrou a existência de uma maior disponibilidade de radicais aniônicos em plantas sensíveis ao Al^{3+} do que em plantas tolerantes ao íon. Um aumento da birrefringência das paredes em plantas sensíveis ao Al^{3+} foi observado após tratamento com $AlCl_3$. Isto foi confirmado por microscopia de força atômica em membranas de celulose de *Acetobacter xylinum* desenvolvidas em meio contendo Al^{3+}. A composição do revestimento extracelular da raiz foi determinada como sendo principalmente de celulose. Nossos resultados indicam que a parede celular é capaz de influenciar a tolerância da planta ao Al^{3+}. Em plantas sensíveis ao Al^{3+}, o cátion desencadeou um processo de morte celular nas raízes, levando à inibição permanente de seu crescimento. A morte destas células apresentou características típicas de apoptose, mas não a fragmentação ordenada da cromatina. Isto sugere a existência de mecanismos alternativos de morte celular em vegetais. Em células animais, a morte celular foi observada em consequência da presença de $AlCl_3$ em concentrações variando de 10^{-8} M a 10^{-3} M. Contudo, a ocorrência de apoptose se deu apenas em $[AlCl_3] < 10^{-5}$ M e necrose foi observada nas demais $[AlCl_3]$. Comprovou-se que o Al^{3+} pode induzir diferentes mecanismos de morte celular em decorrência de sua disponibilidade no meio. Este não é um evento comum, visto que outras drogas, como a violaceína, induzem apenas morte apoptótica independentemente de sua concentração.

SUMMARY

Al^{3+} ions are toxic to cells, causing low productivity in crops and degenerative diseases in animals. The aim of this work was to examine the toxicity of Al^{3+} in maize plants sensitive and tolerant to Al^{3+}, and also in animal cells in culture. The binding of Al^{3+} to DNA reduced DNA viscoelasticity and precipitated the macromolecule as structures in which morphology varied according to the DNA and Al^{3+} concentrations. A model for Al-DNA complex formation is presented, based on our results. The analysis of plant cell walls showed a higher availability of free anionic groups in Al^{3+}-sensitive plants than in Al^{3+}-tolerant plants. An increase in cell wall birefringence was observed after Al^{3+} treatment in Al^{3+}-sensitive but not in Al^{3+}-tolerant plants. This was confirmed by atomic force microscopy analysis of cellulose sheets produced by *Acetobacter xylinum* in the presence of Al^{3+}, which is important because cellulose is the main compound of the root extracellular layer. Our results indicate that the wall structure and composition may modulate the Al^{3+} resistance in plants. In sensitive plants, Al^{3+} triggered cell death in roots and reduced root growth. Although dying cells showed several apoptotic features, no ordered fragmentation of chromatin was observed. This suggested that an alternative death pathway may occur in plants. In animal cells, Al^{3+} caused the death at all concentrations tested (10^{-3}M – 10^{-7}M). However, the cell death pathway was not the same in all cases: apoptosis occurred in cells treated with [AlCl$_3$] < 10^{-5} M and necrosis in cells treated with higher concentrations of AlCl$_3$.

INTRODUÇÃO

1.1 Biodisponibilidade do alumínio: aspectos gerais.

O alumínio é o terceiro elemento mais abundante na crosta terreste (Delhaize & Ryan 1995, Kochian 1995, Matsumoto 2000, Rout *et al.* 2001) e tem sido extensivamente relatado como um dos principais agentes relacionados com a baixa produtividade agrícola de cereais (Kochian 1995, Matsumoto 2000, Rout *et al.* 2001) e com a indução de doenças degenerativas em animais (Jeffery *et al.* 1996, Julka e Gill 1996, Altschuler 1999, Exley 1999, Guo e Liang 2001). As maiores reservas de alumínio ocorrem como $Al(OH)_3$ ou silicatos de alumínio, formas não tóxicas aos seres vivos (Delhaize e Ryan 1995, Harris *et al.* 1996). A biodisponibilidade do alumínio surge em meio ácido (pH < 5), condição típica do ambiente do cerrado brasileiro. Neste tipo de solo ocorre a ionização de compostos de alumínio, originando a espécie tóxica Al^{3+} (Kochian 1995, Harris *et al.* 1996).

O pH do meio exerce profunda influência sobre a concentração de Al^{3+} e, conseqüentemente, sobre seu efeito tóxico e deve ser levado em consideração durante a execução de qualquer análise (Fig. 1). Contudo, a ação tóxica do Al^{3+} não deve ser atribuída diretamente à biodisponibilidade do cátion e sua potencial toxidez, mas à sua capacidade de ligar-se em componentes celulares em quantidade suficiente para causar danos em nível celular e, posteriormente, ao nível de organismo (Kinraide 1991). O Al^{3+} possui um alto valor na relação carga / raio atômico, o que propicia a formação preferencial de ligações eletrostáticas com alto grau de estabilidade com compostos negativamente carregados como fosfatos e grupos carboxila (Berthon 1996).
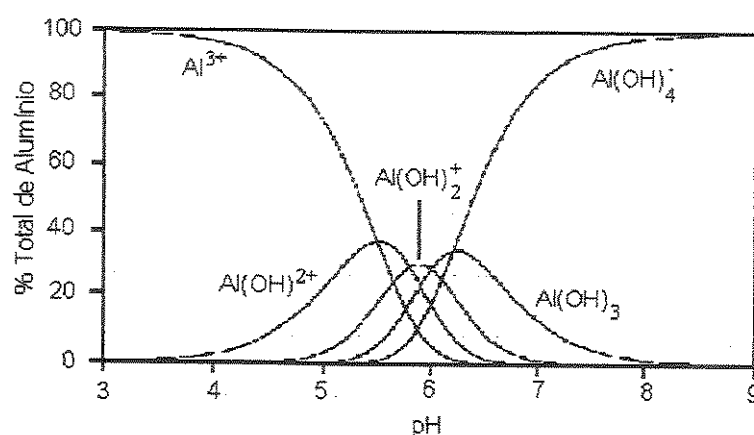

Figura 1: Gráfico ilustrando a variação das espécies de alumínio em meio aquoso. Baseado em Boscolo 2001.

A ingestão de sais de alumínio ainda não é condenada pela Organização Mundial de Saúde (WHO 1998), embora vários artigos tenham sido publicados nas últimas décadas demonstrando o efeito tóxico do Al^{3+} em animais e seres humanos. A classificação do alumínio como metal não tóxico deve ser revista, visto que hoje em dia ocorre um aumento na ingestão de alumínio por seres humanos, não apenas devido à sua utilização na formulação de produtos farmacêuticos (antiácidos em sua maioria) e no processamento de alimentos e posterior embalagem, mas também ao aumento de sua biodisponibilidade nos solos em consequência das chuvas ácidas, introduzindo o alumínio na cadeia alimentar (Berthon 1996).

1.2 O efeito tóxico do Al^{3+}

O Al^{3+} introduz diversas modificações na estrutura e metabolismo celulares que resultam em um efeito tóxico que pode ser considerado bastante similar para células animais e vegetais.

Em células animais, o alumínio é absorvido durante sua passagem pelo trato gastro-intestinal, sendo que a absorção é mais intensa quanto maior a dose ingerida (Berthon 1996) e está potencializada em pacientes com mal de Alzheimer (Moore et al. 2000). Vários autores têm relacionado a presença do Al^{3+} com o surgimento de doenças como o mal de Alzheimer, osteomalacia e mal de Parkinson (Berthon 1996, Jeffery et al. 1996, Julka e Gill 1996, Altschuler 1999, Guo e Liang 2001). Estudos in vitro demonstraram a ocorrência de apoptose em astrócitos cultivados em meio contendo Al^{3+} (Suárez-Fernandez et al. 1999, Guo e Liang 2001), embora os resultados apresentem grandes discrepâncias entre si, possivelmente devido ao fato de que os experimentos foram realizados em condições de pH acima de 6,5.

Os solos ácidos (pH < 5), que compõem cerca de 40 % dos solos cultiváveis do planeta (Kochian 1995), são diretamente responsáveis pelo efeito tóxico do Al^{3+} em vegetais, causando grandes perdas à agricultura, principalmente ao cultivo de cereais. A principal ação tóxica do Al^{3+} em vegetais é a inibição do crescimento longitudinal da raiz (Delhaize & Ryan, 1995, Rout et al. 2001). A parada no desenvolvimento radicular pode ocorrer através da inibição do crescimento da parede celular, através da morte das células do meristema radicular, pela redução no metabolismo celular ou ainda como consequência da ação de todos os mecanismos citados.

1.2.1 O alumínio e seu efeito na parede celular vegetal

Tem-se sugerido que a parede celular vegetal possa representar o sítio inicial de interação do Al^{3+} em plantas (Horst 1995, Horst *et al.* 1999, Matsumoto 2000), hipótese a qual vem obtendo suporte em trabalhos recentes (Li *et al.* 2000, Schmohl *et al.* 2000) e também nesta tese (Schildknecht e Vidal 2002). A parede celular compõe o apoplasto, sendo também denominada matriz extracelular vegetal; é formada basicamente por um arranjo tridimensional, cristalino, polimérico e altamente birrefringente de celulose, β - D- 1,4 glicanas, interligadas por pontes de hidrogênio (Brett e Waldron 1996, Krishnamurthy 1999, Carpita e McCann 2000). A celulose mantém ligações cruzadas com polímeros de hemicelulose, β - D – 1,4 glicanas com resíduos de xilose ou galactose e com birrefringência reduzida ou nula (Krishnamurthy 1999) (Figura 2A). A composição das hemiceluloses na parede celular pode variar entre as espécies de vegetais, sendo constituída basicamente por arabinoxilanas em milho (Carpita 1983). Além das hemiceluloses descritas, as monocotiledôneas apresentam ainda um tipo especial denominados de glicanas mistas, com ligações entre os resíduos de glicose variando entre β - D – 1,4 (70%) e β - D – 1,3 (30%). Tanto as arabinoxilanas quanto as glicanas mistas estão envolvidas com o crescimento celular devido à sua forte interação com a celulose, resultando em uma malha molecular rígida capaz de limitar o tamanho da célula (Nishitani 1997, Inohe *et al.* 2000). Permeando a malha de celulose e hemicelulose, está a matriz de pectina, a qual mantém ligações cruzadas com íons de cálcio (Figura 2B) (Brett e Waldron 1996, Emons e Mulder 1998, Krishnamurthy 1999, Emons e Mulder 2000). As pectinas são polissacarídeos ácidos, isotrópicos (sem birrefringência) e não celulósicos, compostos principalmente por (1, 4) - α - D – galacturonanas, sendo o ácido poligalacturônico sua forma mais abundante nas paredes celulares (Krishnamurthy 1999), cujo caráter ácido é regulado pela enzima pectina metil-esterase e está relacionado com a tolerância ao Al^{3+} (Schmohl *et al.* 2000). Embora seja fisicamente independente da malha formada pelas celuloses e hemiceluloses, a matriz de pectina possui grande importância nos mecanismos de crescimento celular, pois age como barreira à ação enzimática responsável pelo relaxamento da malha de celulose-hemicelulose,
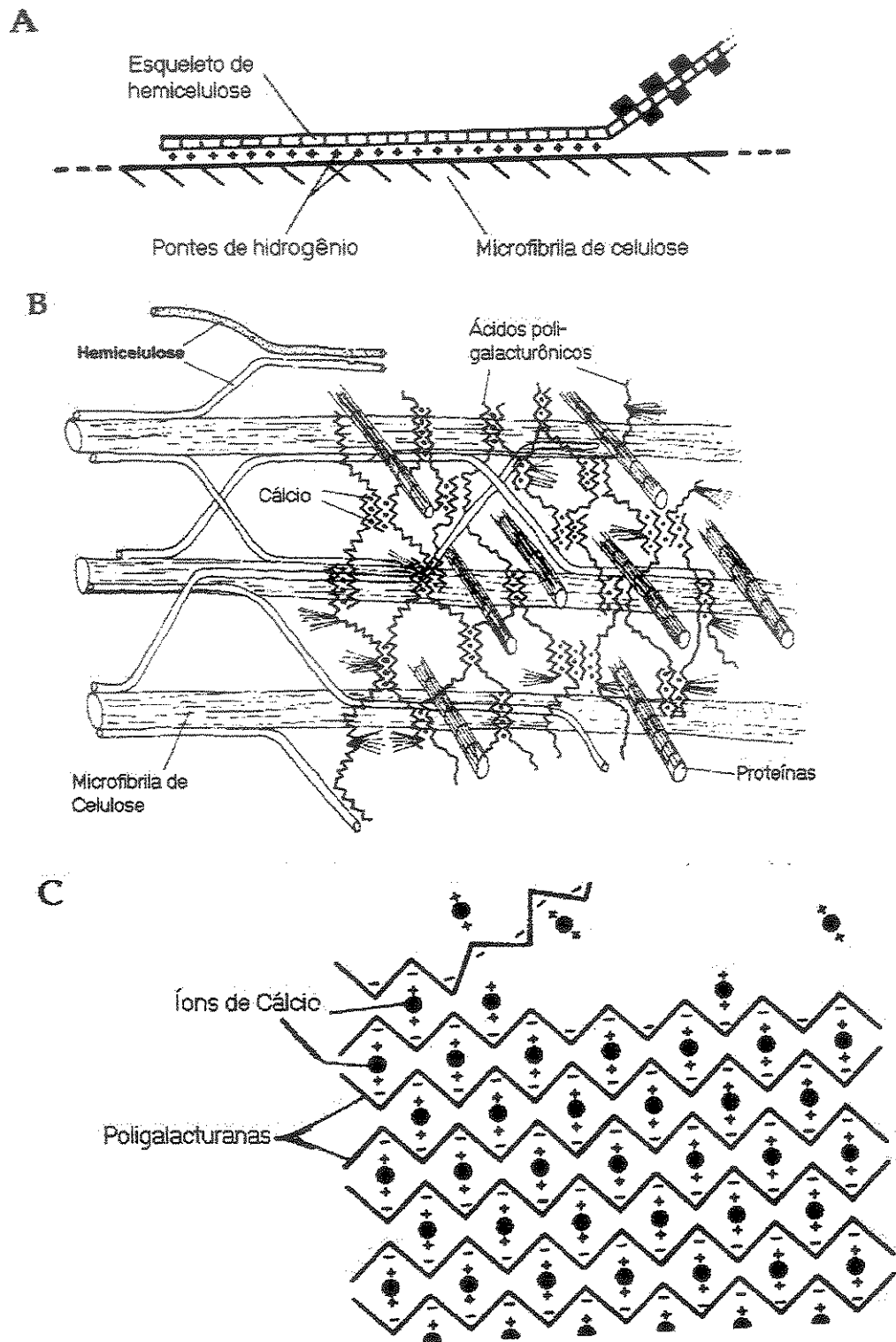
Figura 2: Modelos representando as interações entre os seguintes componentes presentes na matriz extracelular vegetal. A) celulose-hemicelulose B) celulose-hemicelulose-pectina-Ca^{+2} C) Ca^{2+}-pectina. Modificado de Brett e Waldron (1996).

bem como à ação de outras enzimas atuantes no metabolismo de parede celular (Fujino e Itoh 1998).

O cálcio (Ca^{2+}), algumas vezes substituído por magnésio, encontra-se fixado nas carboxilas existentes nas pectinas, constituindo um gel de pectato de cálcio (Brett e Waldron 1996) (Figura 2C). Este gel permeia toda a malha de celulose-hemicelulose e está diretamente ligado à capacidade de troca iônica da parede celular, pois nele estão localizados os grupos aniônicos livres da parede celular (Matsumoto 2000). O Al^{3+} é capaz de deslocar o Ca^{2+} de sua ligação com as pectinas tanto *in vitro* quanto *in vivo*, causando o enrijecimento da matriz de pectina e consequentes perturbações nas ações de enzimas importantes ao metabolismo da parede celular (Blamey e Dowling 1995, Horst 1995, Ostatek-Boczynski *et al.* 1995, Rout *et al.* 2001). Acredita-se que a quantidade de grupos carboxila livres presentes nas paredes celulares esteja relacionada com a afinidade do apoplasto por Al^{3+} e conseqüentemente à sensibilidade ao íon (Horst 1995, Kochian 1995).

A remoção de mucilagem da raiz (composta principalmente por ácidos poligalacturônicos) demonstrou a importância da pectina nos mecanismos de tolerância ao Al^{3+} (Horst 1982) e diversos trabalhos têm dado suporte a esta hipótese. Batata e milho com valores distintos de metilação em suas pectinas apresentaram níveis diferentes de tolerância ao Al^{3+} (Schmohl *et al.* 2000). A comparação da disponibilidade de radicais aniônicos entre plantas sensíveis e resistentes ao Al^{3+} tem sido realizada através de medidas da capacidade de troca de cátions (CEC) da raiz, porém os resultados têm gerado polêmica e ainda não há consenso sobre a maneira correta de realizar estes experimentos (Kochian 1995). Uma alternativa metodológica às medidas de CEC surgiu desta tese e possibilitou observar que a tolerância ao Al^{3+} está diretamente relacionada a disponibilidade de grupos negativamente carregados na parede celular (Schildknecht e Vidal 2002).

Além das modificações na supraorganização e fisiologia dos componentes da parede celular, o Al^{3+} também induz a formação de calose, uma β-D- 1,3 glicana (Zhang *et al.* 1994) que confere impermeabilidade à água aos tecidos onde é depositada (Yim e Bradford 1998). A síntese de calose é dependente de Ca^{2+}, abundante após seu deslocamento do apoplasto pelo Al^{3+}, e resulta na oclusão dos plasmodesmos, causando o fim do transporte intercelular (Sivaguru *et al.* 2000) e possivelmente a morte da célula. A presença de calose tem sido

proposta como um indicador eficaz da ocorrência de danos pelo Al^{3+} em plantas (Zhang et al. 1994, Horst 1995, Budiková 1999, Massot et al. 1999).

1.2.2 O alumínio e a membrana celular

Os mecanismos pelos quais o Al^{3+} é capaz de penetrar no interior das células ainda não são conhecidos. Sabe-se que as membranas celulares são impermeáveis a cátions com grande densidade de cargas, tais como o Al^{3+} (Berthon 1996). Diversos modelos especulativos têm sido propostos com o intuito de elucidar esta questão: o trabalho de Hawes et al. (1995) indicou a possibilidade de ocorrer a endocitose dos cátions; outra proposta é a existência de um canal específico para o transporte de Al^{3+} ou a passagem do cátion através de canais de cálcio ou magnésio (Matsumoto 2000, Ma et al. 2001). Diversos resultados apontam para a existência de um transporte passivo do Al^{3+} para o interior da célula, possivelmente através de um composto neutro que contenha o cátion (Matsumoto 2000). Complexos de Al-citrato são candidatos a realizar este transporte devido a sua neutralidade de cargas, embora esta hipótese tenha sido demonstrada apenas em lipossomos (Rao e Easwaran 1997).

O Al^{3+} pode introduzir altos níveis de peroxidação de lipídeos em células do sistema nervoso central e de raízes de plantas (Cakmak e Horst 1991, Ohyashiki et al. 1998, Campbell e Bondy 2000, Yamamoto et al. 2001), embora a redução do crescimento radicular possa ocorrer em milho sem a presença deste fenômeno (Boscolo et al., 2002). A peroxidação lipídica na presença de Al^{3+} é devida a um desbalanceamento na formação e degradação de espécies reativas de oxigênio (ROS) no interior da célula e possivelmente pela potencialização do estresse oxidativo produzido por ferro (Campbell e Bondy 2000). A manutenção de altos níveis de ROS pode alterar a fluidez da membrana e causar sua despolarização (Olivetti et al. 1995), induzir uma resposta inflamatória aguda em células animais (Campbell e Bondy 2000), danificar o DNA e causar a morte celular tanto em células vegetais quanto animais (Bohr e Dianov 1999, Breusegem et al. 2001, Guo e Liang 2001, Pan et al. 2001).

A adsorção do Al^{3+} a lipossomos tem sido testada in vitro visando compreender sua interação com a membrana plasmática. Alguns resultados indicam que o Al^{3+} é capaz de interagir diretamente com fosfolípides de membrana e de deslocar o Ca^{2+} de suas ligações

17

com estas moléculas (Matsumoto *et al.* 1992), além de possuir uma afinidade por fosfatidilcolina 560 vezes maior do que a do Ca^{2+}. Severas alterações foram observadas em eritrócitos humanos na presença de Al^{3+} (Zatta *et al.* 1998). Acredita-se que a ligação do Al^{3+} nas membranas possa criar uma superfície positivamente carregada e dificultar a aproximação de cátions, tais como Ca^{2+} e Mg^{2+}, inibindo a entrada de cátions no interior da célula. Contudo, recentes resultados demonstram que o Al^{3+} inibe a troca de cátions através da inibição interna de canais específicos para estes, como o bloqueio de canais de K^+ por Al^{3+} (Liu e Luan 2001).

1.2.3 Citoesqueleto e a transdução de sinais na presença de alumínio

Recentemente, diversas alterações de citoesqueleto têm sido relatadas e correlacionadas com os efeitos tóxicos do Al^{3+} (Brancaflor 1998, Sivaguru *et al.* 1999). As células vegetais necessitam da presença de uma rede de citoesqueleto para realizar uma série de funções, tais como a síntese da parede celular (Sivaguru *et al.* 1999) e o direcionamento da morfogênese das raízes (Barlow e Parker 1996). Ainda não se sabe se o efeito do Al^{3+} sobre o citoesqueleto ocorre através de ligação do cátion diretamente com a actina e tubulina ou por vias indiretas. Em plantas, tem-se sugerido que o efeito tóxico do cátion possa ser um resultado da interação do Al^{3+} com o conjunto parede celular-membrana plasmática-citoesqueleto (Horst *et al.* 1999). A hipótese de que a matriz extracelular, tanto animal quanto vegetal (parede), seja capaz de modular a expressão gênica têm sido proposta (Vidal 1993, Wyatt e Carpita 1993, Ingber 1997, Kohorn 2000) e têm suporte em resultados experimentais (Galou *et al.* 1995, Allen *et al.* 2000). Assim, as interações do Al^{3+} com a matriz extracelular, tanto em plantas quanto em animais, bem como com o citoesqueleto, podem representar um importante mecanismo de transdução de sinais.

1.2.4 A indução de morte celular pelo alumínio

O Al^{3+} é capaz de inibir a divisão celular e pode ser encontrado no interior do núcleo (Matsumoto e Morimura 1980). A transcrição de RNA é inibida *in vitro* e *in vivo* em cerca de 50% na presença de Al^{3+} (Matsumoto e Morimura 1980). O Al^{3+} possui grande afinidade pelos grupos fosfato (Kiss *et al.* 1996), o que resulta em sua ligação com o DNA causando a

sua estabilização (Karlik *et al.* 1980) e a alteração da estrutura cromatínica (Matsumoto e Morimura, 1980, Walker *et al.* 1989).

Modificações na organização da cromatina podem afetar a expressão de alguns genes visto que a estrutura da cromatina (p.ex.: níveis de condensação), bem como seu posicionamento no interior do núcleo, são fundamentais para que a maquinaria de transcrição interaja corretamente com as regiões promotoras e também para permitir a ação de sequências epi-regulatórias (Pederson 1998, Allen *et al.* 2000). Além disto, fatores que causem modificações na estrutura do DNA e/ou bloqueios no metabolismo da célula vegetal podem leva-la à morte celular (Havel e Durzan 1996).

Alguns autores têm sugerido a indução de morte em células animais por processos apoptóticos induzidos pelo tratamento com Al^{3+} (Guo e Liang 2001), embora seus resultados permaneçam controversos. A ausência de uma padronização no valor de pH do meio de cultura utilizado nos experimentos dificulta a análise do efeito tóxico do Al^{3+}, visto que este ocorre principalmente em pH < 5.0, e tem levado ao surgimento de resultados contrastantes (Suárez e Fernandez 1999).

Quanto à célula vegetal, ainda não está claro o mecanismo pelo qual ela é levada à morte pelo Al^{3+}; poucos trabalhos têm explorado esta problemática, possivelmente devido à complexidade do tema. A morte celular em vegetais nem sempre apresenta todas as características típicas de apoptose, tais como descritas por Kerr *et al.* (1972). Fath *et al.* (1999) demonstraram a ocorrência de um mecanismo de morte celular geneticamente controlado em plantas, sem a existência da fragmentação ordenada da cromatina e a formação de corpos apoptóticos. Este fenômeno sugere a existência de mecanismos geneticamente controlados de morte celular distintos dos já propostos para a apoptose (Jones 2000). Além disso, caspases ainda não foram identificadas em vegetais, dificultando a análise das etapas metabólicas do processo de morte (Jones 2000). Na situação específica de morte celular induzida por Al^{3+}, ocorre uma baixa disponibilidade de ATP devido à alta afinidade do Al^{3+} pelos fosfatos β e γ do nucleotídeo (Kiss *et al.* 1996, Nelson 1996), e isto dificulta a ativação de vias catalíticas de sinalização intracelular (ex.: caspases). Possivelmente, a geração ROS em consequência ao estresse por Al^{3+} (Boscolo *et al.*, 2002) possa estar relacionada ao processo de sinalização para o início da morte celular (Buckner *et al.* 2000, Jones 2000). A

forte interação do Al^{3+} com o DNA também deve ser considerada, pois a ligação Al-DNA reduz drasticamente a transcrição (Matsumoto e Morimura 1980), o que poderia agir como sinalização para desencadear o processo de morte.

1.3 Tolerância ao Al^{3+}

Os mecanismos pelos quais as plantas são capazes de tolerar ao Al^{3+} ainda estão sob discussão. A exsudação de ácidos orgânicos têm sido proposta como o principal mecanismo de tolerância ao Al^{3+} (Pellet *et al.*, 1994, Ryan *et al.*, 1995, Jorge e Arruda 1997). Este processo envolve exsudação de ânions de ácidos orgânicos, como malato, citrato e oxalato, capazes de complexar o Al^{3+} na rizosfera, evitando assim a entrada do íon no corpo do vegetal. A exsudação de citrato foi induzida em plantas transgênicas resultando na tolerância ao Al^{3+} (de la Fuente *et al.* 1997). Contudo, vários genes relacionados com a tolerância ao Al^{3+} já foram identificados e poucos estão envolvidos na síntese e exsudação de ânions de ácidos orgânicos (Matsumoto 2000). Parker e Pedler (1998) demonstraram que a exsudação de malato não foi capaz de impedir o efeito tóxico do alumínio sobre as plantas e sugeriram a existência de um mecanismo maior de tolerância ao Al^{3+}, composto de vários sub-mecanismos de tolerância e cujos componentes ainda estão por serem descobertos. O estudo dos eventos que ocorrem somente em plantas resistentes ao Al^{3+}, tais como a alteração do pH da rizosfera, produção de compostos anti-oxidantes e baixa negatividade da parede (Matsumoto 2000, Schildknecht e Vidal 2002), e sua correlação com a tolerância ao íon sugerem a existência um conjunto de mecanismos responsáveis pela tolerância ao Al^{3+}. Mais ainda, os resultados atuais sugerem a existência de mecanismos passivos de tolerância, que ocorrem constitutivamente (p.ex.: baixa disponibilidade de radicais aniônicos na parede), e mecanismos ativos de tolerância, que são ativados pelo Al^{3+}, como a exsudação de ânions de ácidos orgânicos. De qualquer maneira, o alvo principal do efeito tóxico do Al^{3+} ainda não é conhecido bem como os mecanismos que levam à sinalização da presença do íon para a ativação de mecanismos de defesa ativos. A parede celular é sugerida como a primeira estrutura vegetal a interagir com o Al^{3+} e portanto o seu papel nos mecanismos de sinalização e tolerância ao íon deve ser estabelecido para auxiliar na compreensão dos eventos decorrentes do efeito tóxico do Al^{3+}.

OBJETIVOS DA TESE

1. Verificar o efeito do Al^{3+} sobre o DNA *in vitro*.
2. Verificar a existência de diferenças quanto a cristalinidade de paredes celulares entre plantas sensíveis e resistentes ao Al^{3+} e comparar a disponibilidade de radicais aniônicos livres nas paredes celulares de plantas sensíveis e resistentes ao Al^{3+}.
3. Verificar a ocorrência e o tipo de morte celular em células de raiz de milho após o tratamento com $AlCl_3$.
4. Verificar a ocorrência e o tipo de morte celular em células animais após o tratamento com $AlCl_3$.

ESTRATÉGIAS COMPLEMENTARES

1. Padronização da metodologia de Cometa para análise da fragmentação cromatínica.
2. Analise da composição da camada que reveste as raízes externamente.

INFORMAÇÕES COMPLEMENTARES

1. Definição da terminologia relacionada ao estresse.

Os termos "resistência" e "tolerância" são definidos por Levitt (1980) como características distintas no que se refere à resposta de uma planta ante ao estresse causado por um agente definido.

A "resistência" de uma planta à um determinado tipo de estresse está relacionada à sua capacidade de sobreviver na presença deste estresse, seja evitando-o ou convivendo com o agente causador do estresse. O termo "tolerância" é menos abrangente, sendo utilizado apenas quando a planta sobrevive na presença de um estresse intracelular causado por um agente qualquer.

Neste trabalho, optou-se por utilizar o termo "tolerância" como definição da maneira pela qual os cultivares estudados convivem com o estresse ao alumínio. Esta escolha tem sua origem na terminologia utilizada pela proprietária dos cultivares estudados (Agroceres S.A.) para a caracterização dos mesmos, com base em estudos realizados por seu corpo técnico. Apenas uma exceção ocorreu no artigo II, pág. 52, onde foi utilizada a nomenclatura "resistente" devido à exigências da revista na qual o manuscrito foi publicado.

Referências Bibliográficas

ALLEN, G.C., SPIKER, S., THOMPSON, W.F. (2000). Use of matrix attachment regions (MARs) to minimize transgene silencing. *Plant Mol. Biol.* **43**, 361-376.

ALTSCHULER, E. (1999). Aluminum-containing antacids as a cause of idiopathic Parkinson's disease. *Med. Hypoth.* **53**, 22-23.

BARLOW, P.W., PARKER, J.S. (1996). Microtubular cytoskeleton and root morphogenesis. *Plant Soil* **187**, 23-27.

BERTHON, G. (1996). Chemical speciation studies in relation to aluminium metabolism and toxicity. *Coord. Chem. Rev.* **149**, 241-280.

BLAMEY, F.P.C., DOWLING, A.J. (1995). Antagonism between aluminium and calcium for sorption by calcium pectate. *Plant Soil* **171**, 137-140.

BOHR, V.A., DIANOV, G.L. (1999). Oxidative DNA damage processing in nuclear and mitochondrial DNA. *Biochemie* **81**, 155-160.

BOSCOLO, P.R.S., MENOSSI, M., JORGE, R.A. (2002) Aluminum-induced oxidative stress in maize. *Phytochemistry,* in press.

BRANCAFLOR, E.D., JONES, D.L., GILROY, S. (1998). Alterations in the cytoskeleton accompany aluminum-induced growth inhibition and morphological changes in primary roots of maize. *Plant Physiol.* **118**, 159-172.

BRETT, C., WALDRON, K. (1996). Physiology and Biochemistry of Plant Cell Walls. London: Chapman & Hall.

BREUSEGEM, F.V., VRANOVA, E., DAT, J.F., INZE, D.L. (2001). The role of active oxygen species in plant signal transduction. *Plant Sci.* **161**, 405-414.

BUCKNER, B., JOHAL, G.S., JANICK-BUCKNER, D. (2000). Cell death in maize. *Physiol. Plantarum* **108**, 231-239.

BUDIKOVA, S. (1999). Structural changes and aluminium distribution in maize root tissues. *Biol. Plantarum* **42**, 259-266.

CAKMAK, I., HORST , W.J. (1991). Effect of aluminium on lipid peroxidation, superoxide dismutase, catalase and peroxidase activities in root tips of soybean (*Glycine max*). *Physiol. Plantarum* **83**, 463-468.

CAMPBELL, A., BONDY, S.C. (2000). Aluminum induced oxidative events and its relation to inflammation: a role for the metal in Alzheimer's disease. *Cell. Mol. Biol.* **46**, 721-730.

CARPITA, N., MCCANN, M. (2000). The cell wall. In: *Biochemistry and Molecular Biology of Plants* (Ed. B.Buchanan, W.Gruissen & R.Jones). New York, USA: American society of plant physiologists.

CARPITA, N.C. (1983). Hemicellulosic polymers of cell walls of Zea coleoptiles. *Plant Physiol.* **72**, 515-521.

DELHAIZE, E., RYAN, P.R. (1995). Aluminum toxicity and tolerance in plants. *Plant Physiol* 107, 315-321.

EMONS, A.M.C., MULDER, B.M. (1998). The making of the architecture of the plant cell wall: How cells exploit geometry. *Proc. Natl. Acad. Sci. USA* 95, 7215-7219.

EMONS, A.M.C., MULDER, B.M. (2000). How the deposition of cellulose microfibrils builds cell wall architecture. *Trends Plant Sci.* 5, 35-40.

EXLEY, C. (1999). A molecular mechanims of aluminum-induced Alzheimer's disease? *J. Inorg. Biochem.* 76, 133-140.

FATH, A., BETHKE, P.C., JONES, R.L. (1999). Barley aleurone cell death is not apoptotic: characterization of nuclease activities and DNA degradation. *Plant J.* 20, 305-315.

FUJINO, T., ITOH, T. (1998). Changes in pectin structure during epidermal cell elongation in pea (*Pisum sativum*) and its implications for cell wall architecture. *Plant Cell Physiol.* 39, 1315-1323.

GALOU, M., GAO, J., HUMBERT, J., MERICSKAY, J., LI, Z., PAULIN, D., VICKART, P. (1997). The importance of intermediate filaments in the adaption of tissues to mechanical stress: evidence from gene knockout studies. *Biol. Cell* 89, 85-97.

GUO, G.W., LIANG, Y.X. (2001). Aluminium-induced apoptosis in cultured astrocytes and its effect on calcium homeostasis. *Brain Res.* 88, 221-226.

HARRIS, W.R., BERTHON, G., DAY, J.P., EXLEY, C., FLATEN, T.P., FORBES, W.F., KISS, T., ORVIG, C., ZATTA, P.F. (1996). Speciation of aluminum in biological systems. *J. Toxicol. Environ. Health* 48, 543-568.

HAVEL, L., DURZAN, D.J. (1996). Apoptosis in plants. *Bot. Acta* 109, 268-277.

HAWES, M.C., CROOKS, K., COLEMAN, J., SATIAT-JEUNEMAITRE, B. (1995). Endocytosis in plants: fact or artefact? *Plant Cell Environ.* 18, 1245-1252.

HORST , W.J., WAGNER, A., MARSCHNER, H. (1982). Mucilage protects root meristems from aluminium injury. *Z. Pflanz. Bodenkunde* 105, 435-444.

HORST, W.J. (1995). The role of the apoplast in aluminium toxicity and resistance of higher plants: a review. *Z. Pflanz. Bodenkunde* 158, 419-428.

HORST, W.J., SCHMOHL, N., KOLLMEIER, M., BALUSKA, F., SIVAGURU, M. (1999). Does aluminium affect root growth of maize through interaction with the cell wall - plasma membrane - cytoskeleton continuum? *Plant and Soil* 215, 163-174.

INGBER, D.E. (1997). Tensegrity: the architectural basis of mecanotransduction. *Ann. Rev. Physiol.* 59, 575-599.

INOUHE, M., INADA, G., THOMAS, B.R., NEVINS, D.J. (2000). Cell wall autolytic activities and distribution of cell wall glucanases in *Zea mays* L. seedlings. *Int. J. Biol. Macromol.* 27, 151-156.

JEFFERY, E.H., ABREO, K., BURGESS, E., CANNATA, J., GREGER, J.L. (1996). Systemic aluminum toxicity: effects on bone, hematopoietic tissue and kidney. *J Toxicol Environ Hlth* 48, 649-665.

JONES, A. (2000). Does the plant mitochondrion integrate cellular stress and regulate programmed cell death? *Trends Plant Sci.* **5**, 225-230.

JORGE, R.A., ARRUDA, P. (1997). Aluminum-induced organic acids exudation by roots of na aluminum-tolerant tropical maize. *Phytochemistry* **45**, 675-681.

JULKA, D., GILL, K.D. (1996). Altered calcium homeostatis: a possible mechanism of aluminium-induced neurotoxicity. *Biochim. Biophys. Acta* **1315**, 47-54.

KARLIK, S.J., EICHHORN, G.L., LEWIS, P.N., CRAPPER, D.R. (1980). Interaction of aluminium species with deoxyribonucleic acid. *Biochemistry* **19**, 5991-5998.

KERR, J.F.R., WYLLIE, A.H., CURRIE, A.R. (1972). Apoptosis: a basic biologic phenomenom with wide-ranging implications in tissue kinetics. *Br. J. Cancer* **26**, 239-257.

KINRAIDE, T.B. (1991). Identity of the rhizotoxic aluminium species. *Plant Soil* **134**, 167-178.

KISS, T., ZATTA, P., CORAIN, B. (1996). Interaction of Aluminum (III) with phosphate-binding sites: biological aspects and implications. *Coord. Chem. Rev.* **149**, 329-346.

KOCHIAN, L.V. (1995). Cellular mechanisms of aluminum toxicity and resistance in plants. *Ann. Rev. Plant Physiol. Plant Mol. Biol.* **46**, 237-260.

KOHORN, B.D. (2000). Plasma membrane-cell wall contacts. *Plant Physiol* **124**, 31-38.

KRISHNAMURTY, K.V. (1999). Methods in Cell Wall Cytochemistry. Washington, USA: CRC press.

LA FUENTE, J.M., RAMÍREZ-RODRÍGUEZ, V., CABRERA-PONCE, J.L., HERRERA-ESTRELLA, L. (1997). Aluminum tolerance in transgenic plants by alteration of citrate synthesis. *Science* **276**, 1566-1568.

LEVITT, J. (1980). Responses of plants to environmental stresses. New York, USA. Academic Press.

LI, X.F., MA, J.F., HIRADATE, S., MATSUMOTO, H. (2000). Mucilage strongly binds aluminum but does not prevent roots from aluminum injury in Zea mays. *Physiol. Plantarum* **108**, 152-160.

LIU, K., LUAN, S. (2001). Internal aluminum block of plant inward K^+ channels. *Plant Cell* **13**, 1453-1465.

MA, J.F., RYAN, P.R., DELHAIZE, E. (2001). Aluminium tolerance in plants and the complexing role of organic acids. *Trends Plant Sci* **6**, 273-278.

MASSOT, N., LLUGANY, M., POSCHENRIEDER, C., BARCELO, J. (1999). Callose production as indicator of aluminium toxicity in bean cultivars. *J. Plant Nutr.* **22**, 1-10.

MATSUMOTO, H., YAMAMOTO, Y., KASAI, M. (1992). Changes of some properties of the plasma membrane-enriched fraction of barley roots related to aluminium stress: Membrane-associated ATPase, aluminium and calcium. *Soil Sci. Plant Nutr.* **38**, 411-419.

MATSUMOTO, H., MORIMURA, S. (1980). Repressed template activity of chromatin of pea roots treated by aluminium. *Plant Cell Physiol* **21**, 951-959.

MATSUMOTO, H. (2000). Cell biology of aluminium toxicity and tolerance in higher plants. *Int. Rev.*

Cytol. **200**, 1-46.

MOORE, P.B., DAY, J.P., TAYLOR, G.A., FERRIER, I.N., FIFIELD, L.K., EDWARDSON, J.A. (2000). Absorption of aluminium[26] in Alzheimer's disease measured using accelerator mass spectrometry. *Dement. Geriatr. Cogn. Disord.* **11**, 66-69.

NELSON, D.J. (1996). Aluminium complexation with nucleoside di- and tri-phosphates and implication in nucleoside binding proteins. *Coord. Chem. Rev.* **149**, 95-111.

NISHITANI, K. (1997). The role of endoxyloglucan transferase in the organization of plant cell walls. *Int. J. Cytol.* **173**, 157-195.

OHYASHIKI, O., SUZUKI, S., SATOH, E., UEMORI, Y. (1998). A marked stimulation of Fe^{2+}-initiated lipid peroxidation in phospholipid liposomes by lipophilic aluminum complex, aluminum acetylacetonate. *Biochim. Biophys. Acta* **1389**, 141-149.

OLIVETTI, G.P., CUMMING, J.R., ETHERTON, B. (1995). Membrane potential depolarization of root cap implication in nucleoside binding proteins. *Plant Physiol.* **109**, 123-129.

OSTATEK-BOCZYNSKI, Z., KERVEN, G.L., BLAMEY, F.P.C. (1995). Aluminium reactions with polygalacturonate and related organic ligands. *Plant Soil* **171**, 41-45.

PAN, J.W., ZHU, M., CHEN, H. (2001). Aluminium induced cell-death in root tip cells of barley. *Exp. Bot.* **46**, 71-79.

PARKER, D.R., PEDLER, J.F. (1998). Probing the "malate hypohesis" of differential aluminum tolerance in wheat by using other rhizotoxic ions as proxies for Al. *Planta* **205**, 389-396.

PEDERSON, T. (1998). Thinking about a nuclear matrix. *J. Mol. Biol.* **227**, 147-159.

PELLET, D.M., GRUNES, D.L., KOCHIAN, L.V. (1994) Organic acid exudation as an aluminum tolerance mechanism in maize (*Zea mays* L.). *Planta* **196**, 788-795.

RAO, K.S.J., EASWARAN, K.R.K. (1997). Al^{27}-NMR studies of aluminum transport across yeast cell membranes. *Mol. Cell. Biochem.* **175**, 59-63.

ROUT, G.R., SAMANTARAY, S., DAS, P. (2001). Aluminium toxicity in plants: a review. *Agronomie* **21**, 3-21.

RYAN, P.R., DELHAIZE, E., RANDALL, P.J. (1995) Malate efflux from root apices: evidence for a general mechanism of Al-tolerance in wheat. *Aust. J. Plant Physiol.* **22**, 531-536.

SCHILDKNECHT, .P.H.P.A., VIDAL, B.C. (2002). A role for the cell wall in Al^{3+} resistance and toxicity: crystallinity and availability of negative charges. *LifeXY* **1**, 1087-1095.

SCHMOHL, N., PILLING, J., HORST, W.J. (2000). Pectin methylesterase modulates aluminium sensitivity in *Zea mays* and *Solanum tuberosum*. *Physiol. Plantarum* **109**, 419-427.

SIVAGURU, M., BALUSKA, F., VOLKMANN, D., FELLE, H.H., HORST, W.J. (1999). Impacts of aluminum on the cytoskeleton of the maize root apex. Short-term effects on the distal part of the transition zone. *Plant Physiology* **119**, 1073-1082.

SIVAGURU, M., FUJIWARA, T., SAMAJ, J., BALUSKA, F., YANG, Z., OSAWA, H.,

MAEDA,T., MORI,T., VOLKMANN,D., MATSUMOTO,H. (2000). Aluminum-induced 1-->3-beta-D-glucan inhibits cell-to-cell trafficking of molecules through plasmodesmata. A new mechanism of aluminum toxicity in plants. *Plant Physiol* **124**, 991-1006.

SUÁREZ-FERNÁNDEZ, M.B., SOLDADO, A.B., SANZ-MEDEL, A., VEGA, J.A., NOVELLI, A., FERNÁNDEZ-SÁNCHEZ, T. (1999). Aluminium-induced degeneration of astrocytes occurs via apoptosis and results in neuronal death. *Brain Res.* **835**, 125-136.

VIDAL, B.C. (1993). Cell and extracellular matrix interaction: a feedback theory based on molecular order recognition-adhesion events. *Rev. Unicamp* **4**, 11-13.

WALKER, P.R., LEBLANC, J., SIKORSKA, M. (1989). Effects of aluminum and other cations on the structure of brain and liver chromatin. *Biochemistry* **28**, 3911-3915.

WYATT, S.E., CARPITA, N.C. (1993). The plant cytoskeleton-cell-wall continuum. *Trends Cell Biol.* **3**, 413-417.

YAMAMOTO, Y., KOBAYASHI, Y., MATSUMOTO, H. (2001). Lipid peroxidation is an early symptom triggered by aluminum, but not the primary cause of elongation inhibition in Pea roots. *Plant Physiol.* **125**, 199-208.

YIM, K., BRADFORD, K.J. (1998). Callose deposition is responsible for apoplastic semipermeability of the endosperm envelope of muskmelon seeds. *Plant Physiol.* **118**, 83-90.

ZATTA, P.F., CERVELLIN, D., ZAMBENEDETTI, P. (1998). Effects of aluminum on the morphology of rabbit erythrocytes: a toxicological model. *Toxicol. in vitro* **12**, 287-293.

ZHANG, G., HODDINOTT, J., TAYLOR, G.J. (1994). Characterization of 1,3 -D-Glucan (callose) synthesis in roots of *Triticum aestivum* in response to aluminum toxicity. *J. Plant Physiol.* **144**, 229-234.

WHO guidelines for drinking-water quality. (1998). 2, 3-13. 1998. Geneva, Switzerland, World Health Organization.

ARTIGOS

Al^{3+}-induced effects on the higher order structure of DNA

Pedro H. P. A. Schildknecht[*], Benedicto de Campos Vidal

Departamento de Biologia Celular, Instituto de Biologia, Universidade Estadual de Campinas (UNICAMP), Campinas, SP, Brazil.

*Author for correspondence: Departamento de Biologia Celular, Instituto de Biologia – UNICAMP. Caixa Postal 6109, 13084-971, Campinas, SP, Brazil. Phone: (55)(19) 37886124; Fax: (55)(19) 37886111. E-mail: pedroh@operamail.com

Abstract

Aluminium (Al^{3+}) is the third most abundant element in soil and an understanding of its role in biological processes could help to answer questions in fields as diverse as crop development and brain diseases. Aluminium represses the template activity of DNA by binding to the phosphates, which in turn stabilizes the superhelix and leads to uncoiling of supercoiled DNA. In this work, we found that the binding of Al^{3+} to DNA phosphates resulted in a stable, rigid structure that was unable to migrate through agarose gels during electrophoresis. The hydrodynamic radius of DNA molecules increased after complexing with Al^{3+}, as well as the amount of light scattered by DNA molecules. The binding of Al^{3+} to DNA also increased the birefringence of this macromolecule, and led to its precipitation in a highly ordered array. However, at low DNA and Al^{3+} concentrations, the DNA precipitated as an amorphous structure that scattered light. Based on these results, we suggested two models for Al^{3+}-DNA binding: one for a high Al^{3+}:DNA ratio in which the DNA macromolecules are crosslinked and arranged in parallel to one another, with an enhancement of DNA birefringence, and andother for a low Al^{3+}:DNA ratio, in which Al^{3+} binds preferentially to the same DNA molecule, causing it to bend. Both models clearly showed the relevance of Al^{3+}-DNA interactions in the biological activity of DNA.

Introduction

Aluminium is the third most abundant element in soil and investigations into its biological role have been stimulated by the toxic effect of this metal on plants (Jorge *et al.*, 2001; Ma *et al.*, 2001; Schildknecht and Vidal, 2002) and by the suspicion that aluminium may be involved in brain diseases (Exley, 1999; Campbell and Bondy, 2000). Most of the aluminium in soil occurs as harmless oxides or silicates. However, in acid soils (pH < 5.0), aluminium is solubilized into the toxic species $Al(H_2O)_6^{3+}$, represented as Al^{3+} (Kochian, 1995; Harris, 1996). The preference of Al^{3+} for electrostatic rather than covalent binding is predictable thermodynamically due to its high charge-to-radius ratio (Berthon, 1996). Therefore, Al^{3+} forms stable complexes with ligands containing negatively charged organic functional groups, including pectin (Blamey and Dowling, 1995), mucin (Exley, 1998) and DNA (Matsumoto and Morimura, 1980; Karlik *et al.*, 1980; Karlik and Eichorn, 1989; Ahmad *et al.*, 1996; Nishino *et al.*, 2001).

Matsumoto and Morimura (1980) suggested intrastrand binding of Al^{3+} to the DNA double helix concomitant to the crosslinking of DNA molecules by an Al^{m+} polymer. However, intrastrand crosslinking of DNA could alter the distance between the two DNA strands, thereby affecting base stacking, although this has not been observed (Karlik *et al.*, 1980). Al^{3+} binds DNA phosphates (Karlik *et al.*, 1980; Ahmad *et al.*, 1996; Kiss *et al.*, 1996) and stabilizes the superhelix and prevent coiling of circular DNA molecules (Rao *et al.*, 1993). The intermolecular cross-linking of DNA by Al^{3+} was described by Karlik *et al.* (1980) and may be responsible by the formation of compact, toroidal structures of Al^{3+}-DNA complexes (Karlik *et al.*, 1989). The influence of ions, particularly multivalent cations, on the structure and mechanical properties of DNA is well known, and there is no evidence against a role for electrostatic interactions in DNA condensation, bending and other structural modifications (Bloomfield, 1991; Bloomfield, 1996; Baumann *et al.*, 1997; McFail-Isom *et al.*, 1999). The Al^{3+}-induced packing of DNA reduces the template activity of chromatin (Matsumoto and Morimura, 1980) and may result in the toxic effects observed in organisms exposed to Al^{3+} (Exley, 1999; Campbell and Bondy, 2000; Matsumoto, 2000; Jorge *et al.*, 2001; Ma *et al.*, 2001). However, there is little information on the mechanisms of DNA condensation induced by Al^{3+} and how this may interfere with the gene activity. In

this work, we examined the DNA packing by Al^{3+} by analyzing of the optical properties of the Al^{3+}-DNA complex and its mobility during electrophoresis.

Material and Methods

Electrophoresis

One microgram of 1kb DNA ladder (Gibco BRL, San Diego, CA) was diluted in 20 µl of 0.9% NaCl, pH 4.5, and $AlCl_3$ was added to final concentrations of 10^{-4} M to 10^{-6} M followed by mixing with a micropipette. Other salts, such as $CaCl_2$ and NaCl, were also tested as described for $AlCl_3$. Three microliters of 0.25% bromophenol blue:0.25% xylene cyanol loading buffer were added to the samples which were then loaded onto 0.7% agarose gels. TAE (0.04 mM Tris, 0.001 mM EDTA, pH 8.0) was used as the electrophoresis buffer and the samples were run at 8 V/cm and 45 A for 90 minutes. The gel was stained with ethidium bromide (2 mg/ml) and observed under UV light.

Light scattering measurements

The transmittance of a solution of 0.001% DNA in 0.9% NaCl, pH 4.5, was measured in a quartz cuvette at 650 nm using a diode-array spectrophotometer (Hewlett-Packard Co., Palo Alto, CA). $AlCl_3$ was added to the DNA solution from stock solutions of 10^{-1} M-10^{-4} M, pH 4.5, to give final concentrations of 10^{-5} M-10^{-7} M.

The number of photons scattered by the Al^{3+}-DNA complexes and the hydrodynamic radius of the complexes were measured by dynamic light scattering (DLS) in a DynaPro MS/X instrument coupled to a temperature control device (Rheometric Scientific, Inc., Piscataway, NJ). The DNA solution (0.001% in 0.9% NaCl, pH 4.5) was prepared with deionized water and filtered through a 0.45 µm filter (Millipore Corp., Bedford, MA). $AlCl_3$ was added to the DNA solution from the stock solutions mentioned above to give final concentration of 10^{-3} M-10^{-7} M. Background readings were obtained with 0.9% NaCl. All measurements were made at 37°C using a quartz cuvette and a monochromatic laser beam ($\lambda = 830nm$) as the source of photons.

The DLS technique measures the oscillations of light scattered from a sample. The readings are called "dynamic" the scattering objects, in this case Al^{3+}-DNA complexes, are in continuous motion through the sample. The hydrodynamic radius of a molecule determined by DLS is defined as the radius of a hypothetical hard sphere that diffuses as fast as the sample under measurement. Since these spheres are only hypothetical, the radius estimated from the diffusional properties of the particle is indicative of the apparent size of the dynamic hydrated/solvated non-spherical particle (as macromolecules are in practice) and is considered the "hydrodynamic" radius.

Polarized light microscopy and histochemistry

Threads of calf thymus DNA (Sigma Chemical Co., St. Louis, MO) were placed on a glass slide and hydrated with 200 μl of 0.9% NaCl, pH 4.5, at an approximate ratio of 1:2 (w/v). The NaCl solution prevented DNA melting by counteracting the negative charges of the phosphates. In addition, the NaCl solution did not act as a buffer, thus allowing low pH values (<5.0) to be reached, as required for formation of amounts of Al^{3+}, but not other aluminium species (Harris, 1996). The material was transferred to a humid chamber for 5 min and then observed under polarized light in a microscope (Carl Zeiss, Germany) equipped with a revolving stage. Fifty microliters of $AlCl_3$ or $CaCl_2$ solution (10^{-3}-10^{-5} M) were added to the DNA solution and the formation of Al^{3+}-DNA complexes was observed with the microscope. The glass slide with the DNA was not removed from the microscope stage during this procedure in order to minimize the impacts of external movements. A Brace-Köhler compensator was used to determine the main direction of vibration of the DNA fibrils. Although this type of compensator can also be used to measure the length of the optical retards caused by birefringent material, in this work this compensator was used only to abolish the birefringence of fibrils that were arranged in the same direction and, hence, determine their orientation. A first-order red compensator ($\lambda/4$) was used to verify the birefringence signal of the DNA molecules. Structures showing birefringence with a negative signal appeared in blue whereas the positive birefringent material was yellow because of the optical path difference of the compensator. These colors shall change if the position of the structures is altered in relation to the γ position of the compensator. The red parts of an object are in the extinction position or are isotropic.

The binding of Al^{3+} to DNA was analyzed by staining DNA with toluidine blue (TB), which binds electrostatically to available DNA phosphates by a reaction of basophilia (Mello, 1997). Two hundred microliters of 0.1% DNA solutions prepared as described above were placed on a glass slide and treated with 50 µl of 10^{-3} M and 10^{-5} M $AlCl_3$ or $CaCl_2$ for 15 min. The cation-DNA solution was subsequently stained with 200 µl of 0.025% TB in McIlvaine buffer (0.05 M citrate, 0.1 M sodium phosphate, pH 4.5) for 15 minutes and observed by ordinary light microscopy.

Salt solutions

$AlCl_3$ was used to prepare stock Al^{3+} solutions in sterile deionized water, pH 4.5. Stock solutions (10^{-1} M to 10^{-5} M) were prepared so as to allow the addition of similar volumes to the DNA solutions to obtain any desired $AlCl_3$ concentration, thus minimizing sample dilution. The Ca^{2+} and Na^+ stock solutions (10^{-1} M) were prepared with $CaCl_2$ and NaCl, respectively, as described for $AlCl_3$. All the stock solutions were discarded after use and were prepared freshly before each experiment.

Data analysis

Each experiment was repeated at least three times, excepted for the DLS measurements, which were done in duplicate, with 20 repeats/sample. All data were analyzed by ANOVA, using the Minitab statistical software package (Minitab Inc., State College, USA). The level of significance was set at $p < 0.05$.

Results

Effect of Al^{3+} on DNA mobility during electrophoresis

The electrophoretic mobility of DNA was highly affected by treatment with 10^{-4} M and 10^{-5} M $AlCl_3$ (Fig. 1, lanes 2 and 3). No migration was observed for those samples, which remained stationary in the gel loading chamber, even after electrophoresis for 3-4 h. At a lower $AlCl_3$ concentration (10^{-6} M), the DNA moved freely through the agarose gel, in a manner similar to the control sample (Fig. 1, lane 4). There were no alterations in the mobility of DNA treated with NaCl or $CaCl_2$, even at high concentrations (10^{-3} M – 10^{-4} M) (Fig. 1, lanes 5-8).

Light scattering by Al³⁺-DNA complexes

The light transmittance of DNA solutions decreased in the presence of increasing Al^{3+} concentrations (Fig. 2A). Pure DNA and $AlCl_3$ solutions showed high transmittance values (> 95%) and were not expected to absorb light at this wavelength, thus showing that the decrease in the transmittance of Al^{3+}-treated DNA solutions resulted from light scattering. No alterations were observed in light transmittance in the samples treated with 10^{-7} M - 10^{-5} M $AlCl_3$ ($p = 0.211$), but a sudden decrease in transmittance was observed in the presence of 10^{-4} M and 10^{-3} M $AlCl_3$ ($p = 0.000$).

DLS analysis confirmed the results of the transmittance measurements by showing higher light scattering (as photons x 10^9/s) of DNA treated with 10^{-5} M $AlCl_3$ ($p = 0.000$) (Fig. 2B). There was no difference in light scattering between the control (without Al^{3+}) and $AlCl_3$ (10^{-7} M) treated samples (p = 0.151), in contrast to the findings for light transmittance.

The hydrodynamic radius of DNA increased in the presence of 10^{-5} M $AlCl_3$ ($p = 0.000$) (Fig. 2C), whereas treatment with 10^{-7} M $AlCl_3$ resulted in a decrease in the hydrodynamic radius compared to the control (p = 0.006).

Influence of Al³⁺ on the liquid-crystalline array of DNA

DNA threads hydrated with 0.9% NaCl showed a crossed fibril array and intense birefringence (Fig. 3A) that was enhanced by the λ/4 compensator (Fig. 3B). The liquid surroundings of the hydrated DNA threads were arbitrarily divided into three regions (a schematic model is given in Fig. 3C); namely 1) a non-dissolved DNA thread, with a dry core and a hydrated surface; 2) a region very close to the DNA thread (VCS) consisting of a saturated DNA solution supplemented with molecules from the DNA thread surface and that showed a strong optical rotatory power; and 3) a region not close to the DNA thread (NCS) and thus not strictly connected to it, with a lower DNA concentration than the VCS region and hence little or no optical rotatory power was detected. There were no real borders between these sectors, but a gradual transition from a region to another. The addition of Al^{3+} to the DNA solution resulted in precipitation of the macromolecule as highly oriented fibrils in the NCS region (Fig. 3D) and as a membrane-like structure in the

VCS region (Fig. 3E). The DNA precipitated in the NCS region maintained the crossed array of fibrils observed in untreated samples. The membrane in the VCS region of Al^{3+}-treated samples was rigid and could not be stretched with a needle without breaking, thus showing the complete loss of DNA viscoelasticity. When observed with the $\lambda/4$ compensator, the Al^{3+}-DNA-membrane maintained fibrils oriented in the direction characteristic of its structure (Fig. 3F).

In contrast, a lower concentration of Al^{3+} (10^{-5} M $AlCl_3$) did not precipitate the DNA as a membrane-like structure in the VCS region and no alterations in the optical properties of DNA were detected in this region. In the NCS region, a non-birefringent, amorphous precipitate was observed (Fig. 4). Although the precipitate appeared bright under crossed polars, no changes in its brightness were observed as the microscope stage was rotated, contrary to what should have occurred with a birefringent precipitate.

There were no alterations in the properties of the hydrated DNA in the presence of Ca^{+2}, even at 10^{-3} M.

Al^{3+} reduces the binding of toluidine blue to DNA phosphates and induces macromolecular fragmentation

Staining with toluidine blue (TB) caused the precipitation of DNA as highly stained, metachromatic fibrils (Fig. 5A). DNA treated with $CaCl_2$ remained soluble, but precipitated as soon as TB was added. There were no differences between the TB-stained fibrils of $CaCl_2$ (10^{-5} M) treated samples and the control. A slight decrease in fibril diameter was observed in all experiments with 10^{-3} M $CaCl_2$ (Fig. 5B), but this decrease was not quantified by direct measurements.

$AlCl_3$ (10^{-3} M) precipitated the DNA as membranes, with the same characteristics as for the VCS environment. The metachromasy was abolished and the membranes did not stain with TB or showed only a pale green color. Samples treated with 10^{-5} M $AlCl_3$ showed two types of precipitates, one similar to the amorphous precipitate already observed in the NCS region, and the other consisting of small aggregates with lower metachromasy (Fig. 5C) after TB staining.

Discussion

Electrophoretic mobility of Al^{3+}-DNA complexes.

The lack of migration of DNA treated with 10^{-4} M – 10^{-5} M $AlCl_3$ could not be attributed to neutralization of the negative charges of DNA phosphates by Al^{3+} since samples treated with $CaCl_2$ and $NaCl$, at a concentration greater than the highest $AlCl_3$ concentration tested, showed no alterations in their electrophoretic profile.

The lack of DNA migration in the presence $>10^{-6}$ M $AlCl_3$ may reflect stiffening of the macromolecule and the formation of a large Al^{3+}-DNA complex unable to pass through the pores of the agarose matrix. As a result, the samples remained in the loading chamber, even after several hours of electrophoresis (lanes 2-3, Fig. 1). At a lower concentration (10^{-6} M), the number of interactions between Al^{3+} and DNA is reduced which may facilitate the disruption of Al^{3+}-DNA complexes by the electrophoretic electric field, so that the DNA fragments could migrate through the gel. Similar results were observed by Rao *et al.* (1993), who analyzed the electrophoretic mobility of Al^{3+}-DNA complexes at low Al concentrations (3.3 x 10^{-7} M – 3.3 x 10^{-9} M) and found no interference of Al^{3+} on DNA mobility. However, these results did not mean that Al^{3+} cannot alter the superstructure of DNA at low concentrations, but rather that electrophoresis may not be sufficiently sensitive to detect such a change. Rao *et al.* (1993) also showed that although an influence of Al^{3+} on DNA structure was not detected in linear fragments of DNA, plasmids were readily uncoiled by Al^{3+} at the same concentrations as those tested with linear DNA.

Al^{3+} caused DNA aggregation and bending

The wavelengths for the light transmittance measurements were chosen in a range where DNA had no absorbance so that all variations in transmittance would be the result of scattered light. As an additional method, the DLS measures were done to detect only scattered light. $AlCl_3$ and DNA solutions showed high light transmittance (Fig. 2A) although some light scattering was detectable in pure DNA solutions (Fig. 2B).

A decrease in transmitted light was detected with 10^{-7} M - 10^{-5} M $AlCl_3$ and differed from the results of the DLS measurements, which showed no differences among samples treated with 10^{-7} M $AlCl_3$ and those without $AlCl_3$. These findings were puzzling

since transmittance measurements indicated light scattering in samples treated with 10^{-7} M AlCl$_3$ whereas DLS measures did not. Light absorption could mask the transmittance results by lowering the number of photons that reach the UV-vis detector of the spectrophotometer. However, no absorbance by the DNA solutions was expected at the wavelength used. Thus, this discrepancy may be related to methodological differences, and can be confirmed by measuring absorbance, transmittance and light scattering simultaneously in a single apparatus. This approach was not used here but is a theme for further analysis. Despite the confusing results for samples treated with 10^{-7} M AlCl$_3$, DNA treated with 10^{-5} M AlCl$_3$ showed a marked decline in light transmittance and increased light scattering compared to the control. These results agreed with the increased hydrodynamic radius of DNA in the presence of 10^{-5} M AlCl$_3$, which showed that the macromolecular length of DNA was enhanced by higher amounts of the cation. This Al^{3+}-induced compaction of DNA, possibly as toroidal aggregates (Karlik *et al.*, 1989), could account for the immobility of DNA during electrophoresis. The microscopic analysis of these aggregates is discussed later.

Al^{3+} binding to DNA phosphates alters the molecular ordering in solution

The core of DNA threads showed high birefringence as a consequence of the elevated concentration of the macromolecule. Entropic packing constraints are sufficient to promote molecular alignment into an orientational, positional order (Stray *et al.* 1998) and this phenomenon that was observed in the core of the DNA threads and, in lower magnitude, in the VCS region. The lack of optical activity in the NCS region reflected the low DNA concentration which did not cause the alignment of the molecules.

The pattern of DNA precipitation in the presence of different concentrations of Al^{3+} suggested the model for Al^{3+}-DNA interactions showed in Fig. 6. High AlCl$_3$ concentrations resulted in a filamentous precipitate in the NCS region, where DNA was less concentrated, and in a membrane-like precipitate in the VCS region, where the DNA solution could be considered to be saturated. Thus, there is enough Al^{3+} to interact with several DNA phosphates, some regions will become positively net charged as a consequence of the residual charge (2+) from the Al-phosphate complex. These positively charged regions would repeal each other, even in saline solution (0.9% NaCl). The

electrostatic interaction of Al^{3+} with phosphates could also occur between two DNA molecules to bring them closer together (Fig. 6A). The occurrence of repulsion and attraction among DNA molecules would subject the double helix to forces from several directions because of the interaction with other DNA molecules. Equilibrium could be reached by the macromolecular orientation of DNA molecules into a common virtual axis (all molecules being parallel to each other), so that the repulsion between two molecules would be balanced by the repulsion from the surrounding molecules. This model should result in highly oriented DNA fibrils with a birefringent precipitate, as observed in the NCS region, and a low viscoelasticity because of the cross-linking of DNA molecules by Al^{3+}.

If this model is applied to saturated DNA solutions, the highly oriented fibrils will be maintained together by intense attraction and repulsion among the molecules and should produce a birefringent, membrane-like structure, such as seen in the VCS region. DNA occurred as a saturated solution in the VCS region so that the intermolecular DNA crosslinking by Al^{3+} involved molecules previously aligned by entropic packing constraints. Such precipitates should also show regions where would be preferential tearing when stretched with a needle, because of the presence of highly positively charged DNA molecules, which would repeal each other. Unsaturated DNA solutions may show crosslinking by Al^{3+} in the same DNA molecule, and this can lead to the molecular bending and toroidal packing of DNA observed by Karlik *et al.* (1989).

However, the model in Fig. 6A cannot explain the lack of visible precipitates at VCS region, or the amorphous precipitate in the NCS region, when a low concentration of $AlCl_3$ was used. In this case, because there is insufficient Al^{3+} to form adjacent Al^{3+}-DNA complexes, the cation will bind to the closest phosphate (in the same DNA molecule as the other phosphate(s) bound) and cause macromolecular bending (Fig. 6B). This mechanism of cation-induced bending has been discussed elsewhere (Maher III, 1998; McFail-Isom *et al.*, 1999) and is driven by an electrostatic collapse of the DNA molecule. Thus, at low $AlCl_3$ and DNA concentrations, only a few Al^{3+} will bind to each DNA molecule that will precipitate as a highly bent, disordered structure without birefringence, as seen in the amorphous precipitate in the NCS region. Likewise, if the Al^{3+}/ phosphate ratio is too high, the Al^{3+} cations will be spread out among different DNA molecules and there will be no

visible alteration in the DNA birefringence or viscoelasticity, exactly as observed in the VCS region following exposure to low amounts of $AlCl_3$.

Although the cross-linking of the two antiparallel strands of the same DNA molecule by Al^{3+} was not contemplated in our model, the results of Karlik *et al.* (1980) and Karlik and Eichhorn (1989) suggest that such binding may occur. However, since no interference with DNA base stacking was observed (Karlik *et al.*, 1980), it seems more probable that the cross-linking involves phosphate groups outside the DNA backbone rather than within the macromolecule.

The weak staining of Al^{3+}-DNA complexes by TB was caused by the blockade of phosphates by Al^{3+}; a similar effect has been observed in plant cell walls treated with this cation (Schildknecht and Vidal, 2002). The abolishment of metachromasy was also a result of Al^{3+} binding to phosphates, since this inhibited the formation of stacked TB molecules. The precipitation of Al^{3+}-DNA complexes as small aggregates may result from the toroidal compaction of DNA (Karlik *et al.*, 1989) by Al^{3+} crosslinks within the same DNA molecule. No real DNA fragmentation was expected, since none was observed by electrophoresis. In any case, Al^{3+} treatment did not result in metachromatic, long-length, DNA filaments such as those seen in control (-Al^{3+}) experiments.

The biological importance of Al^{3+}-DNA complexes

The mechanisms of DNA condensation/unpacking are fundamental to several biological events, including gene transcription and cell division. The geometric specificity of certain proteins for the DNA helix suggests the existence of structural recognition motifs in DNA (Bloomfield, 1996). Hence, the correct order of DNA molecules is essential for cell survival. The condensation of DNA by multivalent cations occurs when ~90% of the electrostatic charge of the macromolecule is neutralized (Bloomfield, 1996). The negative charge of DNA can be neutralized by divalent or trivalent cations but, as shown here, the resulting structures of condensed DNA are not similar. The stiffness of the Al^{3+}-DNA precipitates observed in saturated DNA solutions (at a concentration similar to that observed in the cell nucleus) suggests that DNA cannot be transcribed after the Al^{3+} binding. Matsumoto and Morimura (1980) showed that Al^{3+} repressed the template activity of DNA. The concentration of Al^{3+} in the cell nucleus is well below 10^{-5} M, which was the

lowest concentration used during birefringence analysis. However, the high stability of Al^{3+} binding mean that this cation can accumulate within the nucleus over time before its deleterious effects are observed. The bending of DNA could alter the structure of the recognition sites for regulatory proteins, thereby inhibiting cell metabolism. For some proteins, such as the TATA box binding protein, the bending of DNA is essential for initiation of transcription. However, this will not occur if the DNA molecules are crosslinked into a stiff array that does not allow bending. The binding of Al^{3+} to DNA may be one of the causes of Al^{3+}-induced cell death (Campbell and Bondy, 2000; Matsumoto, 2000).

Conclusions

Al^{3+} binds to DNA phosphates and alters the macromolecular conformation of this nucleic acid. The structures formed by Al^{3+} vary according to the Al^{3+} and DNA concentrations. Solutions with high Al^{3+} and DNA concentrations yielded stiff DNA molecules, oriented in parallel. In contrast, solutions with low concentrations of DNA and Al^{3+} resulted in DNA bending as a result of Al^{3+} crosslinking between phosphates of the same DNA molecule. DNA was also affected by very low concentrations of Al^{3+} ($< 10^{-5}$ M $AlCl_3$). These results suggest that Al^{3+} can alter DNA structurally and that this interaction with DNA may be one of the main causes of the toxic effects of this cation in cells.

Acknowledgements

References

Ahmad,R., M.Naoui, J.F.Neault, S.Diamantoglou, and H.A.Tajmir-Riahi. (1996). An FTIR spectroscopic study of calf-thymus DNA complexation with Al(III) and Ga(III) cations. *J. Biomol. Struct. Dyn.* **13**,795-802.

Baumann,C.G., S.B.Smith, V.A.Bloomfield, and C.Bustamante. (1997). Ionic effects on the elasticity of single DNA molecules. *Proc. Natl. Acad. Sci. USA* **94**,6185-6190.

Berthon G. (1996). Chemical speciation studies in relation to aluminium metabolism and toxicity. *Coord. Chem. Rev.* **149**,241-280.

Blamey,F.P.C. and A.J.Dowling. (1995). Antagonism between aluminium and calcium for sorption by calcium pectate. *Plant Soil* **171**,137-140.

Bloomfield,V.A. (1991). Condensation of DNA by multivalent cations. *Biopolymers* **31**,1471-1481.

Bloomfield,V.A. (1996). DNA condensation. *Curr. Opi. Struct. Biol.* **6**,334-341.

Campbell,A. and S.C.Bondy. (2000). Aluminum induced oxidative events and its relation to inflammation: a role for the metal in Alzheimer's disease. *Cell. Mol. Biol.* **46**,721-730.

Exley,C. (1998). The precipitation of mucin by aluminium. *J. Inorg. Biochem.* **70**,195-206.

Exley,C. (1999). A molecular mechanism of aluminium-induced Alzheimer's disease? *J. Inorg. Biochem.* **76**,133-140.

Harris,W.R., G.Berthon, J.P.Day, C.Exley, T.P.Flaten, W.F.Forbes, T.Kiss, C.Orvig, and P.F.Zatta. (1996). Speciation of aluminum in biological systems. *J. Toxicol. Environ. Health* **48**,543-568.

Jorge,R.A., M.Menossi, and P.Arruda. (2001). Probing the role of calmodulin in Al toxicity in maize. *Phytochemistry* **58**,415-422.

Karlik,S.J. and G.L.Eichhorn. (1989). Polynucleotide cross-linking by aluminum. *J. Inorg. Biochem.* **37**,259-269.

Karlik,S.J., G.L.Eichhorn, P.N.Lewis, and D.R.Crapper. (1980). Interaction of aluminium species with deoxyribonucleic acid. *Biochemistry* **19**,5991-5998.

Kiss,T., P.Zatta, and B.Corain. (1996). Interaction of Aluminum (III) with phosphate-binding sites: biological aspects and implications. *Coord. Chem. Rev.* **149**,329-346.

Kochian,L.V. (1995). Cellular mechanisms of aluminum toxicity and resistance in plants. *Ann. Rev. Plant Physiol. Plant Mol. Biol.* **46**,237-260.

Ma,J.F., P.R.Ryan, and E.Delhaize. (2001). Aluminium tolerance in plants and the complexing role of organic acids. *Trends Plant Sci.* **6**,273-278.

Maher III,L.J. (1998). Mechanisms of DNA bending. *Curr. Opin. Chem. Biol.* **2**,688-694.

Matsumoto,H. (2000). Cell biology of aluminium toxicity and tolerance in higher plants. *Int. Rev. Cytol.* **200**,1-46.

Matsumoto,H. and S.Morimura. (1980). Repressed template activity of chromatin of pea roots treated by aluminium. *Plant Cell Physiol.* **21**,951-959.

McFail-Isom,L., C.C.Sines, and L.D.Williams. (1999). DNA structure: cations in charge? *Curr. Opin. Struct. Biol.* **9**,298-304.

Mello,M.L.S. (1997). Cytochemistry of DNA, RNA and nuclear proteins. *Braz. J. Genet.* **20**,257-264.

Nishino,S., T.Kobayashi, H.Matsushima, T.Tokii, and Y.Nishida. (2001). Enhanced nucleophilicity and depressed electrophilicity of peroxide by zinc(II), aluminum(III) and lanthanum(III) ions. *Z. Naturforsch.* **56**,138-143.

Schildknecht, P.H.P.A. and B.C. Vidal. (2002) A role for the cell wall in Al^{3+} resistance and toxicity: crystallinity and availability of negative charges. *LifeXY* **1**, 1087-1095.

Stray,H.H., R.Podgornik, D.C.Rau, and V.A.Parsegian. (1998). DNA-DNA interactions. *Curr. Opin. Struct. Biol.* **8**,309-313.

[**Figure 1**: Electrophoresis of DNA under different conditions: control (lane 1); 10^{-4} M AlCl$_3$ (lane 2); 10^{-5} M AlCl$_3$ (lane 3); 10^{-6} M AlCl$_3$ (lane 4); 10^{-3} M CaCl$_2$ (lane 5); 10^{-4} M CaCl$_2$ (lane 6); 10^{-3} M NaCl (lane 7); 10^{-4} M NaCl (lane 8).]

[**Figure 2**: A) Light transmittance (%) at 650nm in the presence of different AlCl$_3$ concentrations ([AlCl$_3$]). "DNA only" indicates the control treatment (no Al^{3+}) and "AlCl$_3$ only" indicates pure 10^{-3} M AlCl$_3$ solution. B) Light scattering at 830 nm (10^9 photons/s) of DNA solutions treated with different concentrations of AlCl$_3$. C) Hydrodynamic radius of DNA molecules after treatment with AlCl$_3$.]

[**Figure 3**: DNA threads hydrated in 0.9% NaCl and observed under crossed polars. A) DNA + 0.9% NaCl, compensated with a Brace-Köhler compensator; B) As in "A", but compensated with a λ/4 compensator. The arrows indicate the vibrational orientation of the DNA fibrils; C) Scheme explaining the variation of DNA concentrations around the DNA threads. See text for explanation; D) DNA + 10^{-4} M AlCl$_3$ in the NCS region, compensated with a Brace-Köhler compensator; E) As in "D", but observed in the VCS region; F) As in "E", but compensated with a λ/4 compensator. Bar = 200 μm.]

[**Figure 4**: Amorphous DNA precipitate in the NCS region after treatment with 10^{-5} M AlCl$_3$. A) Bright field microscopy; B) Viewed with crossed polars. Bar = 200μm.]

[**Figure 5**: Toluidine blue stained DNA fibrils. A) Control; B) DNA + 10^{-3} M CaCl$_2$; C) DNA + 10^{-5} M AlCl$_3$. Note the absence of metachromasy in the Al^{3+}-DNA complexes. Bar = 200 μm.]

[**Figure 6**: Model showing Al^{3+} complexed to DNA at different concentrations of the cation. See text for explanation.]
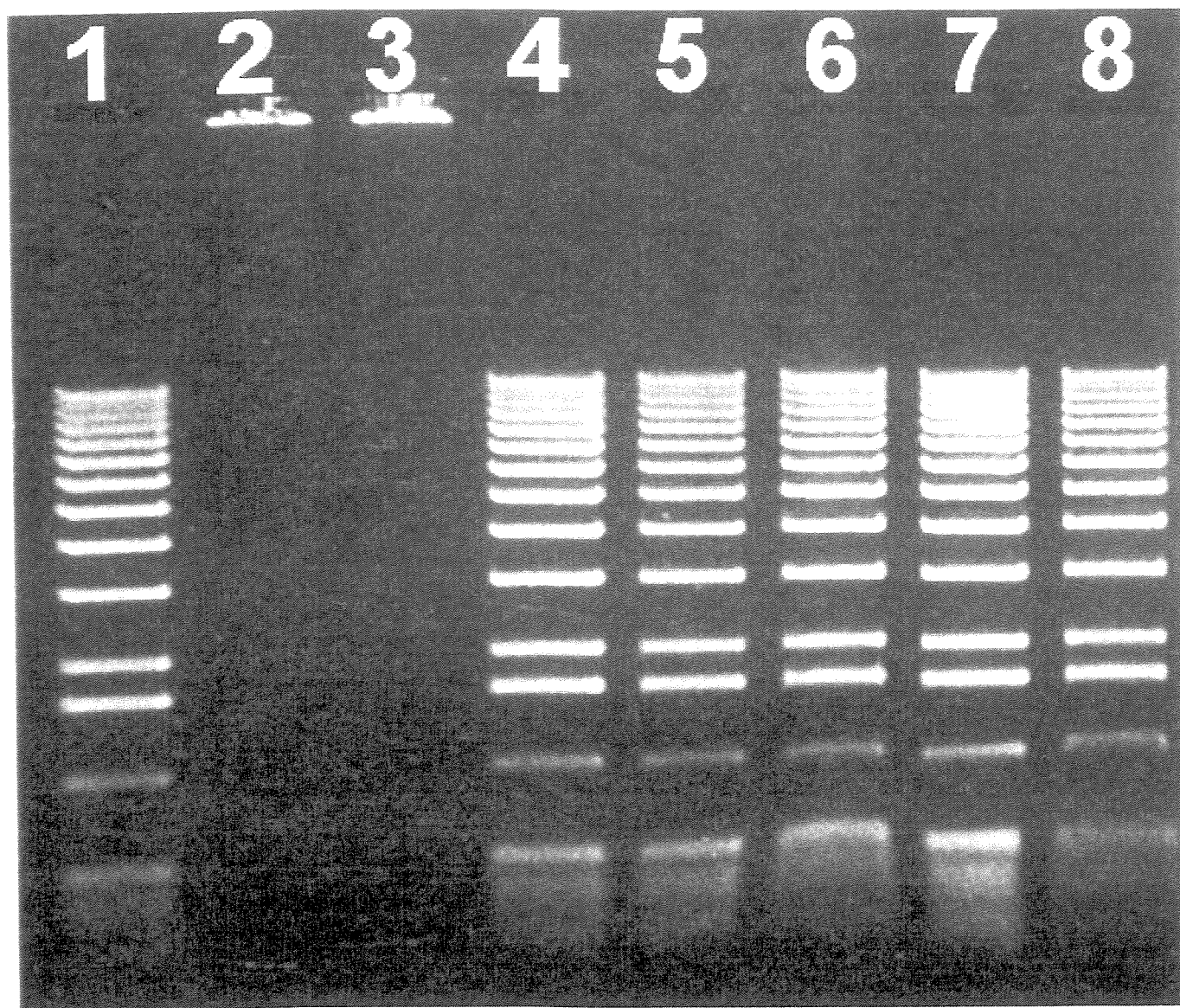
FIG.1

FIG.2
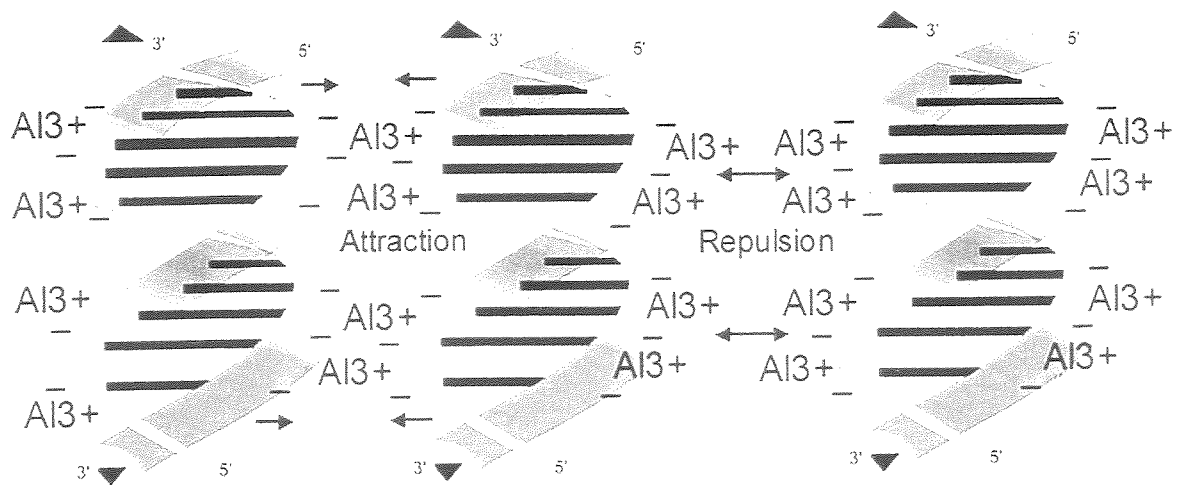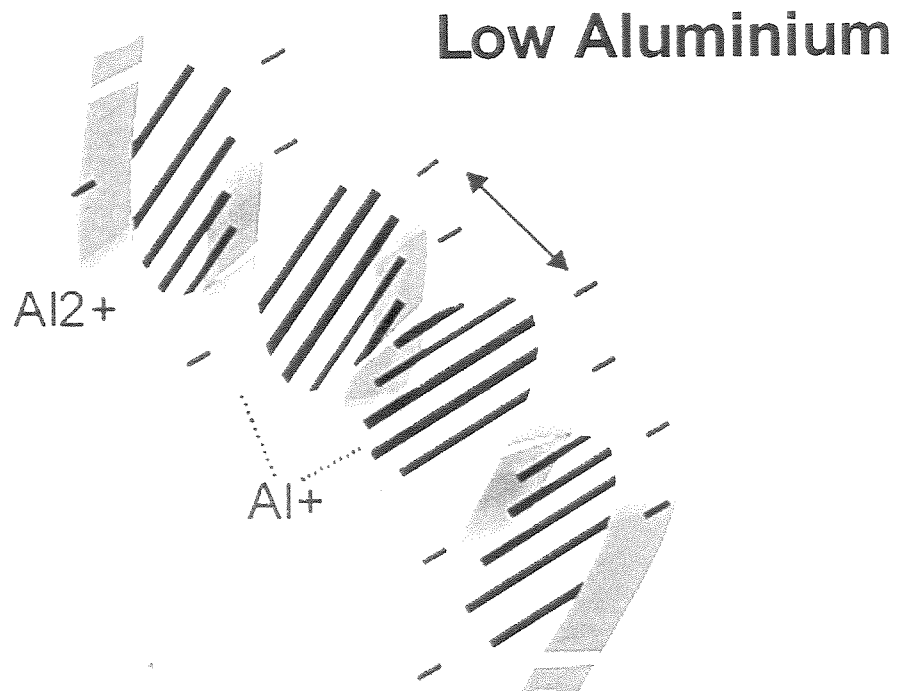
C

NCS
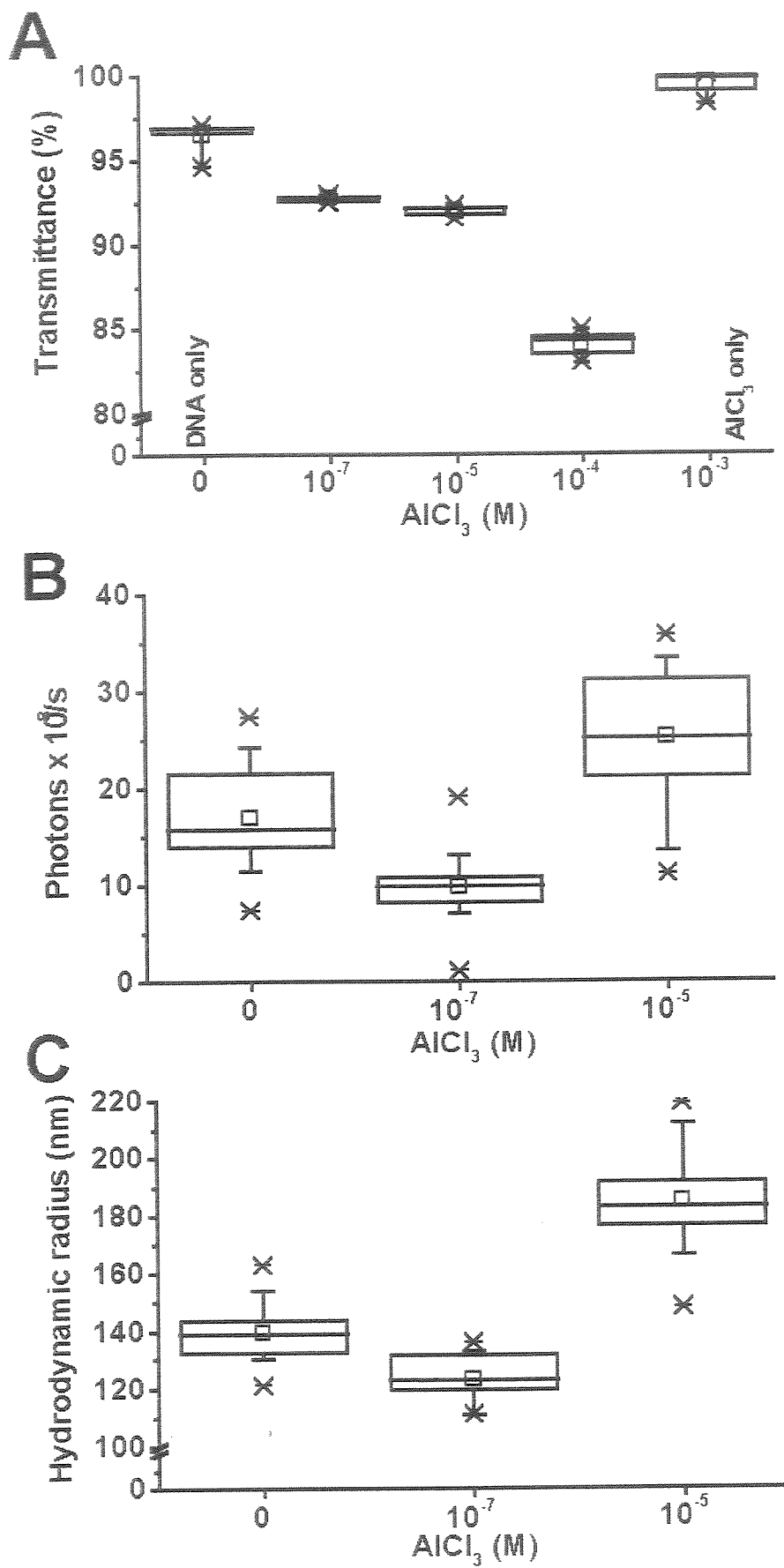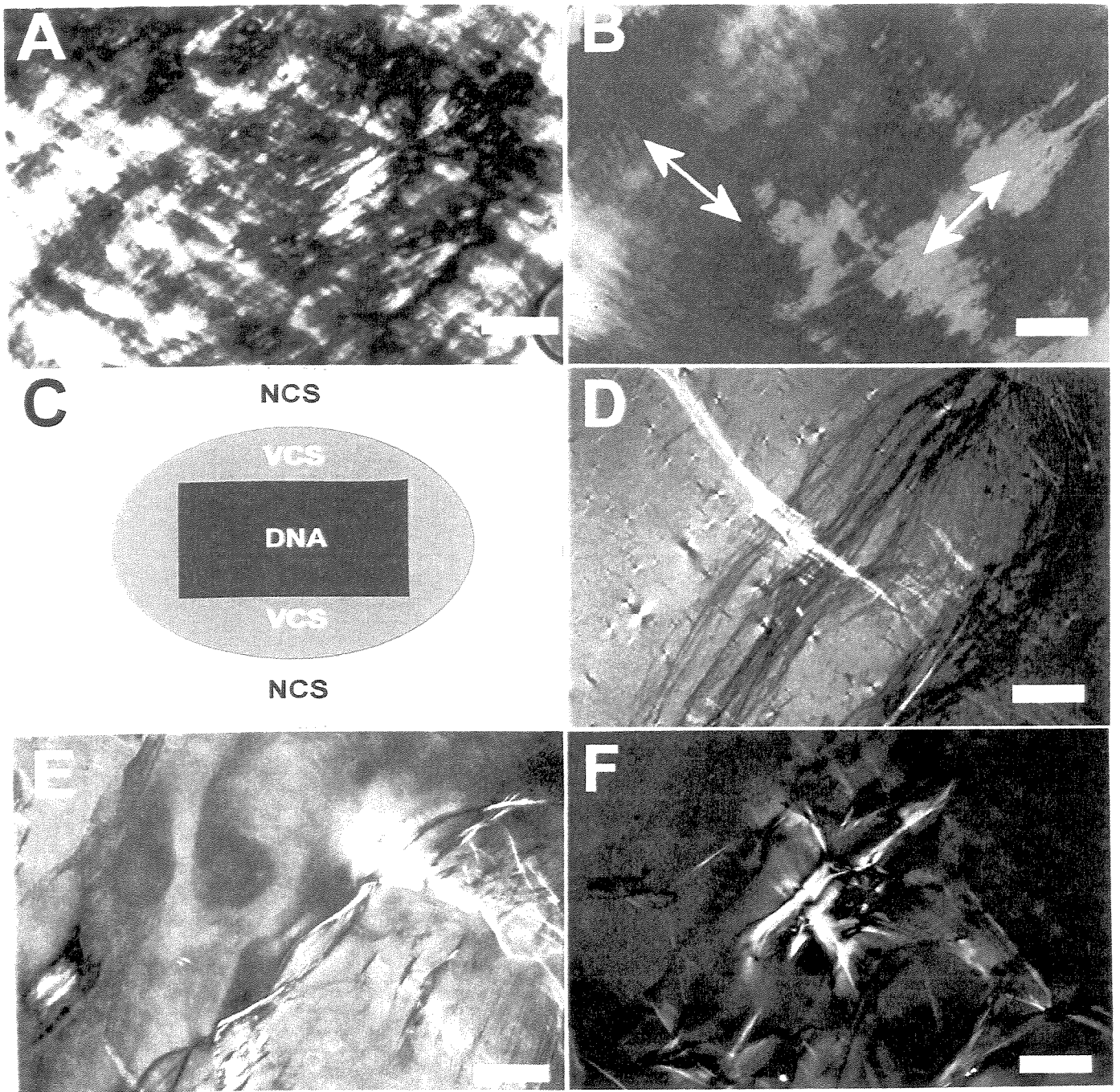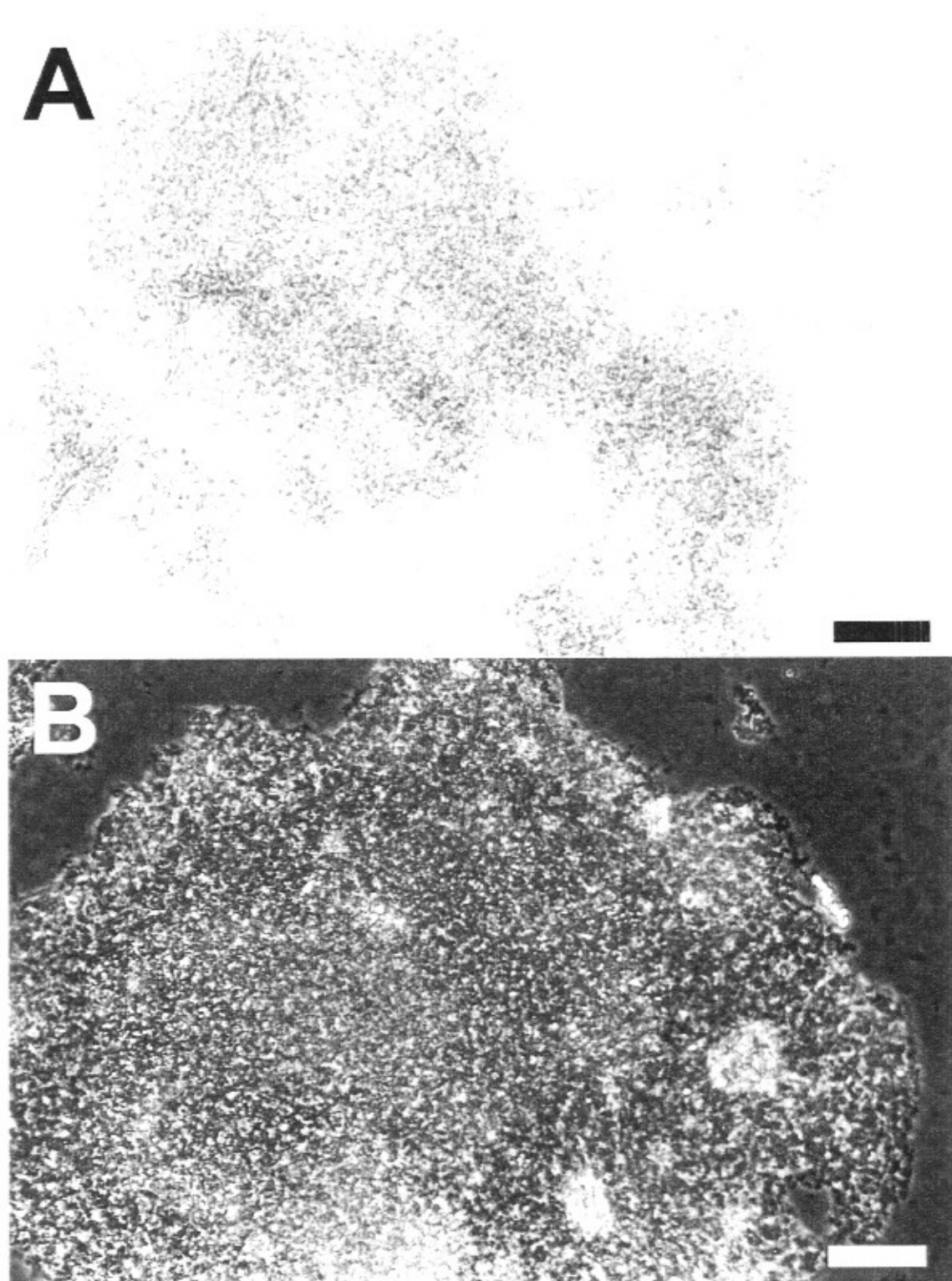
VCS

DNA

VCS

NCS

FIG.3

48

FIG.4

A

B

C

FIG.5

High Aluminium

Attraction   Repulsion

Low Aluminium

Al2+

Al+

FIG.6

51

A role for the cell wall in Al³⁺ resistance and toxicity: crystallinity and availability of negative charges*

Pedro Henrique P. A. Schildknecht [1] #, Benedicto de Campos Vidal [1]

[1]Departamento de Biologia Celular, Instituto de Biologia, Universidade Estadual de Campinas (UNICAMP), 13084899 Campinas, SP, Brazil
#Corresponding author. Tel.: 0055 19 37886124; Fax: 0055 19 37886111; E-mail: pedroh@operamail.com; Address: Departamento de Biologia Celular, Instituto de Biologia, UNICAMP. Caixa Postal 6109. 13084-899 Campinas, SP, BRAZIL.

Abstract

Aluminium (Al) is a toxic ion, which is tolerated by some plants but not by others. In this work, we examined the influence of Al on the structure of root cell walls from Al-resistant and Al-sensitive maize cultivars and on the synthesis and assembly of cellulose by *Acetobacter xylinum*.

Al accumulation and callose synthesis were greater in Al-sensitive plants, as shown by staining with hematoxylin and aniline blue, respectively. Several cracks in the root surface were seen, as well as increased salt accumulation in the roots of Al-sensitive maize cultivars. Walls from Al-resistant control maize had a lower density of negative charges than Al-sensitive plants, and thus less Al binding. However, this difference disappeared after treatment with Al. Quantitative interferometry revealed a higher dry mass content in the walls of Al-resistant maize. Birefringence analysis showed that Al increased the wall crystallinity in sensitive plants as a result of Al crosslinking of pectins, while no alterations were detected in resistant plants. Cellulose synthesis was not inhibited by Al, but the texture of the bacterial cellulose matrix was altered. Atomic Force Microscopy images reveled a greater angular rotation between adjacent fibrils from Al-treated cultures (> 40°) compared to the non-treated controls (< 40°).

Our results support the hypothesis that the availability of wall negative charges, which allow Al binding, are involved in Al resistance. Cell walls are structurally modified by Al, which can alter their plasticity and mechanical strength and may inhibit cell growth and survival.

1. Introduction

The mechanisms by which aluminium (Al) damages cells and how plants can tolerate this metal have been widely studied, but the details of this process still not clear. Most Al in soil occurs as harmless oxides or silicates. However, in acid soils with pH < 5.0, Al is solubilized into the toxic species $Al(H_2O)_6^{3+}$, represented as Al^{3+} [1, 2]. The inhibition of root growth is the major characteristic of Al toxicity, and injuries to the root surface are common, probably as a result of Al accumulation in cell walls [3, 4, 5, 6]. The mechanisms by which plants tolerate Al are still under discussion [5]. Organic acid anions exudation is widely described as a resistance mechanism [7, 8]. However, most of the genes related to Al^{3+} resistance are not involved in the synthesis and exudation of organic acids anions [5]. Parker and Pedler [9] reported that the efflux of organic acids anions plays a minor role in the differential resistance to Al^{3+} and also indicated the need for a multifaceted, more integrative model of resistance. The primary target of Al toxicity remains unknown, but cell wall is apparently the first plant structure to be damaged by Al and may have a role in multiple Al resistance mechanisms [3, 10, 11, 12, 13].

The preference of Al^{3+} for electrostatic rather than covalent binding is predicted thermodynamically because of its high charge-to-radius ratio [14]. Al^{3+} thus forms stable complexes with ligands containing negatively charged organic functional groups [14] which, in the cell walls, are represented by the highly accessible carboxyl residues of pectins [15]. The net negative charge of pectin arises after the removal of methyl residues from uronic acids by pectin methylesterase [16], the enzymatic activity of which is reported to modulate Al resistance in potato plants [12]. NaCl-adapted maize cells with a higher pectin content accumulated more Al, were more Al-sensitive and showed increased callose synthesis than control plants [11]. These results suggested a special role for the pectin matrix in the modulation of Al toxicity. The interaction of Al^{3+} with anionic groups of the apoplast may alter the dynamic characteristics of the cell walls, including plasticity and porosity, thus inhibiting enzymatic activities indispensable to cell elongation and survival [17]. Al also induces rapid disorganization of the cytoskeleton in the distal part of the transition zone (DTZ) in maize roots [18]. Since cellulose orientation is determined by the movement of cellulose synthases, which are driven by the cytoskeleton [19],

disorganization of the cellulose matrix in the cell wall would be expected in Al-sensitive plants. This effect would increase the wall fragility and could contribute to the root cracks observed by several authors [3, 6]. In addition, the importance of the association between the cell wall, plasma membrane and cytoskeleton has been mentioned [11, 20, 21] and may help to elucidate the mechanisms of Al stress signaling from the apoplast to the symplast.

The root cation exchange capacity, which is determined by the availability of ionic groups in the apoplast, is correlated with Al deposition in the cell wall and may play a role in multiple Al-resistance mechanisms [22, 23, 24]. However, there is no consensus as to whether the free anionic residues in the cell wall are involved in Al resistance and toxicity, mainly because of a lack of a precise methods for quantifying ionic groups in cell walls [1, 5]. In this work, we show that the availability of negatively charged residues in the cell wall is not similar for maize cultivars differing in resistance to Al. We also confirm the hypothesis that Al may interfere with the orientation of the cellulose matrix, based on a comparison of the crystallinity and molecular packing of cell walls from both maize cultivars and from cellulose sheets produced by the bacterium *Acetobacter xylinum*.

2. Materials and Methods

Plant material

Seeds from Al³⁺-resistant (Ag 5011) and Al³⁺-sensitive (Ag 6601) maize (*Zea mays* L.) cultivars were generously supplied by Dr. M. Guimarães (AGROCERES S.A., Brazil) and are referred to in the text as resistant and sensitive maize cultivars, respectively. The seeds were germinated for 62 h at 30°C in the dark in a roll of filter paper wetted with sterile deionized water. After germination, the seedlings were transferred to plastic screens floating on nutrient solution (in μM: Ca(NO$_3$)$_2$, 500; KNO$_3$, 500; KH$_2$PO$_4$, 2; NH$_4$NO$_3$, 250; MgSO$_4$, 200; Fe(NO$_3$)$_3$, 2; MnCl$_2$, 2; H$_3$BO$_3$, 11; ZnSO$_4$, 0.35; CuSO$_4$, 0.2; (NH$_4$)$_6$Mo$_7$O$_{24}$, 0.03), pH 4.5. Some of the plantules were treated with 40 μM AlCl$_3$ (Sigma, USA) for 48 h, while others were maintained in the nutrient solution as controls. The solutions were aerated continuously and replaced every 24 h to minimize microbial contamination.

The relative root growth (RRG) of plants was calculated by using the equation

$$RRG = (T_{Al} - T_{initial}) / (C_{control} - C_{initial})$$

where T and C refers to the measured root lengths of Al-treated and control plants, respectively.

Specimen manipulation

After treatment, the apices were sectioned 5 mm from the root tip, fixed for 48 h in 3.7% buffered paraformaldeyde pH 7.4 and dehydrated in butanol under vacuum. The specimens were infiltrated with Paraplast plus wax (Oxford, USA) and 7 μm sections were cut on a microtome (Micron, Germany).

Histochemistry

Aluminium was detected by immersing the roots in a solution containing 0.1% (w/v) hematoxylin and 0.01% (w/v) KIO$_3$, prepared at least 1 h before use [25]. The roots were stained for 20 min and extensively washed in distilled water to remove non-specific staining. Callose was visualized by staining root sections in 0.1% (w/v) aniline blue in 1 M glycine/NaOH buffer (pH 9.5) and observed directly with a fluorescence microscope as described [6].

Measurement of cell-wall negativity

Thick (7μm) sections were stained with 0.025% methylene blue (MB) for 20 min in McIlvaine buffer (0.05 M citrate, 0.1 M sodium phosphate), pH 4.5. MB was chosen because it is a non-metachromatic thiazinic stain with a high affinity for anionic substrates, and shows a high correlation between its molar concentration and its absorbance [26]. Thus, the absorbances of MB stained cell walls were strictly related to the extent of MB binding to anionic radicals and reflected the availability of negative charges in the cell wall. All preparations were washed in distilled water, air dried, cleared in xylene and mounted in Canada balsam (n$_D$=1.54). The average absorbance (OD), which is defined as total absorbance/measured area, was obtained from stained cell walls using a Zeiss automatic scanning microspectrophotometer with a 0.5 μm x 0.5 μm scanning spot and λ = 610 nm, under conditions previously described by Vidal *et al* [27]. The percentage of cell wall surface with an absorbance > 0.6 OD units was also measured and expressed as the S% parameter. Absorbances < 0.02 were considered to be background.

Microincineration.

Microincineration was done as described by Steven [28]. Briefly, non-fixed root tips were placed on a glass slide and immediately put in a high-temperature electronic furnace (EDG Equipments, Brazil). The temperature was gradually increased in 15 min intervals to 100°C followed by incubation at 100°C for 15 min, 350°C for 15 min and 650°C for 60 min. This process left only inorganic constituents of the root tips. The material was subsequently cooled to room temperature, mounted in mineral oil and analyzed under crossed polars.

Dry mass and birefringence quantification.

Dry mass was assessed by measuring the intensity of the interferometric brightness in 7 μm thick sections of roots not treated with Al. The quantitative analysis was done using a Zeiss interferometric microscope equipped with a Zeiss interferometric frontal lens at λ = 546 nm. The images were captured by a CCD camera and analyzed with appropriate software (Global Lab Acquire Software^{TM}, Marlboro, MA, USA). The interferometric brightness is a consequence of the optical path differences (OPD) in the sample, and is positively correlated with the dry mass in samples the of same thickness [29]. The brightness was measured by

converting the images into pixels displaying distinct gray levels, from 0 (black) to 255 (white), which allowed indirect comparison of the dry mass of the maize cultivars.

The birefringence of cell walls from the outer layer of root cells was measured in 7 μm thick sections hydrated for at least 1 h in distilled water. The observations were done using a light polarizing Zeiss microscope with the cell walls set at 45° angle to the axis formed by the crossed polars; the λ was 546 nm. The birefringence was determined by measuring the optical retards using a Brace-Köhler compensator (1/10 λ). The outer layer of cells was chosen for birefringence measurements because it represents the boundary between the roots and the external environment and should therefore be the primary site of interaction with Al^{3+}.

Bacterial culture

Colonies of *Acetobacter xylinum* strain ATCC 23769 were purchased from the Fundação André Tosello (Campinas, Brazil) and grown in liquid culture medium: 2% glucose (Sigma, USA), 2% yeast extract (Biobrás, Brazil), 0.5% peptone (Biobrás, Brazil), and 0.1 % KH_2PO_4 (Sigma, USA), pH 4.7. In some cultures, $AlCl_3$ was added to a find concentration of 100 μM without shaking at 25 °C. *A. xylinum* produces cellulose pellicles in static culture [30], and was harvested after 48 h in our experiments. The pellicles were washed in distilled water and then in 4M HCl for 12 h to remove cell debris followed by washing in ultrapure water for several times to remove the acid. The samples were then air-dried on a steel support appropriate for atomic force microscopy.

Atomic force microscopy

A model TMX 2010 Topometrix instrument (Sunnyvale, CA, USA) was used to image the cellulose sheets obtained from *A. xylinum*. The images were acquired in non-contact mode and the scan rates were typically 10-20 Hz, with the scan angle being varied to obtain optimum contrast. The angles between adjacent cellulose fibers were measured with Scion Image software (Scion Corp., Frederick, MD, USA), available free at http://www.scioncorp.com. Each 3μm x 3μm image was sectioned in 8 sectors of 1.5 μm x 0.75 μm and 50 angular measurements were done per sector to verify the main orientation of the fibers. The angles were determined by marking two points at the body of two adjacent fibers and a third point at the junction of these fibers, then these points were connected by straight lines and the angles between adjacent fibers were determined by the image analysis software.

Statistical analysis.

Each experiment was repeated twice and fifty measurements were obtained from several specimens at each repetition. All data were analyzed by ANOVA, using the Minitab statistical software package (Minitab Inc., State College, USA). The level of significance was set at $p < 0.05$.
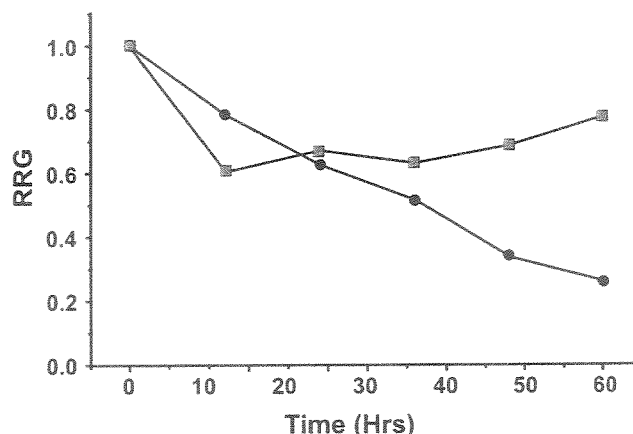
Figure 1. Root elongation responses of Al-sensitive (black circles) and Al-resistant (black squares) cultivars to 40μl of $AlCl_3$ during a 60 h experiment.

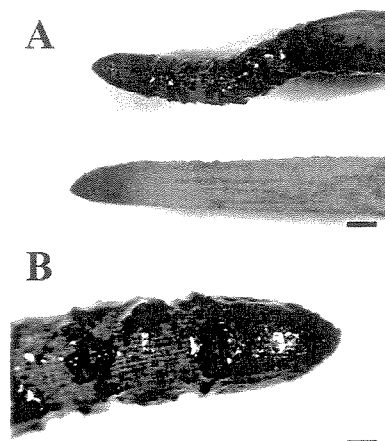**Figure 2.** Detection of Al by hematoxylin staining in maize roots treated with 40μM $AlCl_3$ for 48h. A) Comparison between sensitive (top) and resistant (bottom) maize roots after treatment with Al. Bar = 550 μm. B) Detail of a stained sensitive maize root treated with Al. The cracks on the root surface are deeply stained with hematoxylin. Bar = 400 μm.

3. Results

General aspects of Al-induced damages in maize roots

Root growth was severely inhibited in the sensitive cultivar after 48 h of exposure to $AlCl_3$ [Figure 1] and the roots were heavily stained with hematoxylin (indicative of Al accumulation), in contrast to resistant roots [Figure 2A].

Cracks in the root surface were observed in the sensitive cultivar after a 10 h exposure to 40 μM $AlCl_3$, while no damage was observed in resistant plants. The greatest Al accumulation was observed at the crack periphery, compared to the adjacent layers of intact cells, which stained with a lower intensity [Figure 2B]. Histological sections stained with aniline blue detected callose mostly in the sensitive cultivar, where the deposition of this compound occurred preferentially in walls from meristematic cells and from the root surface [Figure 3]. Resistant roots showed callose only at their surface, with no deposits in meristematic cells.

54
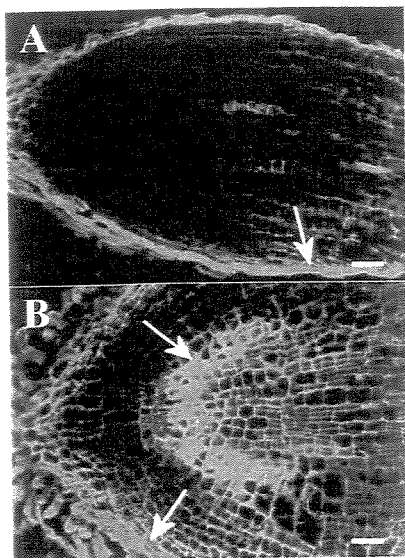
Figure 3. Callose detection by aniline blue staining of histological sections of maize roots treated with 40µM AlCl₃ for 48h. A) Resistant maize root. Callose deposition is indicated by arrow. B) Sensitive maize root. Arrows indicate callose deposition in the meristematic region and at root surface. Bar = 100 µm.
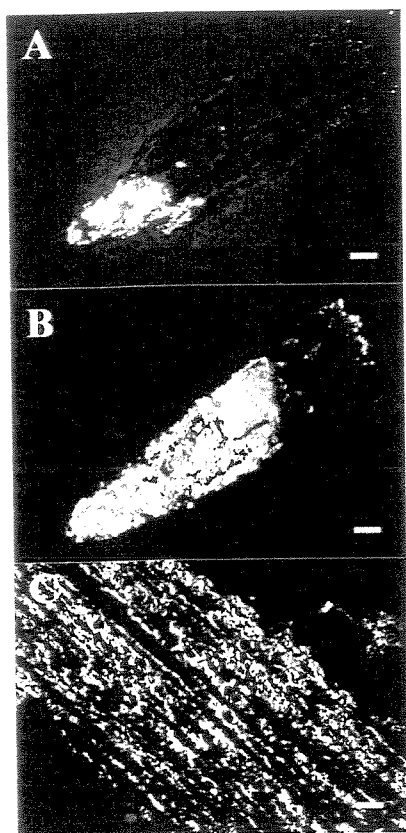
Figure 4. Birefringent images of spodograms from Al-treated maize roots (40µM AlCl₃ for 48h) observed between crossed polars. The long axis of the roots was orientated at 45° to the polarizers. Resistant maize (A) showed a lower accumulation of crystals than sensitive maize (B). Bar = 200 µm. C) Detail of the DTZ in sensitive maize showing the ghost image of cell walls. Bar = 100 µm.

The observation of root spodograms seen under polarized light microscopy revealed that organic material was totally charred after incineration, with only inorganic material remaining. In both maize cultivars, salt crystals were seen as a negative image of the biological structures of the cells, being more abundant in the root tip [Figure 4]. Plants from the resistant cultivar showed no change in the root area covered by crystal deposits after exposure to AlCl₃, with the greatest accumulation in the first 0.5 mm from the tip in the a region of the root cap. In contrast, Al-treated sensitive plants showed enhanced crystal accumulation covering the first 1-2 mm from the root tip, which included the distal transition zone (DTZ) [Figure 4]. These results were consistent among the several slides examined under polarized light.

Measurements of the availability of anionic groups in the apoplast and the interference of Al in the supraorganization of cell wall and cellulose matrix

MB stained cell walls from control roots showed higher absorbances (OD) for the sensitive than for the resistant

Table 1. Optical density of MB stained cell walls from control and Al-treated plants. The average absorbance values of the cell walls are shown for control and Al-treated (Al) roots from sensitive and resistant cultivars. The Al-treated plants were grown in the presence of 40µM AlCl₃ for 48h. The results are given as the mean and standard deviation (SD) for two replicates of $n = 100$ each. The significance of the difference between groups was compared by with ANOVA.

	Control			Al-treated		
	Mean	SD	p	Mean	SD	p
Sensitive	1.066	0.638	0.011	0.950	0.402	0.172
Resistant	0.805	0.319		0.851	0.311	

Table 2. Area (in %) of MB stained cell walls with an OD > 0.6. The percentage of cell wall areas with high absorbance values after MB staining are shown for control and Al-treated (40µM AlCl₃ for 48h) roots from sensitive and resistant cultivars. The results are given as the mean and standard deviation (SD) for two replicates of $n = 100$ each. The significance of the difference between groups was compared by with ANOVA.

	Control			Al-treated		
	Mean	SD	p	Mean	SD	p
Sensitive	11.670	2.031	0.006	05.199	1.191	0.230
Resistant	03.260	0.551		02.894	0.700	

Table 3. Interferometry measurements of cell walls. Grey level values for the interferometric brightness of histological sections from control roots of sensitive and resistant cultivars. The measures were made with an image analysis software (see *materials and methods* for details) and correspond to the dry mass content of cell walls. The results are given as the mean and standard deviation (SD) for two replicates of $n = 50$ each. The significance of the difference between groups was compared with ANOVA.

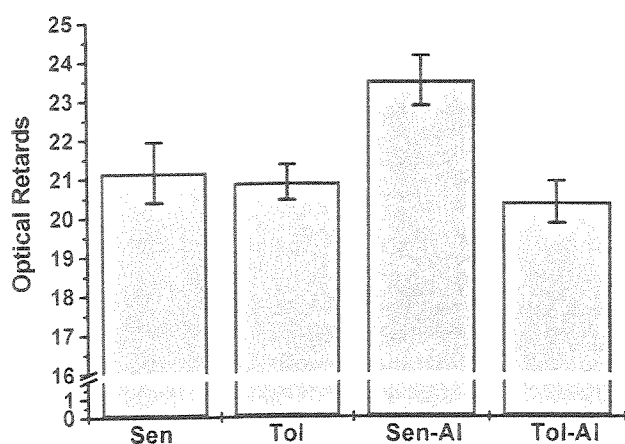|	Mean	SD	p
Sensitive	23.790	1.580	0.000
Resistant	45.440	3.800	

55

cultivar, mainly as a consequence of a higher density of free anionic groups that binds MB [Table 1]. There was no difference in the OD values of both maize cultivars after Al treatment [Table 1]. The percentage of wall area with absorbance values over 0.6 OD units was higher in sensitive than in resistant plants with no exposure to $AlCl_3$; this difference disappeared after treatment [Table 2].

The gray level values corresponding to the interferometric brightness were higher in cell walls from resistant plants compared to sensitive ones, thus indicating a higher dry mass content in walls from resistant plants [Table 3]. The correlation between grey level values, interferometric brightness and dry mass are explained in "Material and Methods".
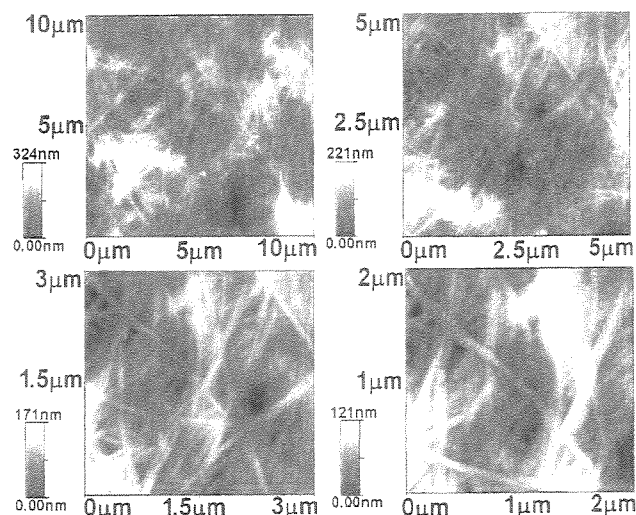
The birefringence was similar in both maize cultivars grown in Al-free nutrient solution. A shift in the birefringence values was seen in cell walls from sensitive plants after treatment with $AlCl_3$, whereas no changes were observed in resistant maize [Figure 5].

Al interference in cellulose assembly

Cellulose pellicles harvested from Al-treated *A. xylinum* cultures were visually similar to those collected from control cultures, but were less resistant to tension forces and were more easily torn by hand than control pellicles. The AFM images showed that the structure of the control pellicles structure involved a more parallel orientation between fibers than the structure of Al-treated cultures [Figure 6, 7, 8]. Measurement of the angles generated by adjacent fibers revealed that the fibrous array in Al-treated pellicles consisted mostly of fibers with an angular rotation >40° relative to each other while control pellicles were structured mostly with fibers rotating less than 40° relative to their neighbours [Figure 8].

Figure 6. AFM images of bacterial cellulose pellicles obtained from control cultures.
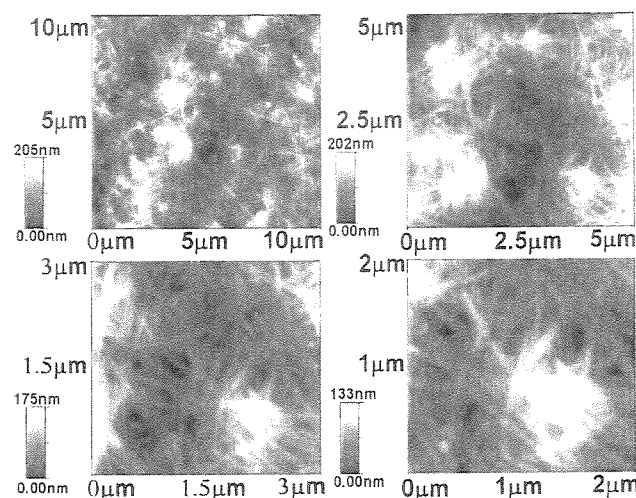
Figure 7. AFM images of bacterial cellulose pellicles obtained from Al treated cultures (100 μM $AlCl_3$ for 48h).

Figure 5. Histogram of the mean optical retard values (± S. E.), measured with a Brace-Köhler compensator, of the cell walls of sensitive and resistant cultivars grown in the absence or presence of Al (40μM $AlCl_3$ for 48h). Note the shift in the wall birefringence of sensitive maize when treated with Al. p = 0.000 compared to the corresponding control (without Al) (ANOVA). The experiment was repeated twice, $n = 100$.

Figure 8. Gaussian distribution of the angular rotation values between adjacent cellulose fibrils assembled in Al treated (100μM $AlCl_3$) cultures and control (without Al) cultures. $p = 0.004$ compared to the control (ANOVA). $n = 200$ for each group.

4. Discussion

The specificity of hematoxylin for apoplastic Al detection is well established [6, 25]. Al³⁺ is proposed to act as a mordant to cause the precipitation of hematein (oxidized hematoxylin) in colored complexes [6], although the histochemical basis of the reaction is still unclear. Hematoxylin does not bind to an Al-citrate complex or to the cation alone, but a purple precipitate readily appears if the stain is added to an Al-pectin or Al-phosphate solution [25]. Thus, the failure of resistant plants to stain heavily with hematoxylin after Al-treatment indicated that a mechanism of resistance was present (or was induced) in resistant but not in sensitive plants, thereby reducing Al binding to the apoplast. The staining of roots in sensitive plants revealed Al deposits not seen in resistant plants after exposure to AlCl₃, as well as a high level of Al accumulation at the periphery of surface cracks. This observation suggested the interactions of Al with the cell wall contributed to the origin of these lesions in maize roots. We observed cracks in the root surface after only 10 h of exposure to Al. Yamamoto *et al* [6] reported similar lesions in peas after 8 h of treatment, while Ikegawa *et al* [31] showed that an Al-induced loss of membrane integrity in tobacco liquid cell cultures occurred only after 24 h of treatment with Al. These findings indicate that the death of root surface cells is a consequence of the cracks and not the contrary, thus showing the importance of the plant extracellular matrix in resistance to Al.

The synthesis of callose is a strong indicator of Al toxicity [32]. Callose makes tissue impermeable to water [33] and blocks the plasmodemata, thereby inhibiting cell-to-cell trafficking [34]. Callose may also might prevent wall-loosening and hence cell wall elongation [5]. The accumulation of callose in the outer cells of both Al-treated maize cultivars indicated that resistant maize also suffered from Al toxicity. However, the stimulus for callose synthesis did not reach the meristem and thus root growth was maintained. The deposition of callose in the meristematic region of sensitive plants could interfere with cell division to reduce root elongation [5]. Al is known to stimulate callose synthesis [32], possibly as a response to cell wall wounding, which has been shown to initiate callose production [35]. Since Al repress the template activity of chromatin [36], the signalling for callose synthesis should occur before Al reaches the nucleus, and indicates that the interaction of Al with the cell wall-plasma membrane-cytoskeleton continuum is an important step [3, 11].

The high accumulation of crystals in root spodograms from Al-treated sensitive plants contrasts with that of resistant plants, and suggests an imbalance of salt exchange between the root and the environment. The disruption of the cell wall structure (cracks) and further loss of membrane integrity could alter the control of salt uptake in root cells, however it is a merely speculative hypothesis. Since no attempt was made to identify Al compounds among the crystals in root spodograms, the salt deposits may not be attributed solely to Al deposits, thus we cannot state that these crystals reflect Al accumulation. These crystals originated from salts that were present inside plant roots and then could be composed of any compound, including Al. We believe that these crystals are composed mainly of Al salts, but further work still necessary to identify the nature of the crystals. The observation that the crystal deposits in Al-treated sensitive roots were located in an area comprising the meristematic region and the DTZ, both of which are reported to be the most Al-sensitive regions in roots [5, 11, 37], supports the hypothesis that the enhanced salt content in sensitive plants is a consequence of Al toxicity.

Availability of negative charges, dry mass content and anisotropy measurements in the cell wall.

Cell walls from sensitive control plants had higher OD values than resistant plants after MB staining, as well as larger areas with high absorbance values [Table 1, 2]. This finding reflects the higher availability of negative charges, thus higher binding of Al, in the cell walls of sensitive compared to resistant plants. The Al bound to cell walls may increase the wall rigidity and reduce the efficiency of enzymes involved in "wall loosening" events, as discussed later. Treatment with Al reduced the size of the area with high absorbances, probably because of the blockade of some MB binding sites. This hypothesis is supported by similar results obtained with root sections that were immersed in an Al solution prior to staining with MB (data not shown). Although these results could reflect a modification of carbohydrate present in the cell walls of sensitive plants in response to Al, this seems improbable since Al inhibits gene activity and binds to ATP molecules, thereby reducing energy metabolism in sensitive plants [36, 38]. The affinity of cell walls for Al cannot be excluded as a mechanism of resistance against this metal. Variations in the density of anionic groups in cell walls reportedly influence the resistance to Al in potatoes, by regulating pectin methyl esterase activity [12]. Our results support the hypothesis that lower binding of Al to cell walls reduces the effects of Al on the pectin matrix and maintains all metabolic processes that occur at the wall, thereby improving the resistance to Al.

The interferometric measurements showed that walls in resistant plants had a larger mass than those of sensitive plants [Table 3]. Thicker walls provide an enhanced filter against the external environment and, together with high methylesterified pectin, reduce the interaction with Al; this may represent another mechanism of Al resistance. Vázquez *et al* [23] reported cell wall thickening in resistant maize roots after treatment with Al, which supports the idea that thicker walls may enhance resistance to Al.

The wall birefringence was similar in both cultivars prior to exposure to Al [Figure 5]; a paradoxical finding when on considers the distinct dry mass contents of the cultivars. However, birefringence measurements cannot detect alterations in isotropic material, whereas interferometry

allows quantification of both isotropic and anisotropic compounds. Hence, two cell walls with a similar amount of an anisotropic compound but distinct levels of isotropic material will have equal birefringence values. Isotropic components, such as pectins and hemicelluloses [39], occur in larger amounts in the apoplast of resistant plants. Although pectins are originally isotropic, with no birefringence, they can become anisotropic after treatment with Al *in vitro* [40]. The birefringence reflects the anisotropy level of the objects, being stronger in highly ordered molecular (crystalline) arrangements [41]. Al reduces the pectin gel volume and water retention capability, and causes gel stiffening with a loss of viscoelasticity [42, 43]. Thus, the increase in wall birefringence in Al-treated sensitive plants was a result of pectin crosslinking by Al and reflected the alterations introduced by Al in the supraorganization of the plant extracellular matrix.

The effects of Al on the pectin matrix result in a more crystalline and less plastic wall that is more susceptible to physical breaks. The increase in the cristallinity of the cell wall also restricts the access of glucanases responsible for cell wall elongation. The lower interaction of Al with the pectin matrix of resistant plant roots (as seen in MB stained roots) results in an unaltered birefringence for walls from Al-treated resistant plants. Although other resistance mechanisms, such as organic acid anions exudation, may have contributed to protect the wall against Al damage and to maintain the molecular configuration and functionality of the cell walls in resistant plants, our results do support a role for the cell wall Al resistance mechanisms.

Al-induced organic acid anions exudation and an alteration in the density of anionic groups can be classified as active (requiring gene activation) or passive (constitutive) resistance mechanisms, respectively. Passive mechanisms of resistance should reduce Al damage in plant cells and may help to trigger gene-activated Al resistance pathways. How Al signals to the nucleus is not yet known, but the evidence for a cell wall-plasma membrane-cytoskeleton continuum [10, 20] and the report of Al-induced cytoskeletal alterations [34] support a role for the plant extracellular matrix in this signaling pathway.

Al interference in cellulose assembly

The observation that control pellicles exhibited mostly low angular values (< 40°) between adjacent fibrils does not mean that the fibrils have a principal orientation axis, but rather that they have a low rotation angle relative to each other [Figure 8]. Thus, both control and Al-assembled pellicles have fibrils oriented in all directions, as seen in [Figure 6, 7]. However, low rotation angles allow several fibrils to run in similar (but not parallel) directions, thereby enhancing electrostatic interactions between fibrils and increasing their mechanical strength (this is not possible with high rotation angles). Fibrils that interact with each other may cluster together in response to a tensile stimulus,

making control pellicles more resistant to hand-tearing than Al-assembled pellicles.

In plant cells, the spatial deposition of cellulose microfibrils in the wall determines many of the mechanical properties of the wall, which in turn govern cell growth [44]. The bacterium *A. xylinum* has been used as a model to understand cellulose synthesis and crystallization in plant cells since, although the genes involved are not the same, both plants and bacteria share similar pathways of cellulose metabolism [45] and may be similarly affected by Al. While the mechanism by which Al interferes with the texture of cellulose pellicles is not known, the functionality of cellulose synthase rosettes is apparently not affected. As demonstrated by Arioli *et al* [46], the correct operation of cellulose synthase is essential for producing a crystalline polymer that is acid-resistant, as in the pellicles obtained here. Both control and Al-assembled cellulose showed high levels of birefringence (data not shown). The modifications in cellulose texture may result from connection of cellulose synthases to the cytoskeleton [19], which is known to be altered by Al [34].

Our results support the hypothesis that cracks on the root surface may have originated from an uncoordinated cell elongation ratio, in which the external cell growth was inhibited while the expansion of inner cells was normal [6]. Al altered the entire molecular arrangement of the apoplast by crosslinking the pectin and enhancing its cristallinity, and possibly by interfering with the texture of the wall cellulose matrix. Together, these events reduce the mechanical strength and growth of cells in contact with Al, particularly the surface cells. Since these cells are unable to resist to the internal pressure generated by cell growth and are also unable to elongate, they break and subsequently die, giving rise to the root surface cracks.

5. Conclusions

The cell walls of the sensitive maize cultivar had a greater content of anionic groups available for Al binding than the resistant maize cultivar. This resulted in increased Al deposition in the apoplast of the sensitive cultivar and greater callose synthesis, as seen by hematoxylin and aniline blue staining. The Al bound to the cell wall increased salt uptake and enhanced pectin crystallinity only in the sensitive cultivar, and also altered the texture of bacterial cellulose. These events would inhibit wall elongation by enzymes and increase wall fragility. The low availability of negative charges in the walls of resistant plants reduced Al binding and provided passive resistance to Al, thus supporting a role for the cell wall in resistance mechanisms to Al.

References

1. Kochian LV: Cellular mechanisms of aluminum toxicity and resistance in plants. Ann Rev Plant Physiol Plant Mol Biol 46:237-260, 1995.

2. Harris WR, Berthon G, Day JP, Exley C, Flaten TP, Forbes WF, et al: Speciation of aluminum in biological systems. J Toxicol Environ Health 48:543-568, 1996.

3. Horst WJ: The role of the apoplast in aluminium toxicity and resistance of higher plants: a review. Z Pflanz Bodenkunde 158:419-428, 1995.

4. Budikova S: Structural changes and aluminium distribution in maize root tissues. Biol Plantarum 42:259-266, 1999.

5. Matsumoto H: Cell biology of aluminium toxicity and tolerance in higher plants. Int Rev Cytol 200:1-46, 2000.

6. Yamamoto Y, Kobayashi Y, Matsumoto H: Lipid peroxidation is an early symptom triggered by aluminum, but not the primary cause of elongation inhibition in Pea roots. Plant Physiol 125:199-208, 2001.

7. de la Fuente JM, Ramirez-Rodriguez V, Cabrera-Ponce JL, Herrera-Estrella L: Aluminum tolerance in transgenic plants by alteration of citrate synthesis. Science 276:1566-1568, 1997.

8. Jorge RA, Arruda P: Aluminum-induced organic acids exudation by roots of an aluminum-tolerant tropical maize. Phytochemistry 45:675-681, 1997.

9. Parker DR, Pedler JF: Probing the "malate hypothesis" of differential aluminum tolerance in wheat by using other rhizotoxic ions as proxies for Al. Planta 205:389-396, 1998.

10. Horst WJ, Wagner A, Marschner H: Mucilage protects root meristems from aluminium injury. Z Pflanz Bodenkunde 105:435-444, 1982.

11. Horst WJ, Schmohl N, Kollmeier M, Baluska F, Sivaguru M: Does aluminium affect root growth of maize through interaction with the cell wall - plasma membrane - cytoskeleton continuum? Plant Soil 215:163-174, 1999.

12. Schmohl N, Pilling J, Horst WJ: Pectin methylesterase modulates aluminium sensitivity in Zea mays and Solanum tuberosum. Physiol Plantarum 109:419-427, 2000.

13. Hawes MC, Gunawardena U, Miyasaka S, Zhao X: The role of root border cells in plant defense. Trends Plant Sci 5:128-133, 2000.

14. Berthon G: Chemical speciation studies in relation to aluminium metabolism and toxicity. Coord Chem Rev 149:241-280, 1996.

15. Ostatek-Boczynski Z, Kerven GL, Blamey FPC: Aluminium reactions with polygalacturonate and related organic ligands. Plant Soil 171:41-45, 1995.

16. Micheli F: Pectin methylesterases: cell wall enzymes with important roles in plant physiology. Trends Plant Sci. 6:414-419, 2001.

17. Inouhe M, Inada G, Thomas B, Nevins D: Cell wall autolytic activities and distribution of cell wall glucanases in Zea mays L. seedlings. Int J Biol Macromol 27:151-156, 2000.

18. Sivaguru M, Baluska F, Volkmann D, Felle HH, Horst WJ: Impacts of aluminum on the cytoskeleton of the maize root apex. short- term effects on the distal part of the transition zone. Plant Physiol 119:1073-1082, 1999.

19. Chaffey N: Microfibril orientation in wood cells new angles on an old topic. Trends Plant Sci 5:360-362, 2000.

20. Wyatt SE, Carpita NC: The plant cytoskeleton-cell-wall continuum. Trends Cell Biol 3:413-417, 1993.

21. Kohorn BD: Plasma membrane-cell wall contacts. Plant Physiol 124:31-38, 2000.

22. Godbold DL, Jentschke G: Aluminium accumulation in root cell walls with inhibition of root growth but not with inhibition of magnesium uptake in Norway spruce. Physiol Plantarum 102:553-560, 1995.

23. Vázquez MD, Poschenrieder C, Corrales I, Barceló J: Change in apoplastic aluminium during the initial growth response to aluminium by roots of a tolerant maize variety. Plant Physiol 119:435-444, 1999.

24. Rout GR, Samantaray S, Das P: Aluminium toxicity in plants: a review. Agronomie 21:3-21, 2001.

25. Ownby JD: Mechanisms of reaction of hematoxylin with aluminium-treated wheat roots. Physiol Plantarum 87:371-380, 1993.

26. Lillie RD: HJ Conn's Biological Stains: A Handbook on the Nature and Uses of the Dyes Employed in the Biological Laboratory. The Williams & Wilkins Company. 1977.

27. Taicheng A, Jinzhang G, Hui C, Xihai Z: Heterogeneous photocatalytic degradation of methylene blue aqueous solution under the coexistence of metalloporphyrin polymer and air. Chem J Internet 1:14-15, 2001.

28. Vidal BC, Silva WJ, Strikis PC: Nuclear phenotypes and DNA content of root cells of Zea mays mays, Zea diploperennis and of a mazoid hybrid. Cell Mol Biol 30:11-22, 1984.

29. Steven ER: Plant microtechnique and microscopy. Oxford University Press.1999.

30. Vidal BC: Variation in dry mass concentrations and protein contents in DNA puffs. Caryologia 30:69-76, 1977.

31. Ross P, Mayer R, Benziman M: Cellulose Biosynthesis and function in bacteria. Microbiol Rev 55:35-58, 1991.

32. Ikegawa H, Yamamoto Y, Matsumoto H: Responses to aluminum of suspension-cultured tobacco cells in a simple calcium solution. Soil Sci Plant Nutri 46:503-514, 2000.

33. Zhang G, Hoddinott J, Taylor GJ: Characterization of 1,3-D-Glucan (callose) synthesis in roots of *Triticum aestivum* in response to aluminum toxicity. J Plant Physiol 144:229-234, 1994.

34. Yim K, Bradford KJ: Callose deposition is responsible for apoplastic semipermeability of the endosperm envelope of muskmelon seeds. Plant Physiol 118:83-90, 1998.

35. Sivaguru M, Fujiwara T, Samaj J, Baluska F, Yang Z, Osawa H, et al: Aluminum-induced 1→3-beta-D-glucan inhibits cell-to-cell trafficking of molecules through plasmodesmata. A new mechanism of aluminum toxicity in plants. Plant Physiol 124:991-1006, 2000.

36. Brett C, Waldron K: Physiology and biochemistry of plant cell walls. Chapman & Hall.1996.

37. Matsumoto H, Morimura S: Repressed template activity of chromatin of pea roots treated by aluminium. Plant Cell Physiol 21:951-959, 1980.

38. Sivaguru M, Horst WJ: The distal part of transition zone is the most aluminium-sensitive apical root zone of maize. Plant Physiol 116:155-163, 1998.

39. Lorenc-Plucinska G, Ziegler H: Changes in ATP levels in Scots pine needles during aluminium stress. Photosynthetica 32:141-144, 1996.

40. Krishnamurty KV: Methods in cell wall cytochemistry. CRC Press, 1999.

41. Schildknecht PHPA, Vidal BC: Al³⁺ induces alterations on DNA and pectin molecular order. Annals XXX Meeting Brazilian Society of Biochemistry and Molecular Biology. E-69, 2001.

42. Hartshorne NH: The microscopy of liquid crystals. Microscope Press, 1974.

43. Blamey FPC, Asher CJ, Kerven GL, Edwards DG: Factors affecting aluminum sorption by calcium pectate. Plant Soil 149:87-94, 1993.

44. Blamey FPC, Dowling AJ: Antagonism between aluminium and calcium for sorption by calcium pectate. Plant Soil 171:137-140, 1995.

45. Emons AM, Mulder BM: How the deposition of cellulose microfibrils builds cell wall architecture. Trends Plant Sci 5:35-40, 2000.

46. Carpita NC, Vergara C: A recipe for cellulose. Science 279:672-673, 1998.

47. Arioli T, Peng L, Betzner AS, Burn J, Wittke W, Herth W et al: Molecular analysis of cellulose biosynthesis in Arabidopsis. Science 279:717-720, 1998.

Aluminium triggers apoptotic-like death in an Al-sensitive but not in an Al-tolerant maize cultivar

Pedro Henrique P.A. Schildknecht[*], Benedicto de Campos Vidal

Departamento. Biologia Celular, Instituto de Biologia, Universidade Estadual de Campinas (UNICAMP), Campinas, SP, Brazil.

[*]*Corresponding author* :

Departamento de Biologia Celular, Instituto de Biologia, Universidade Estadual de Campinas (UNICAMP). Caixa Postal 6109. CEP 13084-971 Campinas, SP, Brasil.
Phone: (55)(19) 37886124; Fax: (55)(19) 37886111
E-mail address: pedroh@operamail.com

This article contains 41,180 characters.

Abstract

The aim of this work was to examine the differences in the susceptibility of aluminium-sensitive and tolerant maize plants to the induction of cell death, which could explain the toxicity of this metal in the irreversible inhibition of root growth and in the promotion of meristem death.

Following exposure to aluminium, cracks were seen only on the root surface of only sensitive plants. Evans blue staining showed a loss of membrane integrity only at the crack periphery. Sensitive plants showed swollen cells at the root tips, with highly condensed nuclei that had a smaller area and DNA content. Karyorhexis was frequent and there was extensive DNA fragmentation in sensitive plant roots. Tolerant plants showed no nuclear condensation or DNA fragmentation. The analysis of nuclear morphology, Feulgen-DNA content, chromatin texture and fragmentation pattern indicated that sensitive plants underwent cell death triggered by aluminium in which not all apoptotic features were present. Aluminium-triggered cell death did not occur with tolerant plants. Aluminium triggered non-apoptotic cell death in the roots from sensitive plants, but not in tolerant plants. This observation could explain the differential root growth of both types of plants after long-term growth in aluminium-rich environment.

Introduction

The toxicity effect of aluminium (Al) is the major factor limiting crop cultivation in acid soils around the world (Kochian, 1995). Most of the Al in soil occurs as harmless oxides or silicates. However, in acid soils with pH < 5.0, Al is solubilized into the toxic species Al^{3+} (Kochian, 1995; Harris, 1996). Al penetrates cells possibly as a neutral complex, and inhibits general cell metabolism, including root growth (Kochian, 1995; Matsumoto, 2000; Ma *et al.*, 2001).

The preference of Al^{3+} for electrostatic rather than covalent binding is predicted thermodynamically because of the high charge-to-radius ratio (Berthon, 1996). Thus, Al^{3+} forms stable complexes with ligands containing negatively charged groups (Berthon, 1996), including pectin, DNA and ATP (Karlik *et al.*, 1980; Kiss *et al.*, 1996). As a consequence of this affinity for anionic radicals, the greatest Al deposits occur in the cell wall and in the nucleus (Marienfeld *et al.*, 2000; Silva *et al.*, 2000). Al^{3+} also induces oxidative stress (Campbell and Bondy, 2000; Pan *et al.*, 2001), and is a consequence rather than a cause of Al^{3+} toxicity in maize (Boscolo *et al.*, 2002). Modifications in the structure of DNA introduced by Al^{3+} (Karlik and Eichhorn, 1989; Ahmad *et al.*, 1996) may trigger genetically controlled cell death (CCD) in plants (Havel and Durzan, 1996), as do high levels of oxidative stress (Buckner *et al.*, 2000; Boscolo *et al.*, 2002). The mechanism whereby Al^{3+} differentially affects root growth in tolerant and sensitive plants is unknown. However, an understanding of the pathways involved could help to elucidate the toxicity of Al^{3+}.

In animal cells, controlled cell death is distinct from passive, uncontrolled, accidental death (often called necrosis) (Majno and Joris, 1995; Jones, 2000). Although apoptosis is the most studied form of controlled cell death, there is clear evidence of non-apoptotic controlled death in eukaryotic cells, especially in plants (Cohen *et al.*, 1992; Majno and Joris, 1995; Mittler and Lam, 1997; Fath *et al.*, 1999; Drew *et al.*, 2000). The biochemical pathways underlying cell death activation in plants are still obscure and the morphological characteristics of this process remain controversial (Fath *et al.*, 1999; Buckner *et al.*, 2000; Jones, 2000), despite attempts to classify the controlled cell death events in plants as apoptosis (Havel and Durzan, 1996; Fojtová and Kovarik, 2000; Pan *et al.*, 2001).

Several authors have described and proposed oligonucleossomal chromatin fragmentation into multiples of 180 bp as a hallmark of controlled cell death in plants. However, this DNA laddering is not always associated with controlled death (Fath *et al.*, 1999; Drew *et al.*, 2000). Recent findings have shown that some hallmarks of apoptosis in animal cells may not occur in classic controlled cell death events, such as hormonally-directed aleurone death or differentiation of tracheary elements and aerenchyma (Fukuda, 1997; Fath *et al.*, 1999; Drew *et al.*, 2000). Chromatin condensation, fragmentation (oligonucleosomal or random pattern) and the decrease of DNA content while the cell membrane is still intact are the only characteristics common to all the controlled death processes in plant cells described ti date (Fukuda, 1997; Mittler and Lam, 1997; Fath *et al.*, 1999; Buckner *et al.*, 2000; Drew *et al.*, 2000; Jones, 2000).

Pan *et al.* (2001) reported Al^{3+}-induced cell death in barley root tips and suggested that this resulted from oxidative stress-activated cell death. However, it is unclear whether Al^{3+}-tolerance can protect cells from the Al^{3+}-triggered cell death. Al^{3+}-induced death of root meristematic cells is an important event that may explain the inhibition of root elongation in Al^{3+}-sensitive plants and cell survival in Al^{3+}-tolerant specimens. In this work, we used plasma membrane integrity tests, morphological analysis, nuclear DNA content measurements, chromatin texture analysis, and DNA fragmentation detection assays to examine whether controlled cell death occurs in both Al^{3+}-sensitive and Al^{3+}-tolerant plants.

Materials and Methods.

Plant material

Seeds from Al^{3+}-tolerant (Ag 5011) and Al^{3+}-sensitive (Ag 6601) maize (*Zea mays* L.) cultivars were generously supplied by Dr. M. Guimarães (AGROCERES S.A., Brazil) and are referred to in the text as tolerant and sensitive maize cultivars, respectively. The seeds were germinated for 62 hours at 30°C in the dark in a roll of filter paper moistened with sterile deionized water. After germination, the seedlings were transferred to plastic screens floating on nutrient solution (composition, in μM: $Ca(NO_3)_2$, 500; KNO_3, 500; KH_2PO_4, 2; NH_4NO_3, 250; $MgSO_4$, 200; $Fe(NO_3)_3$, 2; $MnCl_2$, 2; H_3BO_3, 11; $ZnSO_4$, 0.35; $CuSO_4$, 0.2; $(NH_4)_6Mo_7O_{24}$, 0.03), pH 4.5. Some

seedlings were treated with 40 μM AlCl₃ (Sigma, USA) for 48 hours, while others (controls) were maintained in the nutrient solution alone. The solutions were aerated continuously and replaced every 24 h to minimize microbial contamination.

Specimen manipulation

After treatment, the apices were sectioned 5 mm from the root tip, fixed for 48 hours in 3.7% buffered paraformaldeyde, pH 7.4, and dehydrated in tertiary butyl alcohol series under vacuum. The specimens were infiltrated with Paraplast plus wax (Oxford, USA) and 7 μm sections were cut on a rotary microtome (Micron, Germany).

Histochemistry

The loss of plasma membrane integrity was evaluated visually by Evans blue staining. After treatment with AlCl₃, roots were stained with an Evans blue solution (1%, w/v, in buffered saline, pH 7.2) for 10 minutes and then washed extensively in buffered saline to remove untrapped stain. The roots were observed and photographed using a Zeiss stereoscope (Zeiss, Germany).

Root morphology was assessed by toluidine blue staining of root sections. The material was stained for 15 minutes in 0.025% (w/v) toluidine blue in McIlvaine buffer (0.05 M citrate, 0.1 M sodium phosphate, pH 4.0), then washed in distilled water, air dried, cleared in xylene and mounted in Canada balsam (n_D=1.54).

Nuclear staining was done using the Feulgen reaction as described by Vidal *et al.* (1998), with minor alterations. Freshly sectioned root apices were fixed in ethanol-acetic acid (3:1, v/v) for 15 minutes, then rinsed in 70% ethanol and distilled water. The fixed roots were subjected to the Feulgen reaction *en bloc*, with acid hydrolysis being done in 4 M HCl at 24°C for 60 minutes to provide optimal staining. Afterwards, the hydrolyzed material was immersed in Schiff's reagent, prepared as described by Vidal *et al.* (1993), for 45 minutes and then rinsed three times in sulfurous water (0.5%, w/v, $K_2S_2O_5$ in 0.05 M HCl). The stained roots were squashed in a drop of sulfurous water and the coverslips were removed by freezing in liquid N_2. All roots were fixed and processed at the same time in similar glass recipients in order to keep the experimental conditions as constant as possible. The preparations were dehydrated, cleared in xylene and mounted in Canada balsam (n_D=1.54). The stained preparations were stored in the

dark to prevent stain fading. The Feulgen reaction was chosen because it stoichiometrically labels DNA, which allows the identification, localization and quantification of DNA, in contrast to other methods involving dyes such as ethidium bromide or propidium iodide (Mello, 1997; Dolezel *et al.*, 1998).

Scanning microspectrophotometry and image analysis
Data acquisition

Cytometry was done in two systems to ensure the accuracy of the results. One of the approaches involved video image analysis using a CCD camera (JVC, Japan) for image acquisition and a Global Lab Image System (Data Translation, Inc., Palo Alto, CA) for image segmentation and analysis. Both of these were coupled to a Zeiss photomicroscope equipped with a Pol-Neofluar 25/0.60 objective, 1.25 optovar and 1.4 condenser set, at an emission wavelength of 546 nm. The images to be processed were fed from the microscope to the computer via the CCD video camera. The conversion of pixels to micrometers was done using a micrometer slide. The conversion of gray scales to absorbance was done using the Minitab software (Minitab Inc., State College, PA). The second approach involved the use of a Zeiss automatic scanning microspectrophotometer interfaced to a microcomputer, equipped with a Pol-Neofluar 100/1.3 objective, a 2.0 optovar and a 16/0.3 Zeiss LD-Epiplan condenser. The diameter of the measuring diaphragm was 0.1 mm and the working scanning spot was 0.5 μm x 0.5 μm at a wavelength of 546 nm obtained with a Schott monochromator filter ruler. One hundred nuclei were measured in the first cytometry system and 200 on the second system for each cultivar in each experiment.

Parameters for analysis

The parameters used for the measurement of Feulgen-stained nuclei were the total nuclear area in μm^2 (S), the integrated optical density (IOD or, in this case, Feulgen-DNA values corresponding to DNA content) and the optical density (OD, or absorbances). Absorbances above a selected threshold, in this case 0.3, were considered to be "condensed" chromatin and were chosen from several descriptors provided by the software of both cytometry devices. These parameters allowed the plotting of a scatter diagram (Vidal, 1984; Vidal *et al.*, 1984; Mello *et al.*, 1994; Mello *et al.*, 1995; Vidal *et*

66

al., 1998), of S% (percentage of nuclear area covered with stained chromatin having OD values corresponding to "condensed" chromatin) versus AAR (a dimensionless parameter that expressed how many times the average absorbance of the "condensed" chromatin exceeded that of the entire nucleus, given by [IODc/Sc]/[IODt/St], where IODc is the Feulgen-DNA value for "condensed" chromatin, IODt the Feulgen-DNA value for the entire nuclei, Sc is the "condensed" chromatin-stained area in μm^2, and St is the nuclear stained area in μm^2). Absorbances ≤ 0.02 were considered to be background values and were automatically discarded by the software.

Regression analysis of Feulgen-DNA content and nuclear area

The R-square parameter was obtained from a linear regression of the nuclear area and DNA content. As DNA content is not affected by the nuclear size, the Feulgen-DNA values were chosen as independent variables. The Pearson correlation was also used to analyse these variables.

Immunocytochemistry

The TUNEL assay was done in 7 μm thick root sections obtained as already described. DNA fragmentation was detected using an "*In situ* cell death detection" kit (Böehringer Mannheim, Germany) according to the manufacturer's instructions, except that the samples were incubated in a 3% solution of powdered milk solution in saline buffer, pH 7.2, for 1 hour at 37 °C or overnight at 4 °C, prior to cell permeabilization. This extra step was found to increase the binding specificity of the HRP-coupled anti-fluorescein antibody, and enhanced the accuracy of the results.

Externalized phosphatidylserine was detected with an annexin-V fluos staining kit (Böehringer Mannheim, Germany) as described by the manufacturer.

Comet assay and DNA electrophoresis

The comet assay (or single cell gel electrophoresis) was done with isolated root cell nuclei as described by Navarrete *et al.* (1997). Briefly, the roots were sectioned transversally (one at a time) with a sharp blade between 1 and 1.5 mm from the apex and the terminal section was discarded. The cut surface of the root was brought into contact with a 10 μl drop of 50 mM sodium phosphate buffer, pH 6.8, already placed

on a agarose-coated microscopic slide. This procedure was repeated 15 to 20 times. One hundred and twenty microliters μl of 0.5% low melting point agarose at 30 °C were added to the drops which were then with parafilm. The slides were left on ice and the parafilm was removed after solidification of the agarose-nucleus layer. A second layer of agarose (100 μl at 30 °C) was subsequently spread over the first layer and covered with parafilm for at least 10 min on ice to harden the agarose. After removing the parafilm, the slides were placed in freshly prepared lysing solution (2.5 M NaCl, 100 mM EDTA, 10 mM Tris, pH 10, with freshly added 1% Triton X-100 and 2% DMSO) at 4 °C for 1 h. The samples were subjected to electrophoresis in alkali (0.03 M NaOH, 1 mM EDTA, pH 12.1) at 1 V/cm and 30 mA for 15 minutes, which was preceded by a 20 minutes immersion of the slides in the electrophoresis buffer to allow chromatin unwinding. After electrophoresis, the slides were neutralized in 0.05 M Tris buffer, pH 8.0, rinsed in distilled water, fixed in methanol, air dried and stored in the dark. DNA was stained with propidium iodide (20 μg/ml) for 10 min, after which the slides were washed in distilled water and examined in a fluorescence microscope (Zeiss Axiophot). Al^{3+}-induced DNA fragmentation in sensitive and tolerant cultivars was assessed qualitatively to distinguish between healthy and dying nuclei, as described by Schildknecht and Vidal (2001).

DNA was extracted from roots as described by Pan *et al.* (2001). The root tips (5-10 mm) were ground in liquid N_2, incubated in a buffer containing 2% hexadecyltrimethylammonium bromide. DNA was extracted with chloroform–isoamyl alcohol and precipitated with isopropanol. RNA was removed with RNase A. The DNA was dissolved in 0.5 ml TE buffer (10 mM Tris–HCl, pH 7.4 and 1 mM EDTA) and run on 1.8% agarose gels (w/v) containing 0.5 μg ethidium bromide/ml in Tris–acetate-EDTA buffer. DNA from sensitive plants not exposed to $AlCl_3$ was used as a control.

Statistics

All experiments were repeated at least three times. Where applicable, the results were expressed as means and S.D. The statistical analyses (ANOVA and the non-parametric Mann-Whitney test for heterosedastic samples, regression and correlation analyses) were done with the Minitab software. The significance of results was set at $p < 0.05$ for ANOVA.

Results

Loss of plasma membrane integrity and of histological supraorganization

Compared to the tolerant cultivar, root growth was severely inhibited in the sensitive cultivar after a 48 h exposure to Al (Schildknecht and Vidal, 2002). Cracks on the root surface were seen in the sensitive cultivar after 10 h of treatment with 40 μM AlCl$_3$, whereas no damage was observed in tolerant plants (Fig. 1). Evans blue staining revealed a loss of cell viability only in Al-treated sensitive maize and occurred mainly in the region of the crack with adjacent layers of intact cells, showing no staining (Fig. 1). The root cells of tolerant plants did not stain, thus continuing the membrane integrity after exposure to Al. To determine whether the unstained cells were healthy or if were simply maintaining on intact membrane during death, roots with surface cracks were labeled with annexin V and propidium iodide. Disrupted cells were detected at the crack periphery based on propidium iodide staining of the nucleus and anexin V labeling of the membranes, whereas only annexin-V labeled membranes were seen in regions that did not stain with Evans blue, (Fig. 2)

Aluminium altered the morphology of maize root tissues in the sensitive, but not in the tolerant cultivar (Fig. 3, A-C). In the meristematic region of sensitive plant roots, the cells were enlarged and showed a less organized columnar pattern (Fig. 3B). Broken cell walls were observed in the outer cell layer in transversal sections of roots from Al-treated sensitive plants. These broken walls coincided with the cracks that stained deeply with Evans blue (Figs. 1 and 3C).

Influence of Al treatment in nuclear morphology and DNA content

There were no visible changes in the Feulgen-positive nuclei of roots from control (non-treated) plants. The heterogeneously distributed heterochromatin in maize chromosomes, known as knobs (de la Casa-Esperón and Sapienza 2000), was observed and resulted in an uneven distribution of stained material.

After Al treatment, some pyknotic nuclei were observed only in sensitive plants (Fig. 4C). These nuclei had a small surface area and a high level of chromatin condensation that resulted in very deep Feulgen staining, one of the characteristics of mammalian apoptosis (Majno and Joris, 1995). Micronuclei and nuclear budding were not observed in Feulgen-stained roots from either cultivar after Al treatment (Fig. 4, A-C), although vesicles were found around the nucleus in some cells from sensitive plant roots stained with toluidine blue (Fig. 4D).

Both the approaches used in cytometry gave similar data about the Feulgen-stained nuclei. The results provided by scanning microspectrophotometry were used for further analysis because they were based on a higher number of measurements. Microspectrophotometry of Feulgen-stained nuclei from both maize cultivars grown in control nutrient solution showed no differences in the nuclear DNA content ($p = 0.389$, ANOVA test) as represented by Feulgen-DNA values (Fig. 5). After treatment with Al, sensitive plant nuclei showed a marked decrease in the amount of Feulgen-DNA ($p = 0.000$) whereas tolerant plants were unaffected ($p = 0.227$), although there was a non-significant tendency to smaller values (Fig. 5). The Mann-Whitney test confirmed the results obtained by ANOVA. In addition to the DNA content, the nuclear area (μm^2) also decreased in sensitive plant roots after treatment with Al ($p = 0.005$) but not in tolerant specimens ($p = 0.297$, Fig. 5).

Linear regression (expressed by R^2, see Material and Methods for details) and correlation (*r*) were used to examine the relationship between nuclear area and the corresponding Feulgen-DNA content (Tab. 1). Al treatment increased both R^2 and *r* values in sensitive plants, indicating the correlation of nuclear size with the Feulgen-DNA content was enhanced by Al and that both variables were similarly altered, i.e. a decrease in a DNA content resulted in a smaller nuclear area. In contrast, tolerant plants showed lower values of both R^2 and *r*, indication that the Feulgen-DNA content was

less correlated to nuclear size (Tab.1, Fig. 5). Exposure to Al did not alter the levels of chromatin condensation (expressed in terms of OD) in tolerant plants (Fig. 6), whereas sensitive specimens showed higher levels of condensed chromatin after treatment with Al, an indication of apoptosis (Fig. 6). Differences in chromatin texture were detected using a scatter plot of S% (the nuclear relative area covered with condensed chromatin) versus AAR (the ratio that expresses the contrast between the OD values of condensed and noncondensed chromatin compartments) (Fig. 7). This showed that Al induced a nuclear population with larger S% values accompanied by smaller AAR values in sensitive plants; no alterations in chromatin texture were observed in Al-treated tolerant plants. These results indicate that Al increase the high-order-packing state of chromatin and induces chromatin condensation in sensitive plant roots.

Al induced DNA fragmentation

DNA fragmentation was assessed using the TUNEL immunocytochemical assay, the comet assay and by conventional electrophoresis. Al-induced fragmentation of DNA was detected in sensitive plants by all three methods; there were no changes in the tolerant cultivar (Figs. 8, 9).

Extensive TUNEL labeling was observed in Al-treated sensitive maize roots, with the greatest DNA damage in the meristematic tissue (Figs. 8B and 8D). The Al-treated tolerant cultivar showed no differences in TUNEL labeling when compared to the control plants, except that the root outer cell layer was deeply labeled in both cultivars grown in the presence of Al (Figs. 8A and 8C). The qualitative analysis of the nuclei by the comet assay confirmed the results obtained in the TUNEL assay. The comet assay showed a high percentage of nuclei with damaged DNA in sensitive plants (48% of observed nuclei) exposed to Al compared to the tolerant cultivar (18% of observed nuclei). Electrophoresis of DNA revealed an non-specific DNA fragmentation in Al-treated sensitive plants, with no detectable cleavage in 180 bp multiple fragments (Fig. 9).

Discussion

Al alters meristem organization, but is not the direct cause of the loss of membrane integrity

Cell death in root cracks in Al-treated sensitive plants, detected here by Evans blue staining, was also observed in pea roots (Yamamoto *et al.* 2001) and appears to be a common feature of Al toxicity. The cracks on the root surface may be a consequence of internal pressure created by enlargement of inner cells when outer cell growth has been inhibited by Al rather than a result of direct damage by Al (Yamamoto *et al.* 2001). Our results support this hypothesis above since a loss of membrane integrity was detected only at the crack periphery and not in other root regions in direct contact with the Al-containing solution (Fig. 1). Breaks in the cell wall were observed in histological sections of Al-treated sensitive roots and were the main cause of the loss membrane integrity (Fig. 3). However, the absence of wall breakage did not necessarily mean that the cells were healthy. The labeling of intact cells with annexin V revealed externalization of phosphatidylserine, an early event in animal and plant controlled cell death (Brien *et al.* 1997).

The histological disorganization of meristematic tissues in sensitive roots was clearly caused by Al, since it was not seen in control or in Al-treated tolerant plants (Moon *et al.* 1997). The swollen meristematic cells in Al-treated sensitive plants reflect an osmotic imbalance, as suggested by Schildknecht and Vidal (2002). One of the early and most common characteristics of necrosis (uncontrolled death) is the loss of membrane integrity (Majno and Joris, 1995; Jones, 2000), which did not occur in these cells. The nuclear morphological features observed after Al treatment (pyknosis, karyorhexis and marked chromatin condensation) were also typical of a controlled cell death rather than necrosis. The Al-induced death of root meristematic cells is apparently the main cause of the permanent inhibition of root growth in sensitive plants after a long-term exposure to Al. In Al-tolerant plants there are likely to be mechanims that protect the meristem and allow continuous root elongation.

Al alters the nuclear morphology and DNA content in sensitive plant cells

Higher OD values and a decrease in Feulgen-DNA content and area (S) after treatment with Al were evident nuclear in the root meristematic region of sensitive but

not of tolerant plants. The pyknotic nuclei observed in Feulgen-stained cells represented extreme morphological alterations (Fig. 3). Nuclei with a lower DNA content also had a reduced nuclear area, as seen in Al-treated sensitive plants. In this case, the enhanced chromatin packing state resulted in a more conspicuous reduction of the S values which was seen by the higher correlation (R^2 and r) between Feulgen-DNA content and area after treatment with Al. In tolerant plants, the Feulgen-DNA content and nuclear area were less correlated and there was a decrease in the level of chromatin condensation, as shown by both R^2 and r, and OD values, respectively. AAR plots also showed these phenomena and will be discussed later. Chromatin unpacking in tolerant plants is a phenomenon that facilitates gene expression and may be related to tolerance mechanisms that are dependent on Al signaling, such as the triggering of organic acid anions exudation.

Knobs, regions of highly condensed chromatin in maize chromosomes, are characteristic of healthy maize nuclei (de la Casa-Esperón and Sapienza, 2000) and were seen in almost all Feulgen-stained nuclei of both maize cultivars grown in control nutrient solution and also in the Al-treated tolerant cultivar. This morphological feature was seen in the AAR vs S% scatter plot as nuclei with low S% and high AAR values ("chicken-pox face"-like nuclei) (Fig. 7). The nuclei from Al-treated sensitive plants had high S% and low AAR values, revealing nuclei with a great area covered by highly condensed chromatin. The chromatin condensation could be the result of Al binding to DNA (Karlik and Eichhorn, 1989; Ahmad et al., 1996) or could be caused by a controlled cell death event. The detection of DNA fragmentation by the TUNEL, and comet assay and by electrophoresis supports the second possibility.

Al-induced cell death is not necrotic

The TUNEL reaction detected high levels of DNA fragmentation in meristematic root cells from sensitive but not from tolerant plants grown in the presence of Al. This finding was confirmed by the comet assay which showed intense DNA damage in Al-treated sensitive plants. Both of these assays have been used as molecular tracers for genetically controlled cell death (Östling and Johanson, 1984; Gravrieli et al., 1992) but their use is currently restricted to the detection of DNA fragmentation, which is only one of

several characteristics of a controlled cell death. The TUNEL and comet assays provided the analysis of DNA fragmentation at each cell individually, which was not possible by conventional electrophoresis. In contrast, conventional electrophoresis separated damaged DNA into fragments of known length and allowed the observation of 180 bp ladders. In our experiments, Al-treated sensitive plants showed highly damaged DNA that was fragmented randomly with no specific cleavage into 180 bp fragments. DNA from control and Al-treated tolerant plants showed low levels of fragmentation that was unrelated to Al toxicity, and may have been due to naturally dying cells at the root cap and in vascular tissue. The absence of internucleosomal-specific nuclease activity in dying plant cells does not exclude the occurrence of a genetically controlled death, nor does it support the hypothesis of necrosis (Fath *et al.*, 1999; Jones, 2000). Although no DNA fragmentation was observed after 48h of Al stress, there may have been 180 bp ladder formation during early events from Al-induced cell death. However, the morphological and cytochemical analysis of Al-stressed nuclei and the labeling of intact cells by annexin V suggested that a controlled mechanism of cell death occurred without cleavage of DNA into 180 bp fragments.

There are currently no well-defined hallmarks of plant controlled cell death and it may be unwise to indiscriminately apply the characteristics of animal apoptosis to plants (Fath *et al.*, 1999; Drew *et al.*, 2000; Jones, 2000). Several features common to controlled cell death (or apoptosis-like death) in plants can be used to distinguish this phenomenom from necrosis. The latter is characterized by increased nuclear size, the degeneration of biological membranes and the collapse of adjacent cell walls (Hinrichs-Berger *et al.*, 1999) whereas in apoptosis-like death there is increased nuclear condensation, maintenance of membrane integrity, enhanced nuclease and protease activities, chromatin fragmentation and loss of DNA content (Buckner *et al.*, 2000). The Al-induced death seen here in root tip cells showed all the characteristics of a genetically controlled death. In tolerant plants, Al did not trigger cell death because of tolerance mechanisms.

The death of root meristem in sensitive but not in tolerant plants is probably the main cause of differential root growth after long-term growth in aluminium-rich environment. The mechanisms whereby Al triggers cell death is still unknown, but Al-

induced oxidative stress in barley (Pan *et al.*, 2001) and in maize (Boscolo, 2002) may be involved. Oxidative stress is known to play a role in the release of cytochrome c in plants (Jones, 2000) which will trigger the activation of the downstream caspases. However, it is unclear whether Al modulates cell death by producing different levels of oxidative stress in tolerant and sensitive plants or whether the mitochondria sensitivity to reactive oxygen species is also involved.

Conclusions

Aluminium can trigger an apoptosis-like death in the roots of Al^{3+}-sensitive plants, but not in Al^{3+}-tolerant plants. Dying cells occur mainly in the meristematic region of the root tips of Al^{3+}-sensitive plants. This phenomenon could explain the permanent inhibition of root growth seen in Al^{3+}-sensitive plants, but not in Al^{3+}-tolerant plants, after long-term exposure to aluminium.

Acknowledgements

References

Ahmad, R., M. Naoui, J.F. Neault, S. Diamantoglou, and H.A. Tajmir-Riahi. (1996). An FTIR spectroscopic study of calf-thymus DNA complexation with Al(III) and Ga(III) cations. *J. Biomol. Struct. Dyn.* **13**,795-802.

Berthon G. (1996). Chemical speciation studies in relation to aluminium metabolism and toxicity. *Coord. Chem. Rev.* **149**,241-280 .

Boscolo, P.R.S., M. Menossi, and R.A. Jorge. (2002). Aluminum-induced oxidative stress in maize. *Phytochemstry*, in press.

Brien, I.E., C.P. Reutelingsperger, and K.M. Holdaway. (1997). Annexin-V and TUNEL use in monitoring the progression of apoptosis in plants. *Cytometry* **29**,28-33.

Buckner, B., G.S. Johal, and D. Janick-Buckner. (2000). Cell death in maize. *Physiol. Plantarum* **108**,231-239.

Campbell, A. and S.C. Bondy. (2000). Aluminum induced oxidative events and its relation to inflammation: a role for the metal in Alzheimer's disease. *Cell. Mol. Biol.* **46**,721-730.

Cohen, G.M., X.M. Sun, R.T. Snowden, D. Dinsdade, and D.N. Skilleter. (1992). Key morphological features of apoptosis may occur in the absence of internucleosomal DNA fragmentation. *Biochem. J.* **286**,331-334.

de la Casa-Esperón, E. and C. Sapienza. (2000). Natural selection and the function of genome imprinting: beyond the silenced minority. *Trends Genet.* **16**,573-579.

Dolezel, J., J. Greilhuber, S. Lucretti, A. Meister, M.A. Lysak, L. Nardi, and R. Obermayer. (1998). Plant genome size estimation by flow cytometry: inter-laboratory comparison. *Ann. Bot.* **82**,17-26.

Drew, M.C., C.J. He, and P.W. Morgan. (2000). Programmed cell death and aerenchyma formation in roots. *Trends Plant Sci.* **5**,123-127.

Fath, A., P.C. Bethke, and R.L. Jones. (1999). Barley aleurone cell death is not apoptotic: characterization of nuclease activities and DNA degradation. *Plant J.* **20**,305-315.

Fojtová, M., A. Kovarik. (2000) Genotoxic effect of cadmium is associated with apoptotic changes in tobacco cells. *Plant Cell Environm.* **23**, 531-537.

Fukuda, H. (1997). Tracheary element differentiation. *Plant Cell* **9**,1147-1156.

Gravrieli, Y., Y. Sherman, and S.A. Ben-sasson. (1992). Identification of programmed cell death *in situ* via specific labeling of nuclear DNA fragmentation. *J. Cell Biol.* **119**,493-501.

Harris, W.R., G. Berthon, J.P. Day, C. Exley, T.P. Flaten, W.F. Forbes, T. Kiss, C. Orvig, and P.F. Zatta. (1996). Speciation of aluminum in biological systems. *J. Toxicol. Environ. Health* **48**,543-568.

Havel, L. and D.J. Durzan. (1996). Apoptosis in plants. *Bot. Acta* **109**,268-277.

Hinrichs-Berger, J., M. Harfold, S. Berger, and H. Buchenauer. (1999). Cytological responses of susceptible and extremely resistant potato plants to inoculation with potato virus Y. *Physiol. Mol. Plant Pathol.* **55**,143-150.

Jones, A. (2000). Does the plant mitochondrion integrate cellular stress and regulate programmed cell death? *Trends Plant Sci.* **5**,225-230.

Karlik, S.J., G.L. Eichhorn, P.N. Lewis, and D.R. Crapper. (1980). Interaction of aluminium species with deoxyribonucleic acid. *Biochemistry* **19**,5991-5998.

Karlik, S.J. and G.L. Eichhorn. (1989). Polynucleotide cross-linking by aluminum. *J. Inorg. Biochem.* **37,**259-269.

Kiss, T., P. Zatta, and B. Corain. (1996). Interaction of Aluminum (III) with phosphate-binding sites: biological aspects and implications. *Coord. Chem. Rev.* **149,**329-346.

Kochian, L.V. (1995). Cellular mechanisms of aluminum toxicity and resistance in plants. *Ann. Rev. Plant Physiol. Plant Mol. Biol.* **46,**237-260.

Ma, J.F., P.R. Ryan, and E. Delhaize. (2001). Aluminium tolerance in plants and the complexing role of organic acids. *Trends Plant Sci.* **6,**273-278.

Majno, G. and I. Joris. (1995). Apoptosis, oncosis and necrosis. *Am. J. Pathol.* **146,**3-15.

Marienfeld, S., N. Schmohl, M. Klein, W.H. Schröder, A.J. Kuhn, and W.J. Horst. (2000). Localisation of aluminium in root tips of *Zea mays* and *Vicia faba*. *J. Plant Physiol.* **156,**666-671.

Matsumoto, H. and S. Morimura. (1980). Repressed template activity of chromatin of pea roots treated by aluminium. *Plant Cell Physiol.* **21,**951-959.

Matsumoto, H. (2000). Cell biology of aluminium toxicity and tolerance in higher plants. *Int. Rev. Cytol.* **200,**1-46.

Mello, M.L.S., B.C. Vidal, W. Planding and U. Schenck (1994) Image analysis: video system adequacy for the assortment of nuclear phenotypes based on chromatin texture evaluation. *Acta Histochem. Cytochem.* **27**, 23-31.

Mello, M.L.S., S. Contente, B.C. Vidal, W. Planding and U. Schenck (1995) Modulation of *ras* transformation affecting chromatin supraorganization as assessed by image analysis. *Exp. Cell Res.* **220**, 374-382.

Mello, M.L.S. (1997). Cytochemistry of DNA, RNA and nuclear proteins. *Braz. J. Genet.* **20,**257-264.

Mittler, R. and E. Lam. (2001). Characterization of nuclease activities and DNA fragmentation induced upon hypersensitive response cell death and mechanical stress. *Plant Mol. Biol.* **34**,209-221.

Moon, D.H., L.M.M. Ottoboni, A.P. Souza, S.T. Sibov, M.Gaspar and P. Arruda (1997). Somaclonal-variation-induced aluminium-sensitive mutant from an aluminium-inbred maize tolerant line. *Plant Cell Rep.* **16**, 686-691.

Navarrete, M.H., P. Carrera, M. Miguel, and C. de la Torre. (1997). A fast comet assay variant for solid tissue cells. The assessment of DNA damage in higher plants. *Mutat. Res.* **389**,271-277.

Östling, O. and J.P. Johanson. (1984). Microelectrophoretic study of radiation-induced DNA damages in individual mammalian cells. *Biochem. Biophys. Res. Commun.* **123**,291-298.

Pan, J.W., M.Y. Zhu, and H. Chen. (2001). Aluminum-induced cell death in root-tip cells of barley . *Environm. Exp. Bot.* **46**,71-79.

Schildknecht, P.H.P.A. and B.C. Vidal (2001) Annexin V and Comet assay detection of violacein-induced apoptosis . *Clin.Med.Health Res.* **1**,
http://clinmed.netprints.org/cgi/content/abstract/2001100002v1

Schildknecht, P.H.P.A. and B.C. Vidal. (2002) A role for the cell wall in Al^{3+} resistance and toxicity: crystallinity and availability of negative charges. *LifeXY* **1**, 1087-1095.

Silva, I.R., T.J. Smyth, D.F. Moxley, T.E. Carter, N.S. Allen, and T.W. Rufty. (2000). Aluminium accumulation at nuclei of cells in the root tip. Fluorescence detection using lumogallion and confocal laser scanning microscopy. *Plant Physiol.* **123**,543-552.

Vidal, B.C. (1984). Polyploidy and nuclear phenotypes in salivary glands of the rat. *Biol. Cell* **50**, 137-146.

Vidal, B.C., W.J. Silva and P.C. Strikis (1984). Nuclear phenotypes and DNA content of root cells of *Zea mays, Zea diploperennis* and of a mazoid hybrid. *Cell. Mol. Biol.* **30**, 11-22.

Vidal, B.C., M.L.S. Mello, and R.D. Illg. (1993). Chromosome number and DNA content in cells of a biotechnologically selected somaclone of garlic (*Allium sativum* L.). *Rev. Brasil. Genet.* **16**,347-356.

Vidal, B.C., J. Russo, and M.L.S. Mello. (1998). DNA content and chromatin texture of Benzo[a]pyrene-transformed human breast epithelial cells as assessed by image analysis. *Exptl. Cell Res.* **244**,77-82.

Yamamoto, Y., Y. Kobayashi, and H. Matsumoto. (2001). Lipid peroxidation is an early symptom triggered by aluminum, but not the primary cause of elongation inhibition in Pea roots. *Plant Physiol.* **125**,199-208.

Figure legends

[**Table 1.** Results from the statistical analysis of regression (R^2) and correlation (r) between the nuclear area and Feulgen-DNA content from both sensitive and tolerant cultvars.]

[**Figure 1.** Evans blue-stained roots grown in the presence Al. Tolerant roots (T) were not stained while sensitive (S) were highly stained at surface cracks. Bar = 400 μm.]

[**Figure 2.** Micrograph of intact roots from sensitive plants stained with propidium iodide and annexin V, observed by fluorescence microscopy. Bar = 50 μm.]

[**Figure 3.** Toluidine blue-stained root sections of tolerant (A) and sensitive (B, C) plants treated with Al. Sensitive plants showed structural disorganization, with larger cells in the meristematic zone (B, arrow) and ruptures of cell walls on root surface (C). Bar = 100 μm.]

[**Figure 4.** Micrographs of Feulgen stained (A – C) and Toluidine blue stained (D) root sections obtained from Al-treated plants. Tolerant plants showed nuclei with unpacked chromatin and highly contrasting knobs (A, arrow) whereas pyknotic nuclei were observed only in sensitive plants (B and C, arrows). Several vesicles, similar to micronuclei, were observed in sensitive plants (D). Bar = 50 μm.]

[**Figure 5.** Feulgen-DNA values (white bars), corresponding to nuclear content, and nuclear area measures (gray bars) obtained for tolerant (Tol) and sensitive (Sens) cultivars grown in the absence or presence of Al. The standard deviations are shown for each columns. The coefficient of Feulgen-DNA values x area correlation is given at the top of each column.]

[**Figure 6.** OD (546 nm) values, corresponding to the levels of chromatin condensation, in tolerant (Tol) and sensitive (Sens) cultivars grown in the absence or presence of Al. The standard deviations are shown for each column.]

[**Figure 7.** Scatter diagram of AAR vs S% values for sensitive (A) and tolerant (B) plant nuclei, exposed to Al (red symbols) or not (black symbols). The inset in B shows a schematic scatter diagram with the approximate point position acquired by nuclear phenotypes differing in chromatin texture.]

[**Figure 8.** Detection of chromatin fragmentation by TUNEL assay in root sections of tolerant (A, C) and sensitive (B, D) plants treated with Al. The meristematic tissue (M) is shown in A and B, which is separated

from the root cap (RC) by a clear boundary of cells (B). Nuclei with fragmented chromatin (F) were abundant in the meristem of sensitive plants, whereas healthy nuclei (H) were predominant in the meristematic zone of tolerant plants. The root protoderm (P) was also affected by Al and is seen in detail in C and D. The protoderm of tolerant plants showed dying nuclei only in the outer cell layers (C) and sometimes chromatin fragments (DB) were seen in the rhizosphere. Sensitive plants showed nuclei positive to the TUNEL reaction in several cell layers close to the protoderm (D). Bar = 50 μm.]

[**Figure 9.** Electrophoresis of DNA isolated from sensitive (lane 2) and tolerant (lane 3) plants exposed to Al, and from untreated plants (lane 4). A 123 bp ladder is shown in lane 1. Sensitive plants showed the greatest DNA fragmentation after exposure to Al as compared to control and Al-treated tolerant plants. No significant difference was observed between control and Al- treated tolerant plants.]

Table 1: Analysis of the correlation between nuclear area and DNA content				
Cultivar	Sensitive	Sensitive + Al	Tolerant	Tolerant + Al
R^2	0.407	0.529	0.470	0.310
r	0.643	0.727	0.685	0.550

FIG.1

84

Crack
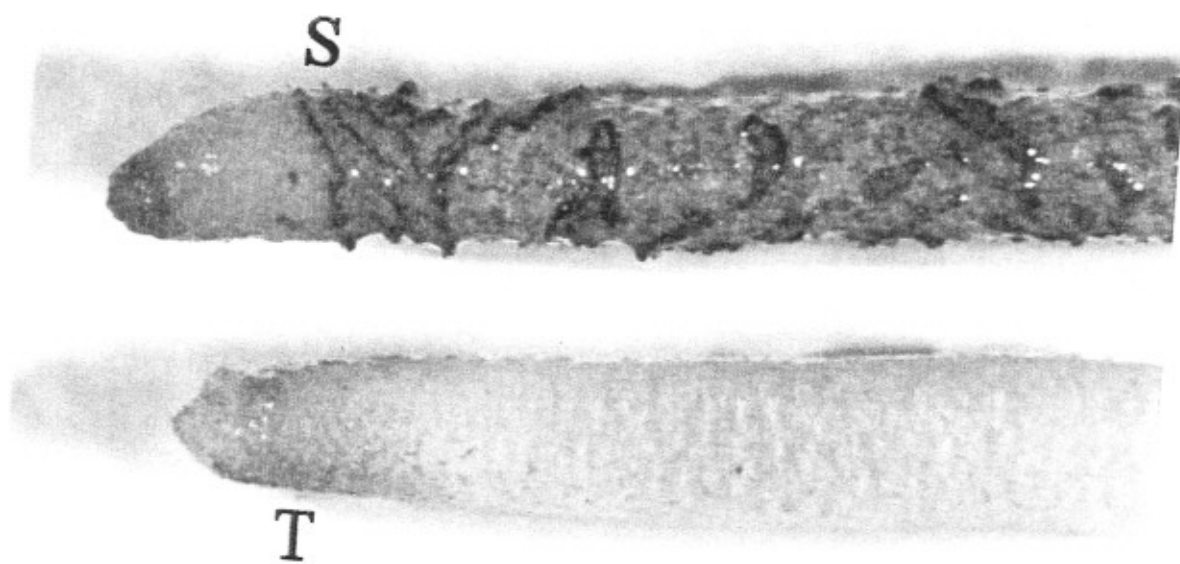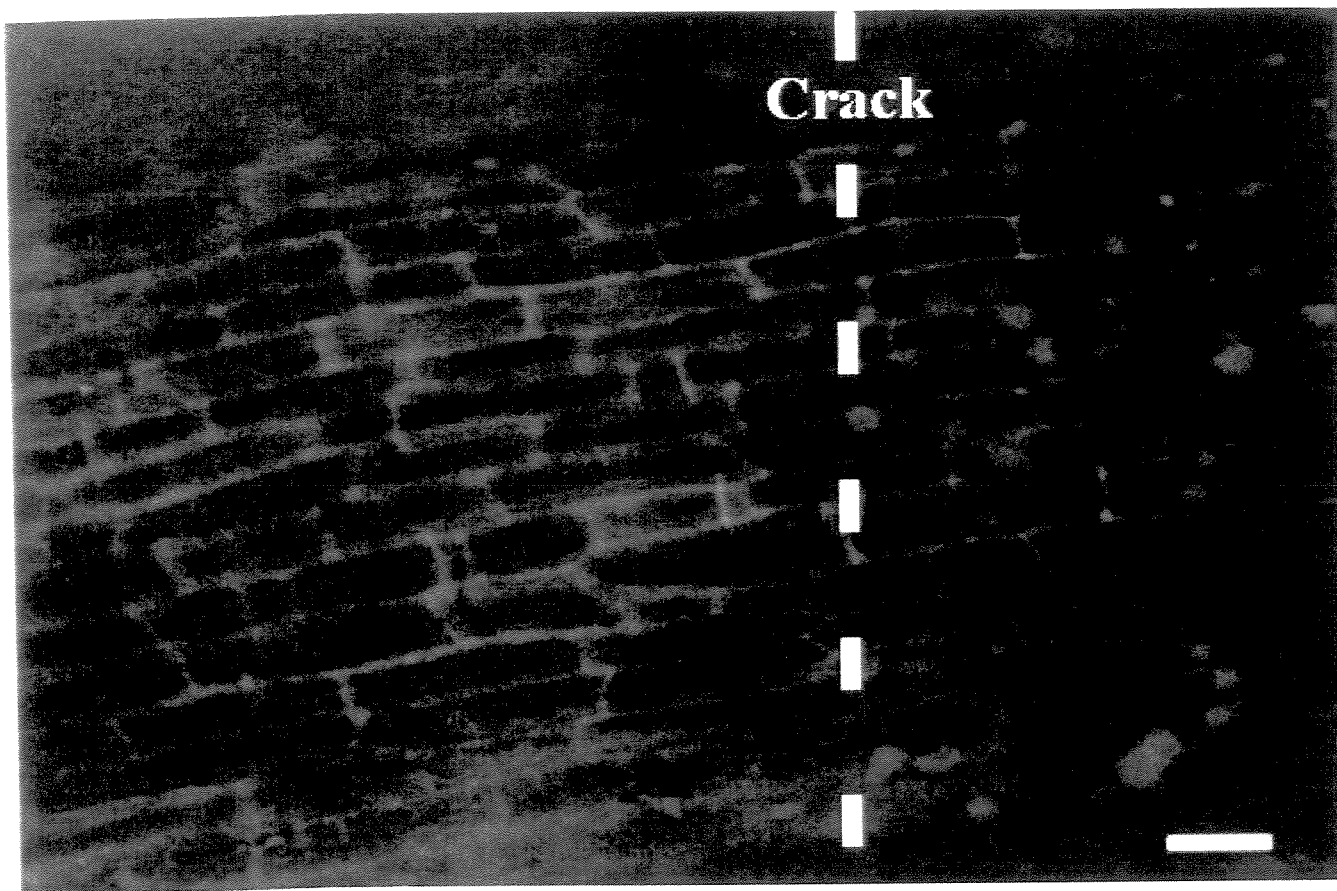
FIG.2
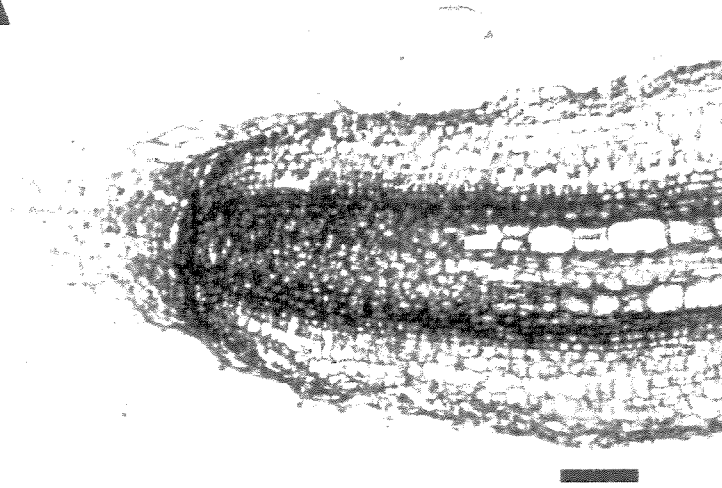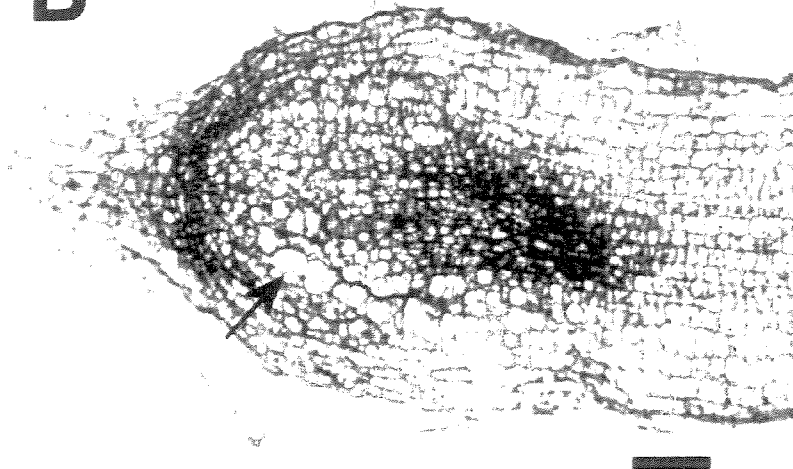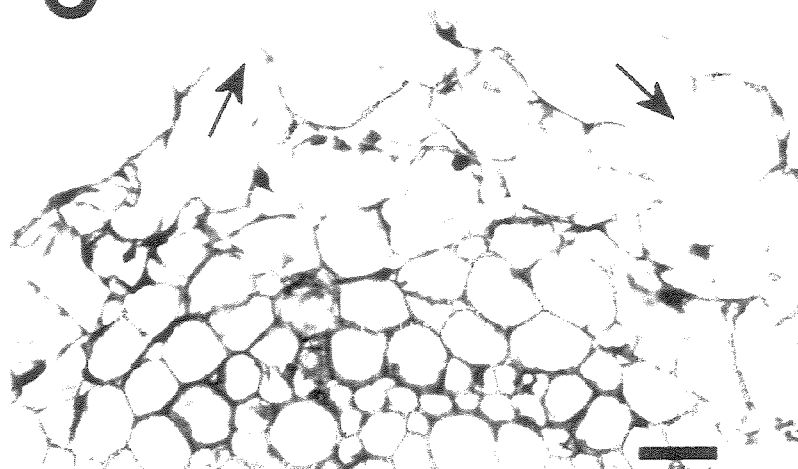
FIG.3

FIG.4
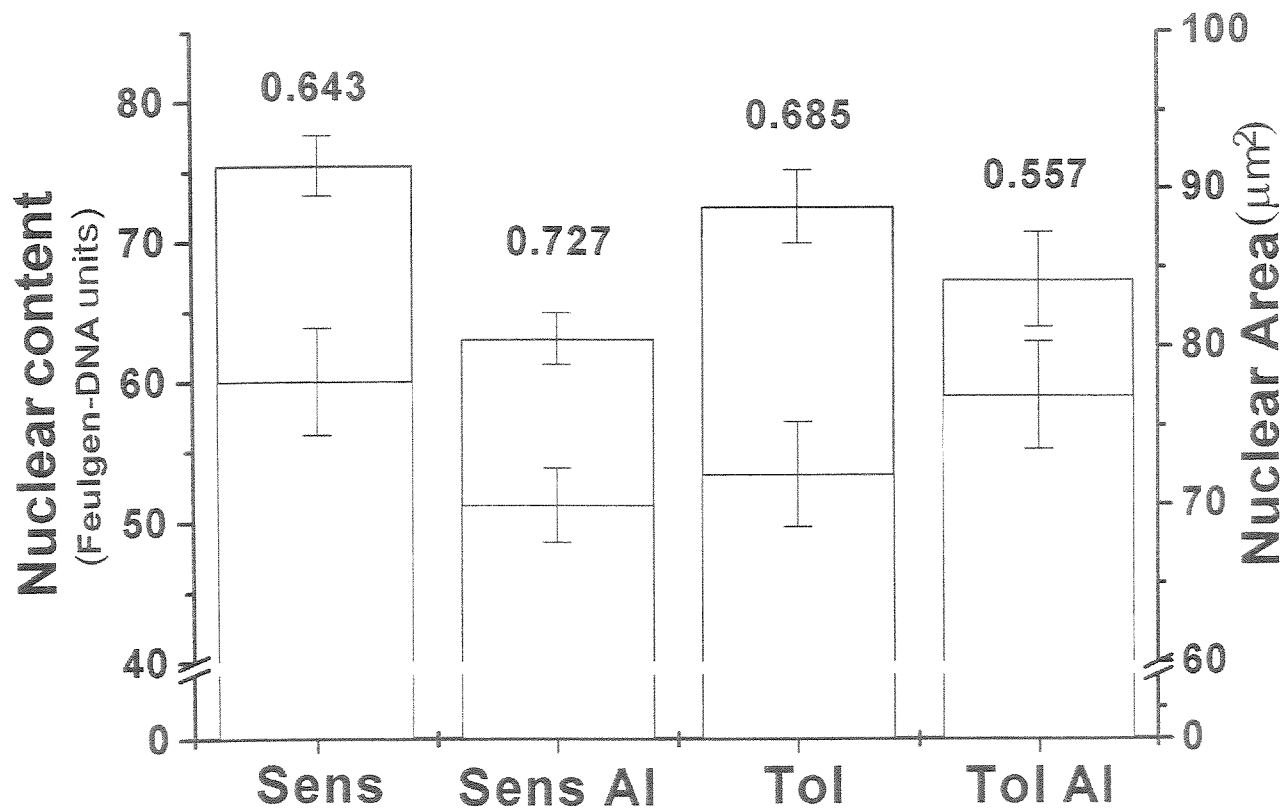
FIG.5
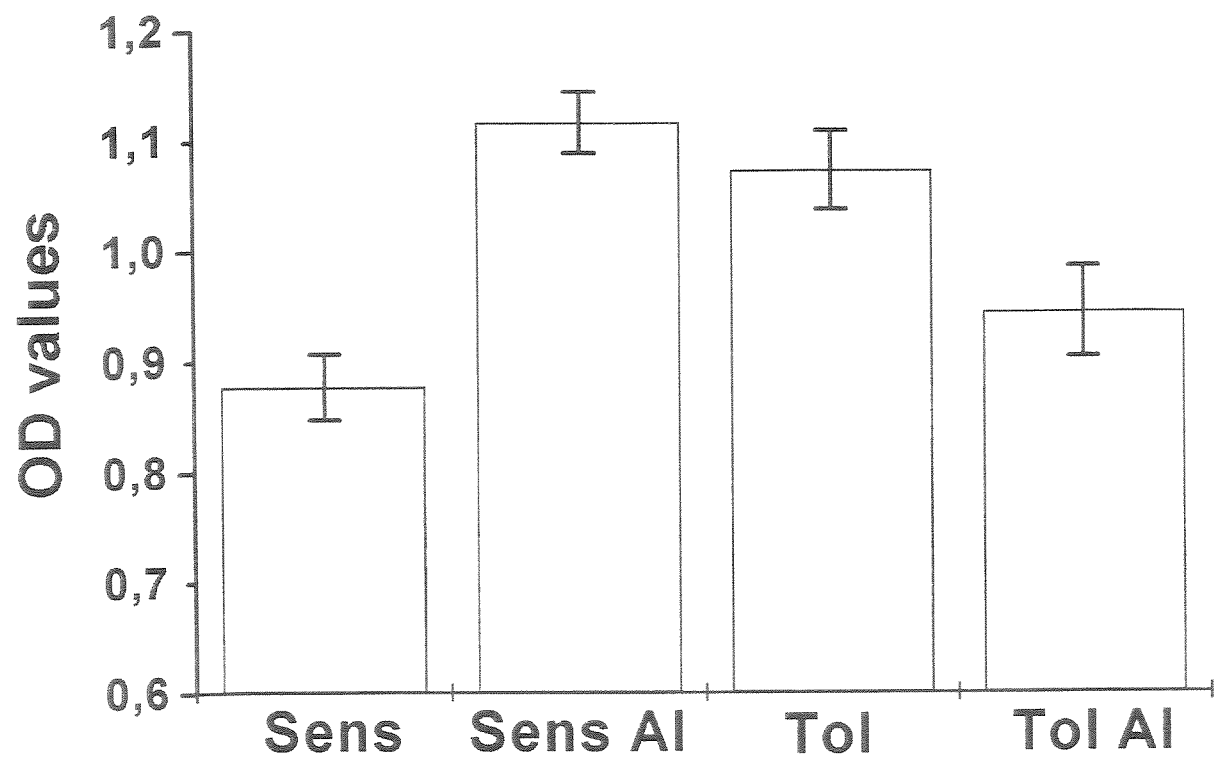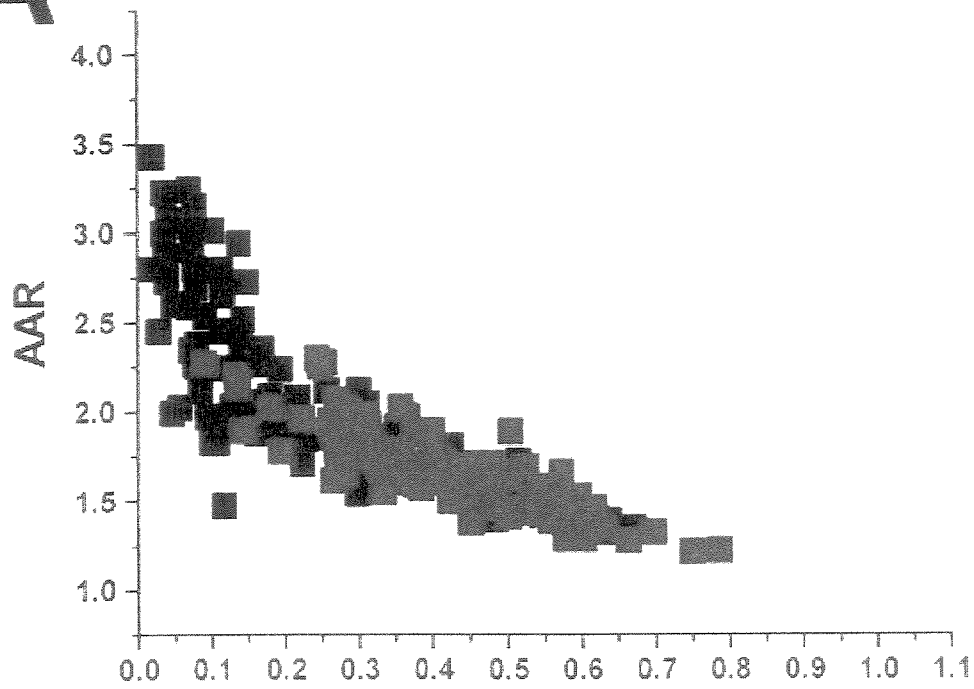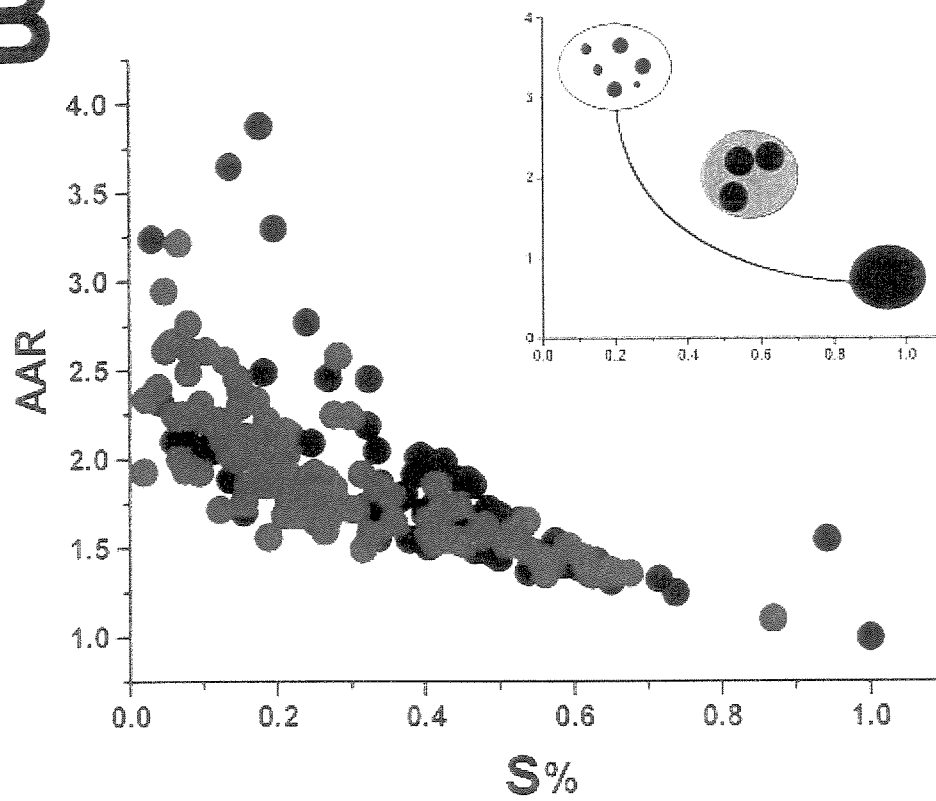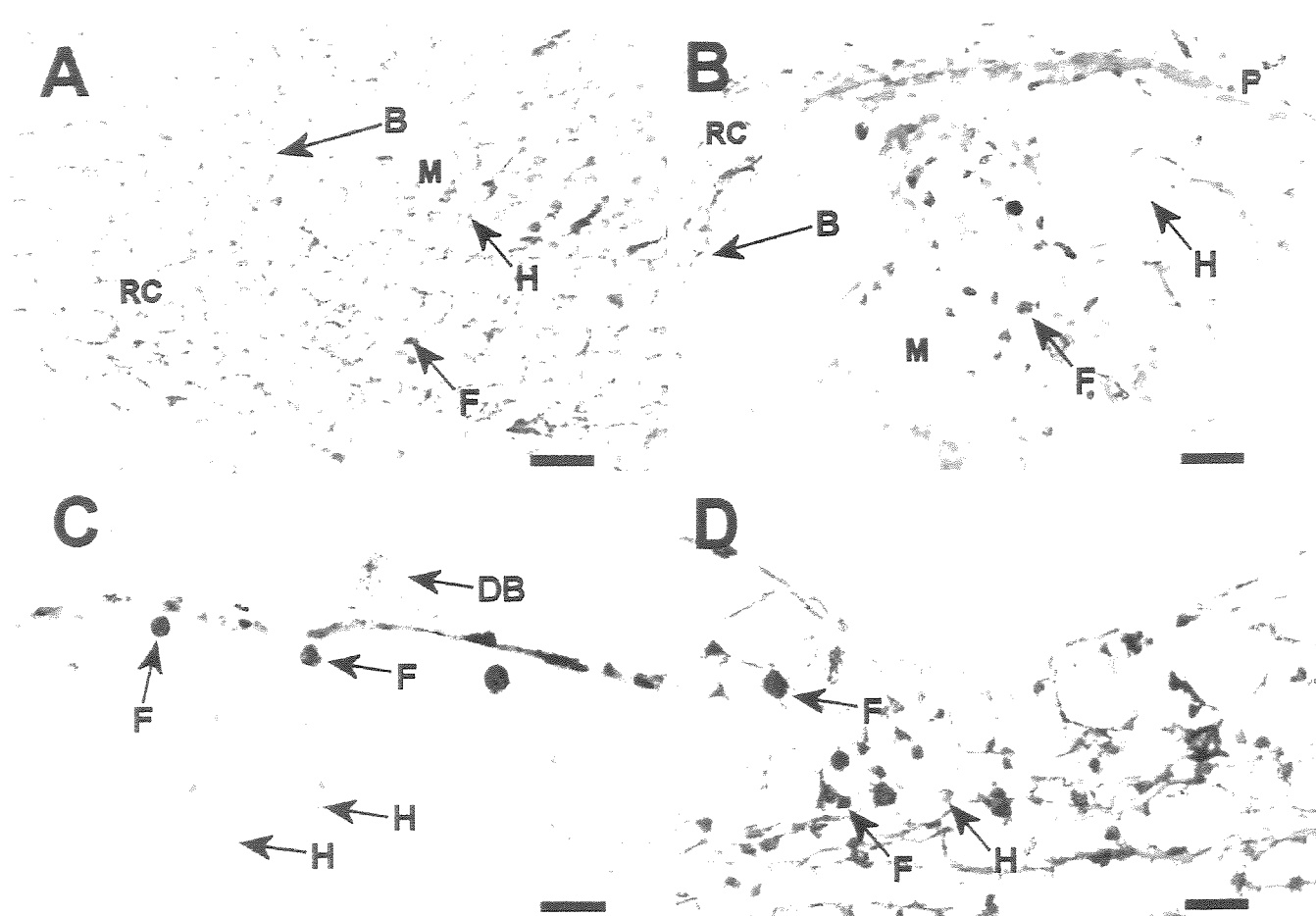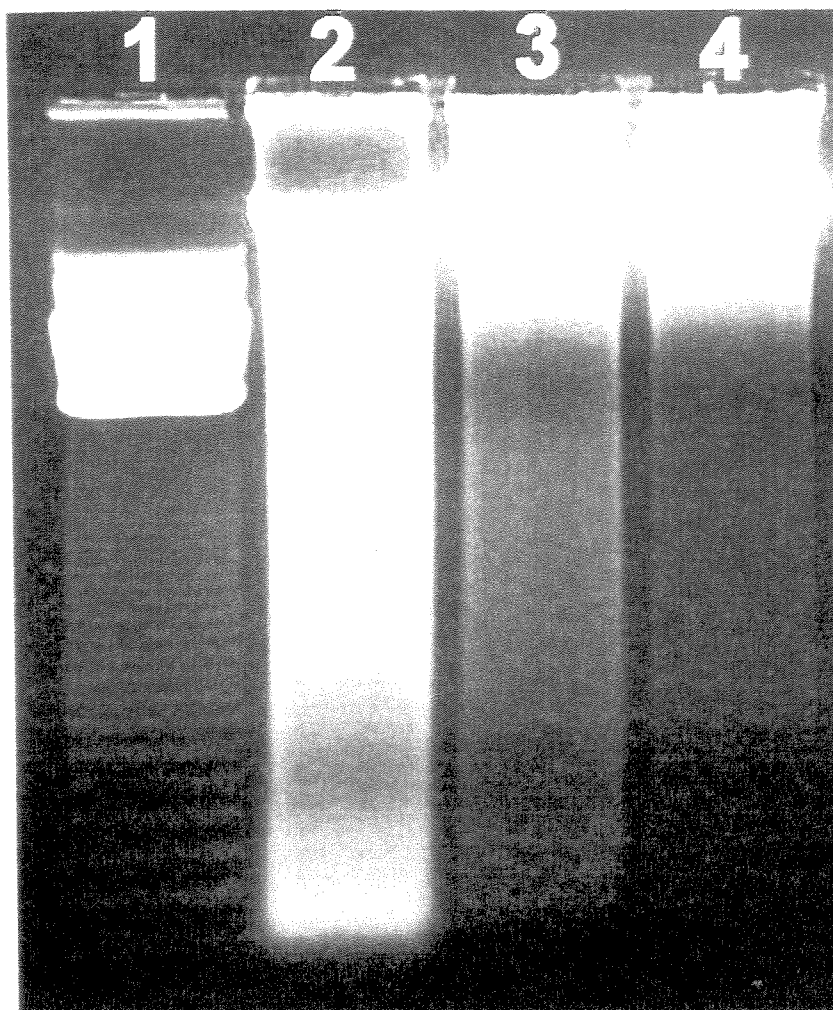
FIG.6

FIG.7

FIG.8

FIG.9

Al triggers necrosis and apoptosis in V79 cells

Pedro H.P.A. Schildknecht* and Benedicto C. Vidal

Departamento de Biologia Celular, Instituto de Biologia, Universidade Estadual de Campinas (UNICAMP), Caixa Postal 6109, 13085-970 Campinas, SP, Brazil..

* To whom correspondence should be addressed: . Phone/fax: (55)(19)3788-6111, e-mail: pedroh@operamail.com

Keywords: aluminium toxicity, apoptosis, necrosis, TUNEL assay, annexin-V.

Abbreviations: Al - aluminium, 8HQ - 8-hydroxyquinoline, PBS - phosphate buffered saline, TUNEL -terminal deoxynucleotidyl transferase-mediated dUTP nick end labeling, IOD - integrated optical density.

Abstract

Aluminium (Al), widely used in antacids, is supported to be involved in several human diseases such as osteomalacia and Parkinson's dementia. The rapid absorption of Al by humans and the competition between this metal and calcium for specific binding sites appear to be the main causes of the adverse effects of Al. In this work, Chinese hamster V79 lung fibroblasts were used to study the toxic effects of different Al concentrations under optimal conditions for ion activity (pH 4.5). Al had a high affinity for the cell nucleus and cytoplasm, as shown by 8-hydroxyquinoline. This is the first time that distinct cell death mechanisms were observed depending on the Al concentration in acid culture medium. Necrosis was detected with 10^{-5}-10^{-3} M Al and apoptosis was observed only at 10^{-8}-10^{-5} M Al. Apoptosis was differentiated from necrosis by image analysis, and by TUNEL and annexin V labeling assays.

Introduction

Aluminium (Al), one of the most abundant elements in the earth's crust and widely used as medication (antacids) for heartburn, is a serious toxicant. The adverse effects of Al have been extensively documented and include several disorders in plants and animals, particularly neurodegenerative diseases in the latter [1-9]. Al can alter intracellular functions by interacting with DNA [10-12] and influencing inflammatory and oxidative events [7].

Al has a higher gastrointestinal absorption rate in Alzheimer's disease [13], which leads to rapid intracellular accumulation [14-16]. The physical and chemical characteristics of Al result in stronger binding to metabolites than that of calcium and magnesium and this explains the efficiency of Al in interfering with some intracellular biochemical pathways [1-9].

Oxidative stress trigger cell death by apoptosis and necrosis [17,18], and Al enhances these events [7,19]. Environmental Al stress results in metabolically altered nuclei in garlic [20], and apoptosis in fish [21] and plants [22,23]. Studies *in vitro* done at pH 7.0-7.4, have shown Al-mediated apoptosis in astrocytes [8,9]. However, the Al concentration necessary to trigger cell death remains controversial [8,9]. The overall solubility and speciation of Al in biological systems is highly affected by the pH of the solution and the most active of Al species (Al^{3+}) is present only at pH < 5.0 [24].

In this work, we used Chinese hamster lung fibroblasts to study the mechanisms of cell death triggered by increasing concentrations of Al^{3+}.

Cell culture and treatment: V79 Chinese hamster lung fibroblasts were plated and grown on glass coverslips immersed in DMEM medium pH 4.5, supplemented with 10% BSA, penicillin (100 U/ml) and streptomycin sulfate (100 μg/ml) in a 5% CO_2 atmosphere at 37°C. After 3 days, $AlCl_3$ was added to the medium to final concentrations of between 10^{-3} M and 10^{-8} M. The cells were harvested after 24 h and washed in 0.9% NaCl, pH 4.5.

Aluminium detection: The slides were stained for 10 min in 0.01% 8-hydroxyquinoline (8HQ), prepared in 50% ethanol [25,26]. The cells were washed free of stain in 50% ethanol and observed under fluorescence microscopy, with excitation at $\lambda = 365$ nm and a $\lambda = 395$ nm barrier filter.

Feulgen reaction: The specimens were subjected to the Feulgen reaction according to Vidal *et al* [27]. Briefly, cells were fixed in ethanol-acetic acid (3:1) and then rinsed in PBS and 70% ethanol. This was followed by the Feulgen reaction, with acid hydrolysis in 4 M HCl at 24°C for 60 min. This length of hydrolysis provided the best staining reaction. After treatment with Schiff reagent, the cells were rinsed in sulfurous water. The preparations were dehydrated, cleared in xylene and mounted in Canada balsam (n_D=1.54). Stained slides were stored in the dark to prevent stain fading. The Feulgen reaction was chosen because its stoichiometric labeling of DNA, which allows the identification, localization and quantification of DNA, in contrast to other methods involving dyes like ethidium bromide or propidium iodide [28].

Image analysis: The image analysis settings were those reported by Vidal *et al* [27]. Images were analyzed using a Zeiss Pol-photomicroscope coupled to equipment for image acquisition, segmentation and highlighting (Global Lab Acquire Software[TM], Marlboro, MA, USA).

The parameters used for image analysis of the Feulgen-stained nuclei included the integrated optical density (IOD) and total nuclear area in μm^2 (S), as described by Vidal *et al* [26,29]. The IOD represents the total optical density of a segmented and digitized nuclear image resulting from the integration of the grey

level values of the segmented area. An IOD value corresponding to 2n nuclei was obtained by measuring the IOD values of a few prophases, with half of the average value obtained (41.12/2) being used as a parameter to identify 2n nuclei. Two hundred interphase nuclei were measured in control and in aluminium-treated cells; disrupted nuclei were not considered.

Detection of cell death: DNA fragmentation in fibroblasts was assessed *in situ* using a TUNEL assay [30] kit (Boehringer-Mannheim, Germany). Annexin-V labeling kit (Boehringer-Mannheim, Germany) was used to detect phosphatidylserine exposed on the extracellular surface of live cells. The integrity of the nuclear envelope was assessed with propidium iodide staining.

Statistical analysis: Each experiment was repeated at least three times. All data were analyzed using the Minitab statistical software (Minitab Inc., State College, PA, USA). A value of $p < 0.05$ and $F > 5.0$ indicated a significant difference in the ANOVA and Mann-Whitney test, respectively.

Results and discussion

After exposure to Al^{3+}, the cells showed a high content of vacuoles which was interpreted as an effort to detoxify the cytoplasm (see Figure 1). Some Al^{3+}-treated cells lacked cytoplasm prolongations and were surrounded by vesicles possibly related to the DNA filled vesicles found after the Feulgen reaction (see Figure 1). Although the mitotic index was not determined, the frequency of cell division decreased after treatment with Al^{3+}.

Aluminium detection. Nucleus and cytoplasm were stained by 8-hydroxyquinoline (8HQ) only in Al^{3+}-treated cells, and this reflected the intracellular accumulation of Al^{3+}, as also detected elsewhere [14-16]. The intensity of intracellular 8HQ-fluorescence increased as the Al^{3+} concentration rose and more Al^{3+} complexes were formed within the cell (Fig. 2).

Although the mechanisms of aluminium entrance into the cell are not completely understood, Al^{3+} is known to cross the cell membrane after 15 min at pH 5.0 [16]. At pH 4.0-5.0, Al^{3+} species predominate in $AlCl_3$ solutions and its activity is 100 times higher than other aluminium species that occur at pH 7.4, where insoluble $Al(OH)_3$ is more abundant [24]. A neutral Al-citrate complex occurs at

pH 3.0 and may help Al^{3+} to cross cell membranes; higher pH values do not favor Al^{3+} transport across membranes [16]. The Al-citrate complex is very stable intracellularly and contributes to Al^{3+} detoxification [31].

Feulgen-stained DNA image analysis. Figure 3 illustrates DNA-filled vesicles and nuclear buds that were observed in Feulgen-stained nuclei after $AlCl_3$ treatment. The DNA-filled vesicles may have originated from nuclear buds and can be considered as micronuclei. Nuclear fragments with highly condensed chromatin were also observed and were related to apoptotic death.

The integrated optical density (IOD) values, which correspond to nuclear DNA content [27, 29], decreased after Al^{3+}-treatment, indicating a loss of DNA as a result of Al^{3+} toxicity (Fig. 4). The decrease in DNA content may have occurred through nuclear budding and micronuclei formation (Fig. 3), and is shown in figures 4 and 5 by IOD values under 5.0. The variation in the IOD values of control cells probably reflected the presence of different cell cycle phases and physiological conditions, as discussed by others [27,29]. This study was not designed to examine the cell cycle; the IOD values for diploid cells were determined as stated in the methods. Cells with IOD values around 20 were considered to be interphasic and diploid, whereas cells with IOD values around 40 were regarded as interphasic tetraploid or S phase diploid cells, as seen in Figures 4 and 5. The latter population of cell was drastically reduced after treatment with Al^{3+} probably because of the inhibition of cell division and DNA synthesis. The nuclear area was generally reduced after exposure to Al^{3+} as a consequence of DNA loss (from mean values of 38.8 $\mu m^2 \pm$ 12.6 in control cells to 31.0 $\mu m^2 \pm$ 12.4 in treated cells, $p=$ 0.008, F=7.13).

The relationship between nuclear area and IOD (which represents the DNA content) provides an efficient tool for monitoring the chromatin packing levels. Since a Feulgen-positive nucleus cannot exist without DNA, two nuclei of similar area but different IOD values necessarily have distinct levels of chromatin packing. The variation in nuclear areas for a similar DNA content was greatly reduced after treatment with Al^{3+}, as observed in Figure 5. The dispersion of values around the fitted line was assessed by regression (R^2) and correlation (r) analyis, with a value of 100% indicating total correlation, 0% indicating a complete absence of correlation. Using these values, the variability in the chromatin packing levels of control cells was significantly reduced after exposure to Al^{3+}, suggesting higher

levels of chromatin condensation in treated cells. An increase in chromatin packing and nuclear shrinkage are typical apoptotic features and were confirmed by the TUNEL and annexin-V labeling assays.

Detection of cell death. Cell death was assessed by the extent of chromatin fragmentation, which reflects both apoptosis and necrosis, and by the translocation of phosphatidylserine from the inner surface of the plasma membrane to the outer surface in intact cells, a feature only of apoptosis.

The TUNEL assay provides a highly accurate estimate of chromatin fragmentation in single cells and is widely used in apoptosis detection [9,30]. No fragmented chromatin was observed in control cells. All Al^{3+} treatments induced chromatin fragmentation, although the extent varied according to the metal concentration. At low $AlCl_3$ concentrations (10^{-8}-10^{-6} M), nuclei with slightly fragmented chromatin were seen and were considered as apoptotic (Fig. 6). Cells treated with higher concentrations (10^{-4}-10^{-3} M) showed intense chromatin fragmentation, particularly with 10^{-3} M, and represented necrotic cells (Fig. 6). At 10^{-5} M $AlCl_3$, the cells showed fragmented chromatin that represented both apoptosis and necrosis, as showed by annexin V labeling.

Annexin-V is a Ca^{2+}-dependent phosphatidylserine-binding protein that can be used as a sensitive probe to detect apoptosis in live cells since the phospholipid translocation to the outer cell surface occurs in the early stages of apoptosis. Propidium iodide can be used to evaluate the integrity of the cell membrane. Neither apoptosis nor necrosis was detected in control cells. Cells treated with 10^{-8}-10^{-6} M of $AlCl_3$ showed increasing levels of apoptosis, but no necrosis. At 10^{-5} M of $AlCl_3$, both apoptosis and necrosis were detected, whereas at higher Al^{3+} concentrations only necrotic cells were observed (Fig. 7). These results suggest a dose-dependent nature for Al^{3+} toxicity. High concentrations of Al^{3+} can cause a failure of cell homeostasis, as this metal can displace Ca^{+2} and Mg^{+2} from their binding sites [32], and induce necrosis [18]. At low concentrations of Al^{3+}, apoptosis results not from a metabolic collapse as in necrosis, but from the binding of Al^{3+} to DNA [10-12] and from a tendency to favor the oxidative stress produced by iron [7,19]. Since Al^{3+} complexes tightly with DNA and is not displaced by bivalent cations, long-term exposure to very low doses of Al^{3+} ($<10^{-8}$ M) could lead to the accumulation of Al-complexes within the cell and result in cell death.

The activity of the Al species has a considerable influence on the results obtained in studies of toxicity of this cation. In consequence, reports have described healthy, or strictly apoptotic cells, at very high $AlCl_3$ concentrations (e.g. 0.2 mM [9] and 1 mM [8]). The real toxicity was masked by the high pH and the use of citrate-buffered culture media or stock solutions without chemicals to prevent Al^{3+} hydrolysis [24]. To the author's knowledge, this is the first report to assess cell death at pH environments with high Al^{3+} activity. Other salts, as aluminium gluconate or aluminium maltolate, should be used when high pH values are unavoidable [24], otherwise the Al^{3+} activity will be reduced because of its precipitation as inactive $Al(OH)_3$.

In this work, we found that aluminium toxicity was triggered apoptosis and necrosis, depending on the Al^{3+} concentration, in a low pH environment. Long-term exposure to very low amounts of Al^{3+} could also result in cell death.

References

1. H. Matsumoto, *Int. Rev. Cytol.* **200**, 1 (2000).

2. E.H. Jeffery, K. Abreo, E. Burgess, J. Cannata, and J.L. Greger, *J. Toxicol. Environ. Health.* **48**, 649 (1996).

3. C. Exley, *J. Inorg. Biochem.* **76**, 133 (1999).

4. C. Exley and J.D. Birchall, *J. Theor. Biol.* **159**, 83 (1992).

5. D. Julka and K.D. Gill, *Biochim. Biophys. Acta* **1315**, 47 (1996).

6. E. Altschuler, *Med. Hypoth.* **53**, 22 (1999).

7. A.Campbell and S.C. Bondy, *Cell. Mol. Biol.* **46**, 721 (2000).

8. M.B. Suárez-Fernández, A.B. Soldado, A. Sanz-Medel, J.A. Vega, A. Novelli and T. Fernández-Sánchez, *Brain Res.* **835**, 125 (1999).

9. G.W. Guo and Y.X. Liang, *Brain Res.* **888**, 221 (2001).

10. S.J. Karlik, G.L. Eichhorn, P.N. Lewis and D.R. Crapper, *Biochemistry* **19**, 5991 (1980).

11. K.S.J. Rao and B.S. Rao, *Biochim. Biophys. Acta* **1172**, 17 (1993).

12. H. Matsumoto and S. Morimura, *Plant Cell Physiol.* **21**, 951 (1980).

13. P.B Moore, J.P. Day, G.A. Taylor, I.N. Ferrier, L.K. Fifield and J.A. Edwardson, *Dement. Geriatr. Cogn. Disord.* **11**, 66 (2000).

14. U. DeBoni, J.W. Scott and D.R. Crapper, *Histochemistry* **40**, 31 (1974).

15. I.R. Silva, J.T. Smyth, D.F. Moxley, T.E. Carter, S.N. Allen and T.W. Rufty, *Plant Physiol.* **123**, 543 (2000).

16. J.K.S. Rao and K.R.K. Easwaran, *Mol. Cell. Biochem.* **175**, 59 (1997).

17. M. Pallardy, M. Perrin-Wolff and A. Biola, *Toxicol. In Vitro* **11**, 573 (1997).

18. M. Raffray and G.M. Cohen, *Pharmcol. Ther.* **75**, 153 (1997).

19. T. Ohyashiki, S. Suzuki, E. Satoh and Y. Uemori, *Biochim. Biophys. Acta* **1389**, 141 (1998).

20. K.A. Roy, A. Sharma and G. Talukder, *Mutat. Res.* **227**, 221 (1989)

21. C. Exley, J.S. Chappel and J.D. Birchall, *J. Theor. Biol.* **151**, 417 (1991).

22. P.H.P.A. Schildknecht and B.C. Vidal, *Gen. Mol. Biol.* **23**, 365 (2000)

23. J.W. Pan, M. Zhu, H. Chen, *Environ. Exp. Bot.* **46**, 71 (2001).

24. W.R. Harris, G. Berthon, J.P. Day, C. Exley, T.P. Flaten, W.F. Forbes, T. Kiss, C. Orvig and P.F. Zatta, *J. Toxicol. Environ. Health.* **48**, 543 (1996).

25. A.R. Llorente, P. Del Castillo and J.C. Stockert, *J. Microsc.* **155**, 227 (1989).

26. P. Del Castillo, A.R. Llorente, A. Gómez, J. Gosálvez, V.J. Goyanes and J.C. Stockert, *Anal. Quant. Cytol. Histol.* **12**, 11 (1990).

27. B.C. Vidal, J. Russo and M.L.S. Mello, *Exp. Cell Res.* **244**, 77 (1998).

28. M.L.S. Mello, *Braz. J. Genet.* **20**, 257 (1997).

29. B.C. Vidal, W.J. Silva and P.C. Strikis, *Cell. Mol. Biol.* **30**, 11 (1984).

30. F. Labat-Moleur, C. Guillermet, P. Lorimier, C. Robert,.S. Lantuejoul, E. Brambilla and A. Negoescu, *J. Histochem. Cytochem.* **46**, 327 (1998).

31. J.F. Ma, P.R. Ryan and E. Delhaize, *Trends Plant Science* **6**, 273 (2001).

32. D.L. Godbold and G. Jentschke, *Physiol. Plantarum* **102**, 553 (1998).

Figure Captions

FIG. 1. Control (A) and $AlCl_3$ (10^{-5} M) - treated (B) V79 cells under phase-contrast microscopy. A treated cell without cytoplasmatic connections and surrounded by vesicles is showed in B (arrow). Bar = 50 μm.

FIG. 2. V79 cells grown in 0 (A), 10^{-8} (B), 10^{-7} (C), 10^{-6} (D), 10^{-5} (E) and 10^{-4} (F) M $AlCl_3$ and stained with 8HQ for Al^{3+} detection. Heavily stained cells, indicating a high aluminium content, are partially detached from the glass surface and show no cytoplasm prolongations (arrow 1 in D, E and F). Some morphological abnormalities induced by $AlCl_3$ are also visible (arrow 2 in E and F). Bar = 50 μm.

FIG. 3. A) Control V79 cells stained by the Feulgen reaction. Mitosis was frequent in all preparations (arrow 1). B) Feulgen-stained V79 cells grown in 10^{-5} M $AlCl_3$. Micronuclei and nuclear buds (arrow 2) were seen, as well as apoptotic bodies (arrow 3) Bar = 25 μm.

FIG. 4. IOD average values (corresponding to DNA content) and S.D. of control and Al (10^{-5} M)-treated V79 cells.

FIG. 5. Regression of nuclear area (μm^2) versus IOD of control (A) and Al (10^{-5} M) -treated (B) cells. The regression (R^2) and correlation (r) coefficients are given for each graph.

FIG. 6. V79 cells subjected to the TUNEL assay. No chromatin fragmentation was detected in control cells (A). The treatment with 10^{-8} (B), 10^{-6} (C), 10^{-5} (D), 10^{-4} (E) and 10^{-3} (F) M $AlCl_3$ resulted in TUNEL-positive cells. Bar = 50 μm.

FIG. 7. V79 cells labeled with annexin-V and stained with propidium iodide. The cells were grown in 10^{-8} (A), 10^{-7} (B), 10^{-6} (C), 10^{-5} (D), 10^{-4} (E) and 10^{-3} (F) M $AlCl^3$. Only necrotic cells are stained by propidium iodide. Bar = 50 μm.

FIG.1

FIG.2

FIG.3
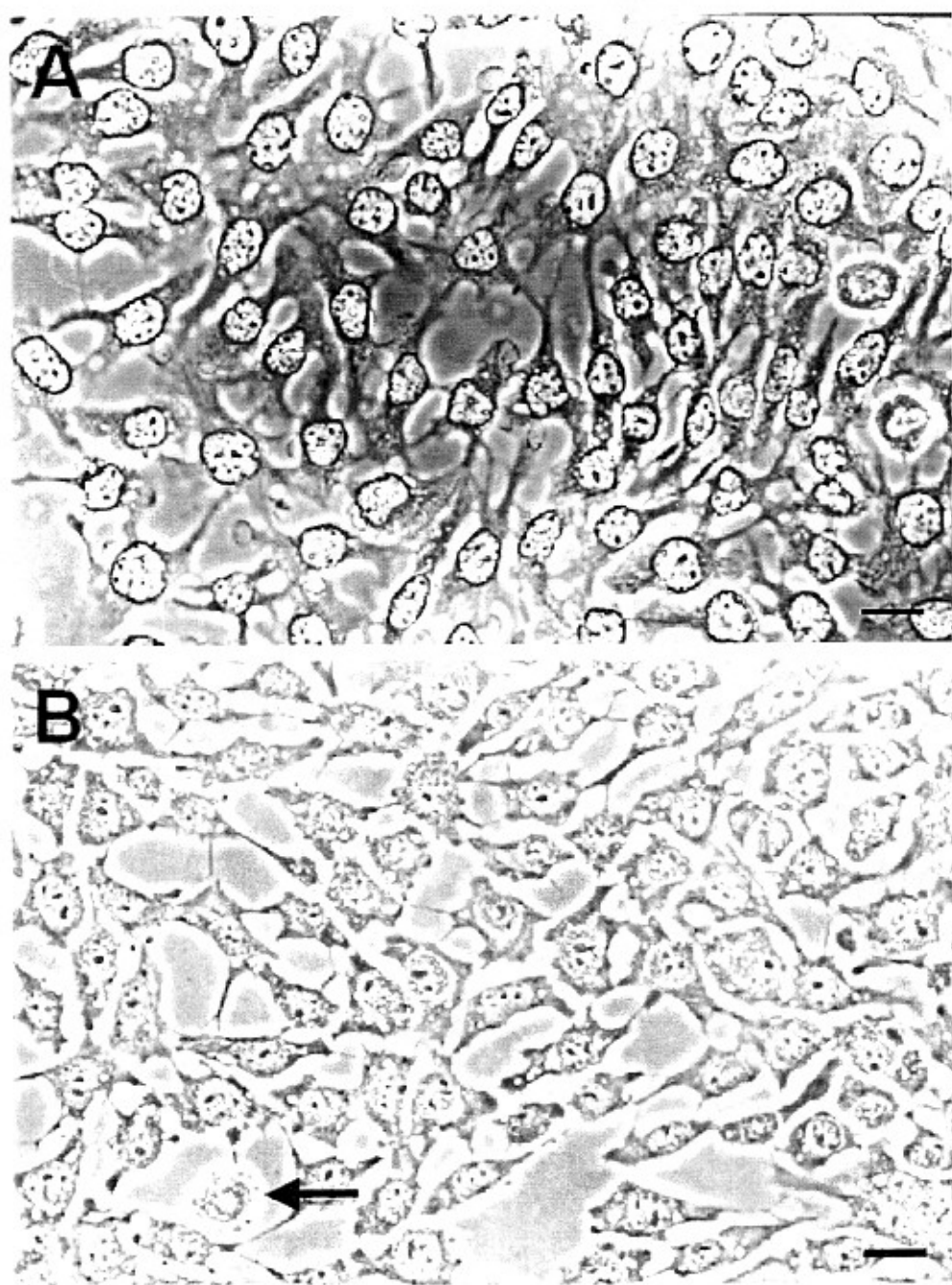
FIG.4
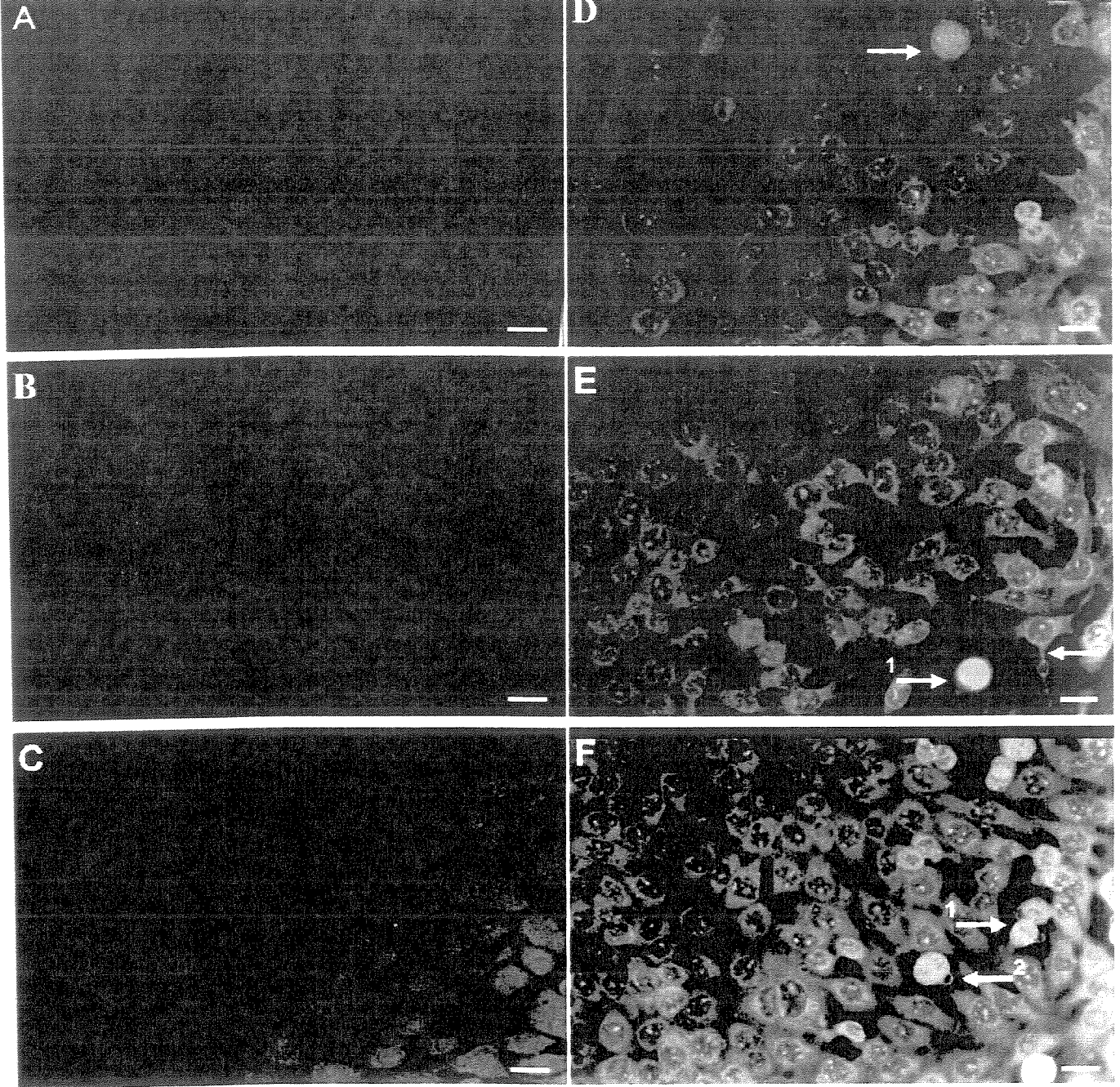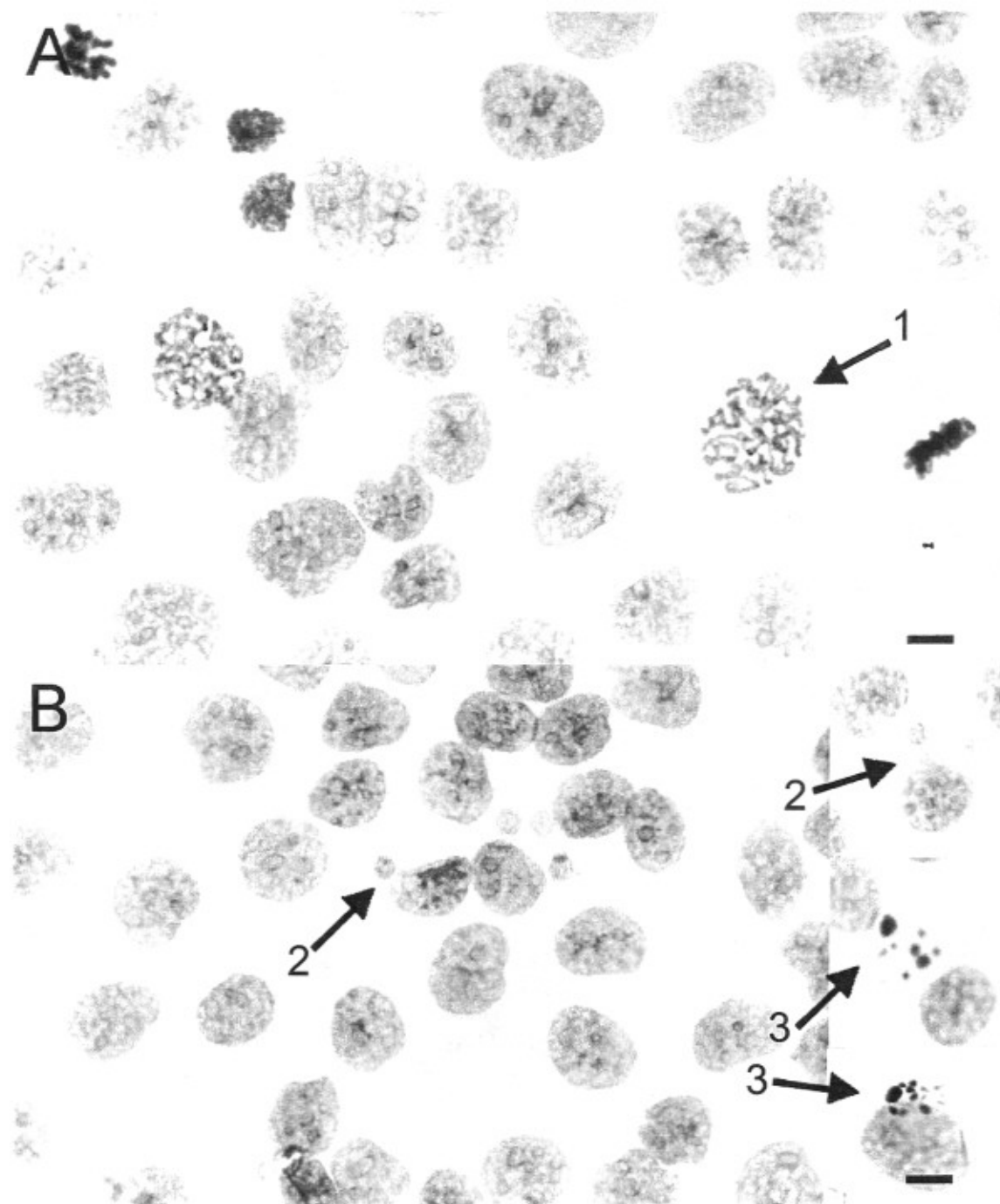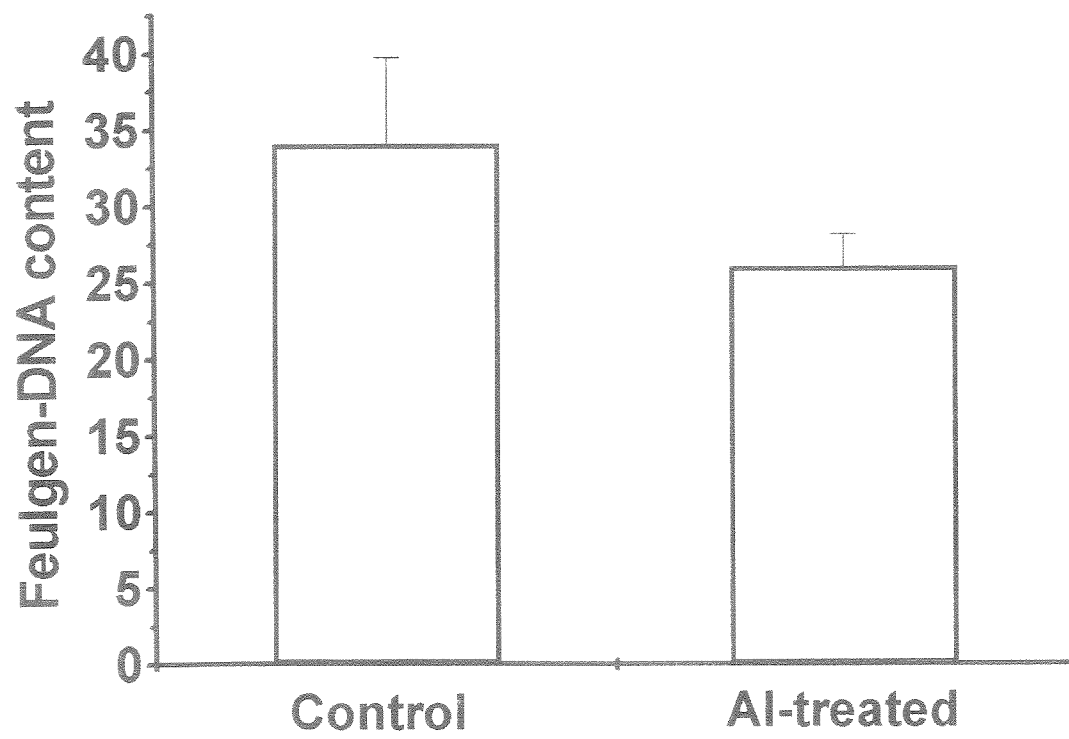
A Control

r = 0.722
R^2=0.522
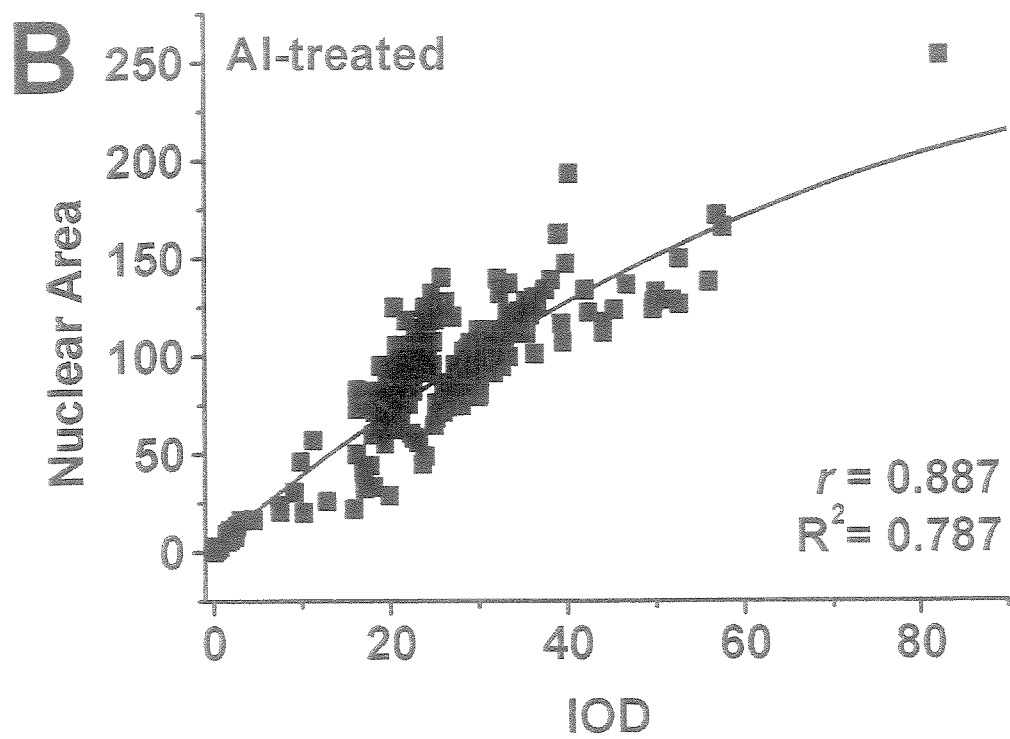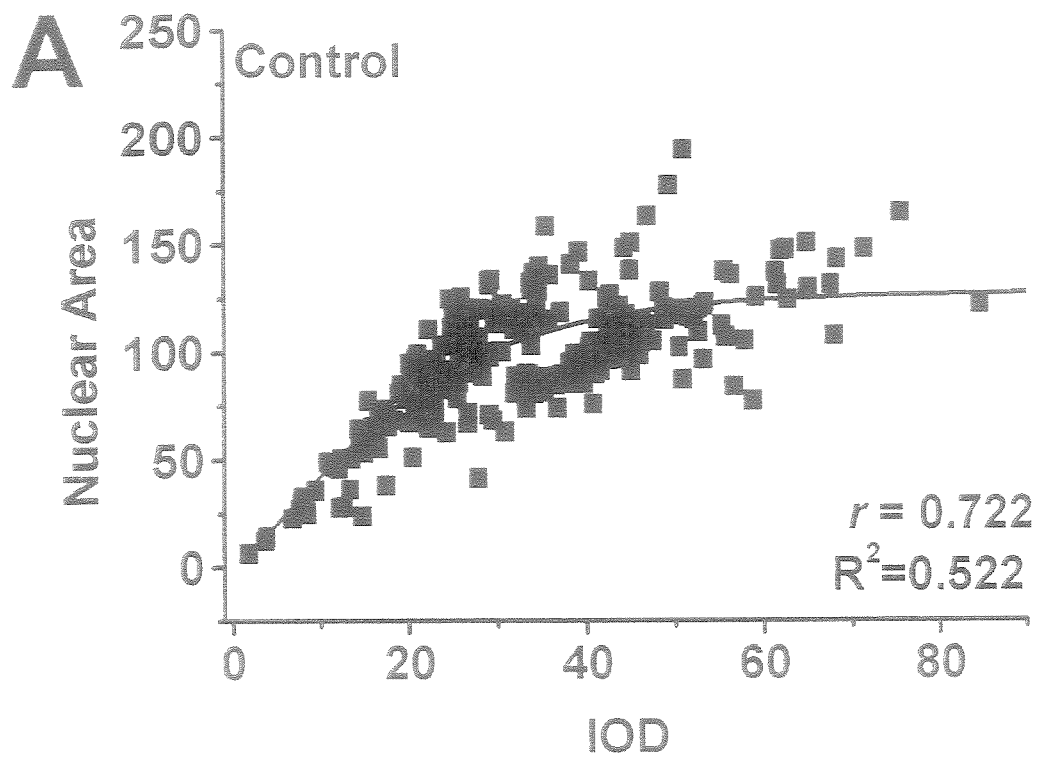
IOD
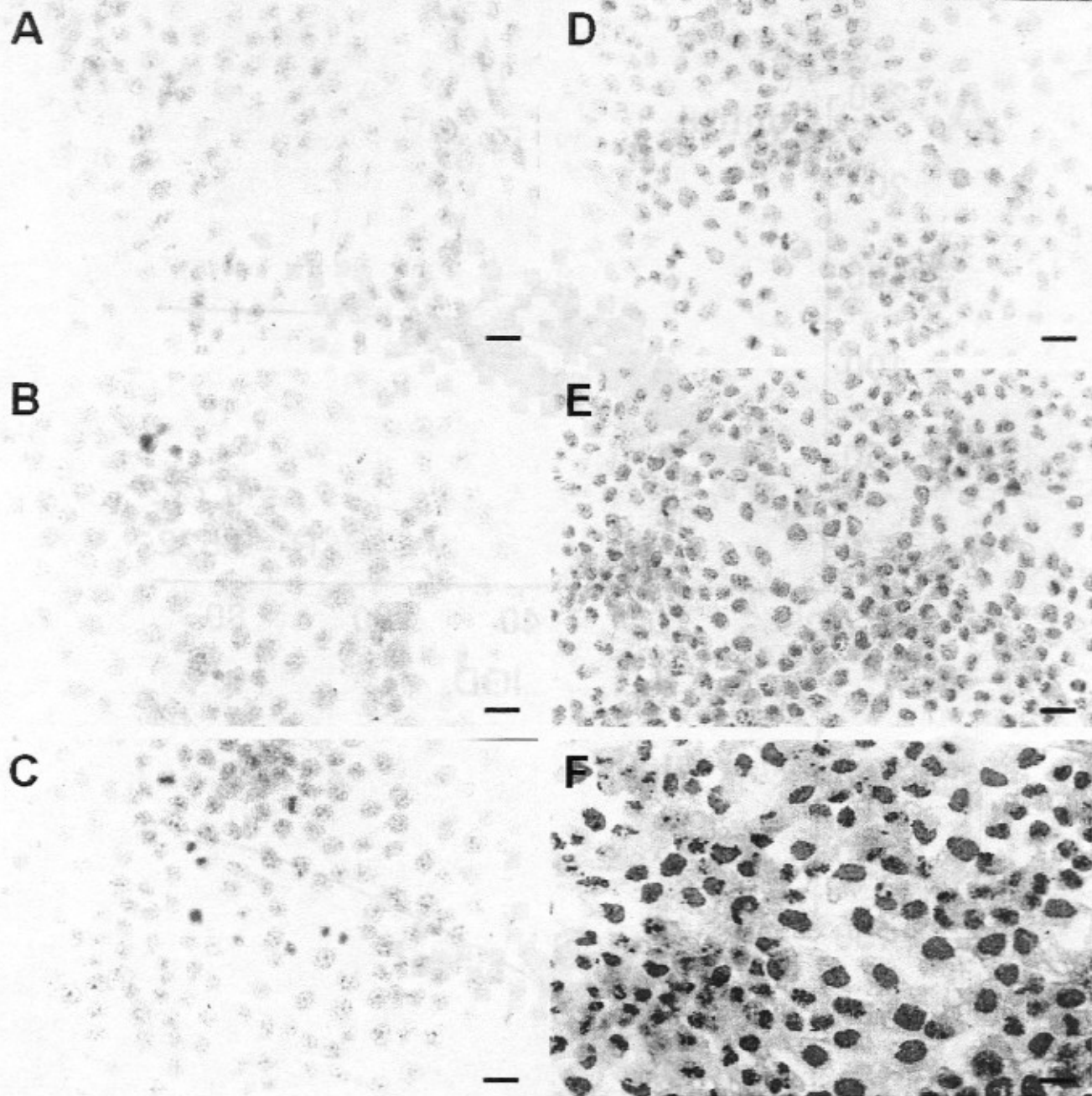
B Al-treated

r = 0.887
R^2 = 0.787

IOD

FIG.5

FIG.6

FIG.7
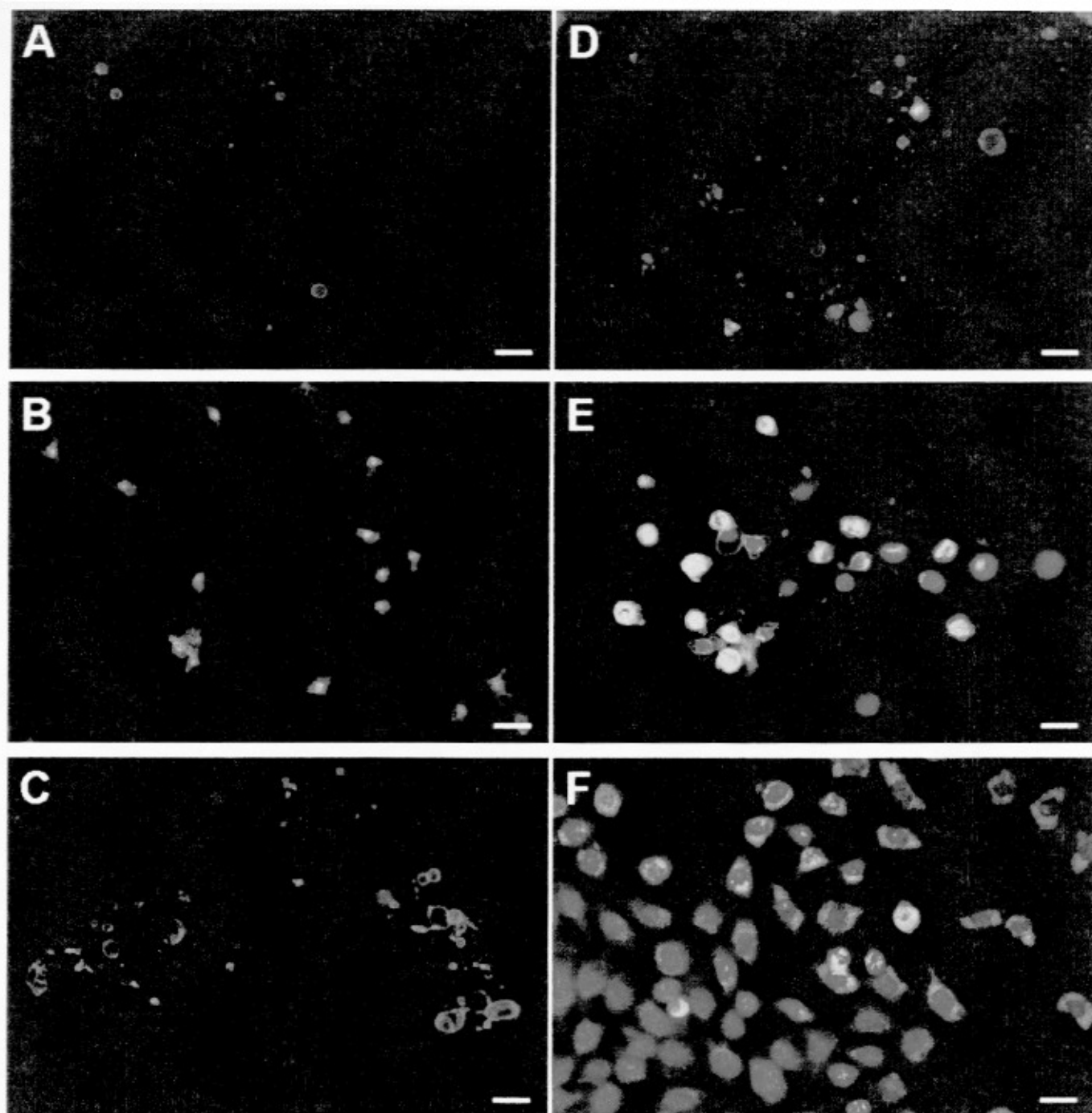
ANNEXIN V AND COMET ASSAY DETECTION OF VIOLACEIN-INDUCED APOPTOSIS

Pedro H.P.A. Schildknecht* and Benedicto C. Vidal

[1]Departamento de Biologia Celular, Instituto de Biologia, Universidade Estadual de Campinas (UNICAMP), CP 6109, Campinas, SP 13085-970, Brazil.

* To whom correspondence should be addressed: pedroh@unicamp.br or pedroh@operamail.com. Phone +551937886124, Fax +551937886111.

Abstract

Although violacein is known to cause chromatin fragmentation and death of cells, the mechanism of cell death is still to be determined. Annexin V/propidium iodide labeling and the comet assay were used to analyse the violacein toxicity. No necrosis was detected by propidium iodide staining. Apoptotic nuclei were labeled by annexin V, and the results agreed with those with the Comet assay in weak alkaline solution. Characteristic apoptotic nuclear phenotypes were obtained from violacein-treated cells just lysis step. The use of annexin V/propidium iodide staining together with the Comet assay provided a fast, reliable means of characterizing cell death. Chromatin fragmentation and the externalization of phosphatidylserine were visualized by annexin V/propidium iodide staining after less than 48 h of exposure to violacein.

Keywords: annexin-v, apoptosis, comet assay, single cell gel eletrophoresis (SCGE), violacein.

Introduction

The morphological characteristics of apoptosis include cell shrinkage, membrane blebbing, nuclear condensation and the emergence of apoptotic bodies (Wyllie I et al. 1981, Palardy et al. 1997, Raffray & Cohen 1997, Maria et al. 2000). In contrast to necrosis, apoptosis is an active process with well organized, regulated biochemical events, involving cell signaling and ordered enzyme cascades (Raffray & Cohen 1997).

The treatment of currently incurable human cancers and the improvement of therapy for other diseases, such as Chagas' disease, represent important applications for the knowledge about apoptosis. Rather than promoting a general, irretrievable collapse of cellular homeostasis and necrosis, as usually occurs with chemotherapics, apoptosis-triggering drugs such as violacein (Melo et al. 2000) induce less pronounced tissue damage but with a similar therapeutic effect .

Apoptosis has been detected by agarose gel electrophoresis , as well as histochemical (Wyllie I et al. 1980, Koopman et al. 1994, Mello 1999), cytochemical (Singh et al. 1988, Singh 2000) and immunochemical (Gavrieli et al. 1992, Mello et al. 2000) methods as discussed by Singh (2000). In this work, violacein-induced apoptosis was detected using the Comet assay and annexin V labeling. This approach provided a fast, accurate method for assessing chromatin fragmentation and biochemical modifications present in apoptotic cells.

Results and Discussion

Violacein, a pigment produced by *Chromobacterium violaceum*, is a potential drug for treating leukemia, lymphoma cells and Chagas' disease (*Melo et al.* 2000). The antitumoral and apoptotic-promoting activities, as well as the National Cancer Institute assays for validation of violacein were described by Melo et al. (2000). Based on these results, violacein is a useful tool for studying apoptosis.

The labeling of apoptotic cells with annexin V conjugated to fluorescein isothiocyanate

112

is very useful for detecting apoptosis (Koopman *et al.* 1994). Annexin V is a Ca^{2+}-dependent protein with a strong affinity for phosphatidylserine (PS), which is externalized in the early stages of apoptosis (Koopman *et al.*, 1994). In non-apoptotic cells, PS is present only on the inner surface of the membrane and false positive results may occur if the membrane is damaged, as occurs in necrotic cells. Cell damage and false positive PS labeling were assessed by staining with propidium iodide which does not enter an intact cell.

Positive labeling by annexin V (indicative of apoptotic cells) was rare in control culture. The apoptotic cells were usually detached from the coverslip, probably as a result of cell-cell interactions (Park *et al.* 1999, Maria *et al.* 2000). Violacein-treated cells were round and smaller than control cells, and showed no citoplasmic prolongations (Fig. 1). The cell shrinkage observed was typical of apoptotic cells (Loo & Rillena, 1998, Maeno *et al.* 2000). In agreement with a previous report (Melo *et al.* 2000), no micronuclei was seen; this absence appears to be peculiar to violacein toxicity. About 50% of the cells treated with violacein were positive for annexin V labeling, but no necrosis was observed after propidium iodide staining of control or violacein-treated cultures. The possibility of triggering apoptosis without necrosis reinforces the usefulness of violacein as a therapeutic agent and a tool in apoptosis research.

The Comet assay (single cell gel electrophoresis) is a fast, reliable method for detecting DNA damage in individual cells (Singh 1988, Olive *et al.* 1992, Klaude *et al.*, 1996). Alkaline lysis followed by a weak alkaline medium for DNA unwinding and electrophoresis enhanced the sensitivity of the test (data not shown), in agreement with Olive *et al.* (1992). Good results were also obtained if TAE buffer (40 mM Tris-acetate, 1 mM EDTA, pH 8) was used instead of alkaline buffer during electrophoresis (data not shown).

After lysis and chromatin unwinding, the nuclei of control cells were uniformly stained by propidium iodide, with small "halos" of DNA (Fig. 2). The "halo" phenotype resulted form the removal of histone by the high-salt concentration lysis solution which allowed chromatin loops to disperse within and outside the nuclei while still attached to nuclear

matrix proteins and to the nuclear envelope (Olive *et al.* 1992, Vidal 2000). Violacein-treated cells had a granular appearance and the higher level of DNA condensation meant there were no halos (Fig. 2). The apoptotic nature of violacein-treated cells was clearly seen in some nuclei showing the marginalization of chromatin at the periphery of the nuclear envelope (Fig. 2). The extent of chromatin diffusion in agarose gels was also useful for distinguishing healthy cells from apoptotic and necrotic cells, as reported by Singh (2000).

Apoptosis was also assessed after electrophoresis with the cells being classified according to their tail extent, as described in experimental procedures (Fig. 3). Although some subjectivity is involved in classifying nuclei as type 1 or 2 or as type or 3 or 4, it is unlikely that a normal nucleus (type 1 and 2) was mistakenly identified as apoptotic (type 3 or 4) or vice versa, because of the marked difference in the nuclear appearance of these two groups. Thus, the interpretation of the Comet assay without the need for image analysis makes this a fast, reliable and non-expensive method.

The Comet assay showed that control cells had few nuclei with fragmented chromatin whereas a high number of nuclei had no detectable tail (type 1 and 2) (Fig. 4). Apoptotic nuclei (type 3 and 4) were more frequent in violacein-treated cells. These results reinforce those obtained with annexin V labeling and confirm previous data suggesting that the expressive chromatin fragmentation in violacein-treated cells was a consequence of apoptosis (Melo *et al.* 2000).

Conclusions

Our results showed that violacein was a potent inducer of apoptosis and its use in apotosis research is recommended. Annexin V and the Comet assay provide a fast and efficient tools for studying apoptosis in animal cells and may be of diagnostic use in the future.

Experimental procedures

Cell culture. For annexin V labeling, V79 Chinese hamster lung fibroblasts (clone M-8) were plated on coverslips in 5 ml of Dulbecco's modified Eagle medium containing antibiotics (100 U penicillin/ml, 100 μ g streptomycin/ml) and supplemented with 10% fetal calf serum, in a 5% carbon dioxide-humidified atmosphere at 37° C. After 48 h, the cells were treated with 2 μ M violacein, (generously supplied by Dr. N. Durán, Institute of Chemistry, UNICAMP) for 24 h. For further details, see Melo *et al.* (2000). For the Comet assay, V79 cells were grown in culture bottles and treated with violacein in the same conditions as described above.

Annexin V labeling. The coverlips with V79 cells were washed twice in 0.05 M phosphate-buffered saline (PBS) and immediately incubated with annexin V and propidium iodide in HEPES buffer as recommended by the manufacturer (Boheringer-Mannheim, Germany). The observations were done using live cells in an Axiophot fluorescence microscope (Zeiss, Germany) with an excitation filter of 515-560 nm and a barrier filter of 590 nm. For longer analysis, the cells were maintained in a humidified chamber for up to 1 h.

Comet (SCGE) assay. After treatment, the cells were trypsinized, washed in ice-cold PBS containing calcium and resuspended in calcium-free ice-cold PBS. The cell suspension was mixed with an equal amount of 1% low melting point agarose kept at 37° C. Immediately after mixing, 100 μ l of the suspension was pipetted on to microscope slides pretreated according to Klaude *et al.* (1996), then covered with a 25 mm x 50 mm parafilm coverslip and placed on a glass tray on ice. The parafilm was removed after the agarose had set and the slides were immersed in cold lysis solution (2.5 M NaCl, 100 mM EDTA, 10 mM Tris, pH 10, with freshly added 1% Triton X-100 and 2% DMSO) followed by incubation at 4° C for at least 1 h. The electrophoresis in weak alkali (0.03 M NaOH, 1 mM EDTA, pH 12.1) at 1 V/cm and 30 mA for 15 min was preceded by a 20 min immersion of the slides in the electrophoresis buffer to promote chromatin unwinding.

After electrophoresis, the slides were neutralized in 0.05 M Tris buffer pH 8.0, rinsed in distilled water, fixed in methanol, air dried and stored. DNA was stained with propidium iodide (20 μ g/ml) for 10 min, washed in distilled water and examined in a fluorescence microscope (Zeiss Axiophot).

Apoptosis was estimated by analyzing 200 nuclei from each treatment (50 nuclei per slide). Nuclear phenotypes identified according to their tail length (Fig. 3): type 1-no tail or DNA diffusion halo, type 2-no tail but with a DNA diffusion halo, type 3-a tail and a DNA diffusion halo, and type 4-a tail and not a DNA diffusion halo. Type 3 and 4 were markers for the early and late apoptotic stages, respectively.

Acknowledgements

References

A.H. Wyllie, G.J. Beathe, A.D. Hargreaves. Chromatin changes in apoptosis. Histochem. J. 13 (1981) 681-692.

S.S. Maria, B.C. Vidal, M.L.S. Mello. Image analysis of DNA fragmentation and loss in V79 cells under apoptosis. Gen. Mol. Biol. 23 (2000) 109-112.

M. Pallardy, M. Perrin-Wolff, A. Biola. Cellular stress and apoptosis. Toxicol. In vitro 11 (1997) 573-578.

M. Raffray, G.M. Cohen. Apoptosis and Necrosis in Toxicology: A continuum or distinct modes of cell death? Pharmacol. Ther. 75 (1997) 153-177.

P.S. Melo, S.S. Maria, B.C. Vidal, M. Haun, N. Duran. Violacein cytotoxicity and induction of apoptosis in V79 cells. In Vitro Cell Dev. Biol. Animal 36 (2000) 539-543.

A.H. Wyllie, J.F.R. Kerr, A.R. Currie. Cell death: the significance of apoptosis. Int. Rev. Cytol. 68 (1980) 251-306.

L.F. Barbisan, M.L.S. Mello, J. Russo, B.C. Vidal. Apoptosis and catastrophic cell death in benzo[a]pyrene-transformed human breast epithelial cells. Mutat. Res. 431 (1999) 133-139.

N.P. Singh, M.T. McCoy, R.R. Tice, E.L. Schneider. A simple technique for quantitation of low levels of DNA damage in individual cells. Exp. Cell Res. (1988) 184-191.

N.P. Singh. A simple method for accurate estimation of apoptotic cells. Exp. Cell Res. 256 (2000) 328-337.

M.L.S. Mello, S.S. Maria, P.H.P.A. Schildknecht, N.A. Grazziotin. DNA fragmentation in programmed cell death in nucleate erythrocytes: a cytochemical analysis. Acta Histochem. Cytochem. 33 (2000) 355-359.

Y. Gravieli, Y. Sherman, S.A. Bem-Sasson. Identification of programmed cell death in situ via specific labeling of nuclear DNA fragmentation. J. Cell Biol. 119 (1992)493-501.

M.L.S. Mello. Discrimination of Feulgen-stained apoptotic nuclei by image analysis. Proc. Am. Assoc. Cancer Res. 40 (1999) 691 (Abstract).

G. Koopman, C.P. Reutelingsperger, G.A. Kuiiten, R.M. Keehnen, S.T. Pals. Annexin V for flow cytometric detection of phosohatidylserine expression on B cells undergoing apoptosis. Blood 85 (1994) 332-340.

M. Klaude, S. Eriksson, J. Nygren, G. Ahnström. The comet assay: mechanisms and technical considerations. Mutat. Res. 363 (1996) 89-96.

P.L. Olive, D. Wlodek, R.E. Durand, J.P. Banáth. Factors influencing DNA migration

from individual cells subjected to gel electrophoresis. Exp. Cell Res. 198 (1992) 259-267.

B.C. Vidal. Extended chromatin fibres: crystallinity, molecular order and reactivity to concanavalin-A. Cell Biol. Int. 24 (2000) 723-728.
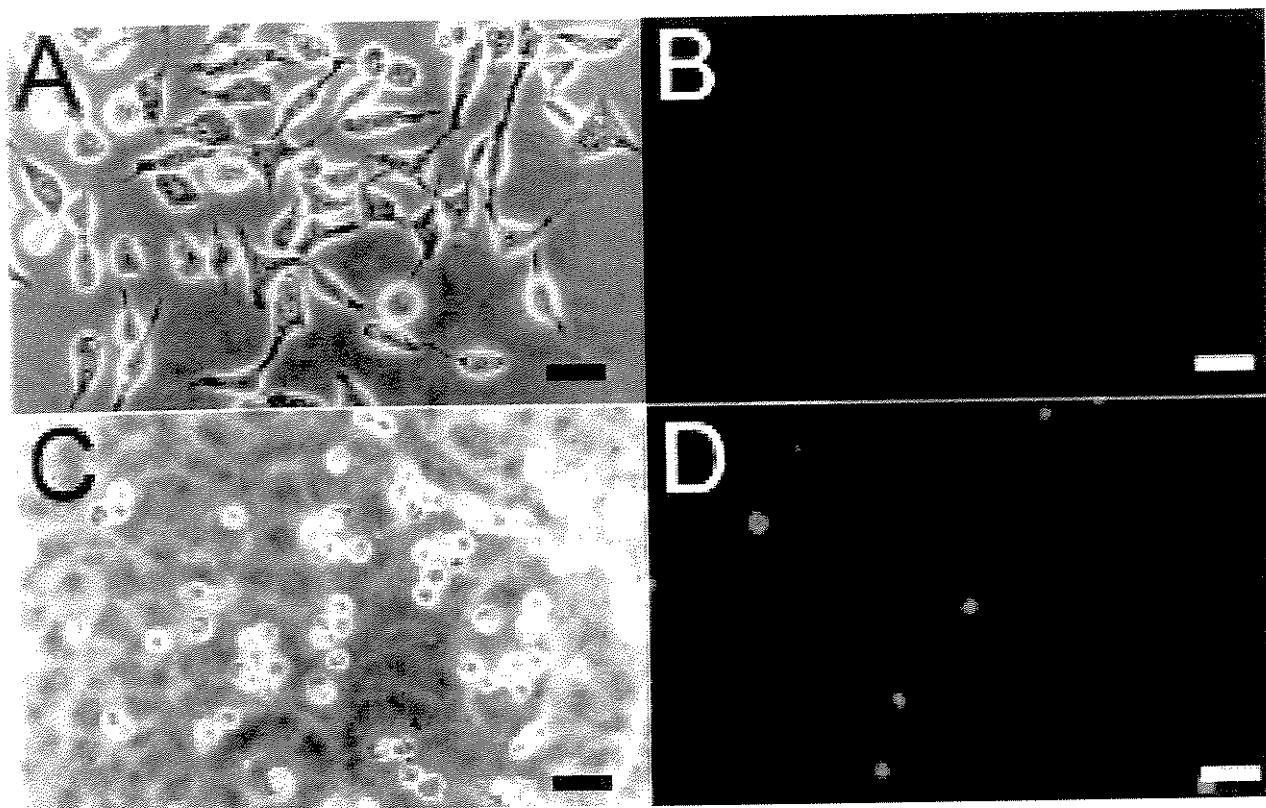
Figure 1: Annexin V / propidium iodide labeled V79 cells under phase contrast (A, C) and fluorescence (B, D) microscopy for apoptosis detection . Apoptotic cells were not detected in control cells (A, B), but only in violacein-treated cells (C, D). Necrosis was not observed in both control and treated cells. Bar = 50 μ m.
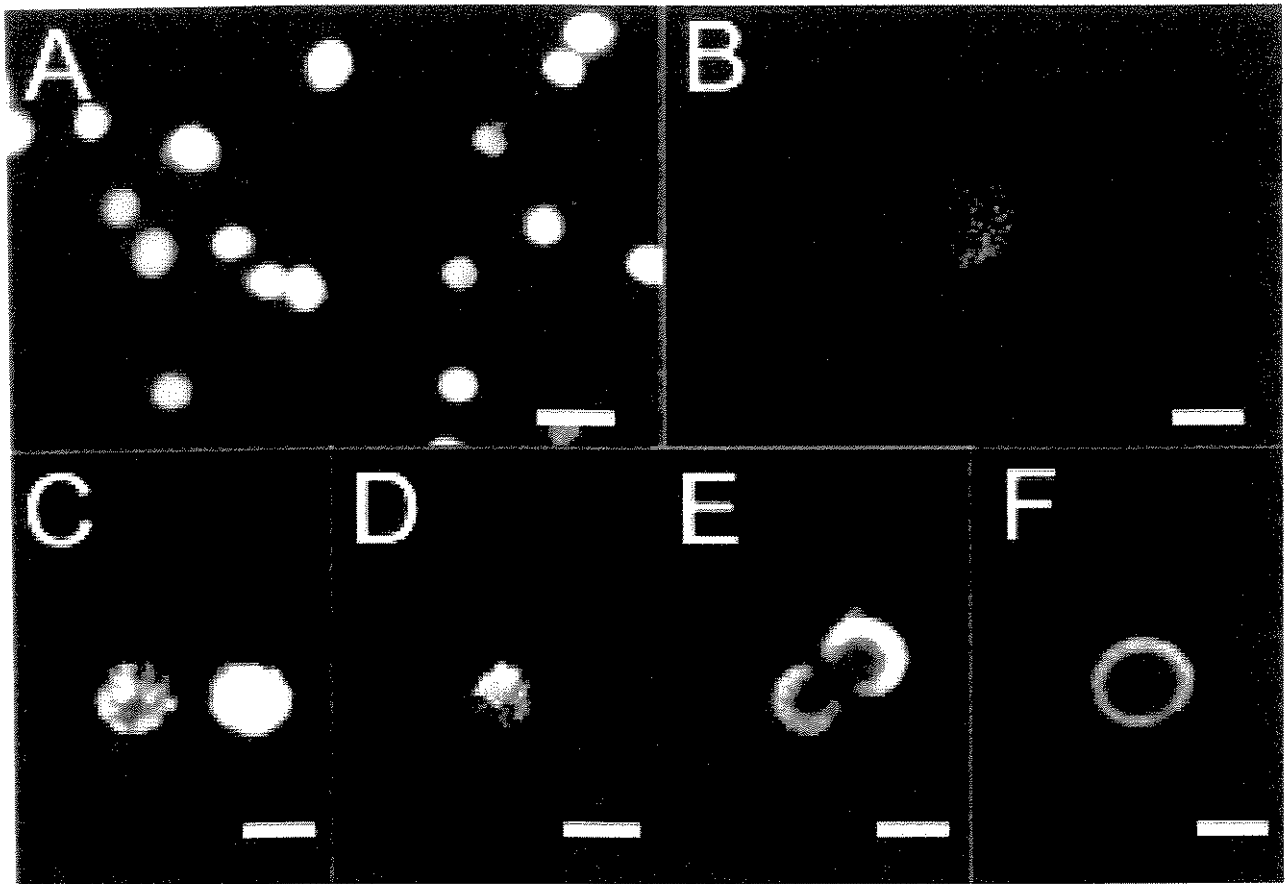
Figure 2: V79 cells after the alkaline lysis step stained with propidium iodide. In control cells (A), a DNA halo is observed around some nuclei while in violacein-treated cells (B-F) only condensed chromatin could be seen displayed in small granules or in nuclear periphery. Bar = 20 μ m.
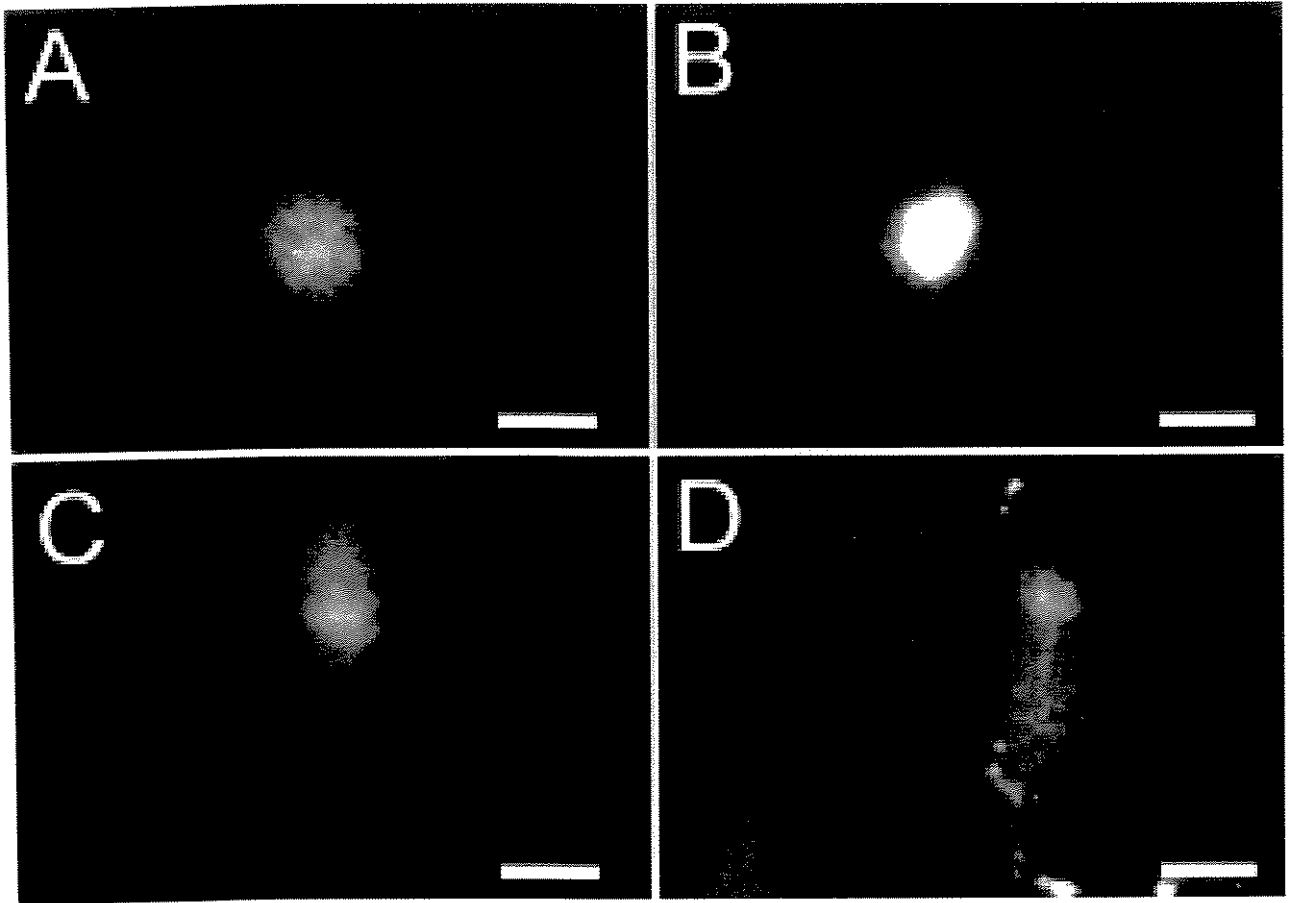
Figure 3: V79 nuclei subjected to Comet test and stained with propidium iodide. The nuclei can be classified by the phenotypes: type 1 (A) and type 2 (B) retract healthy nuclei while type 3 (C) and type 4 (D) are regarded to apoptotic nuclei. Bar = 20 μ m.
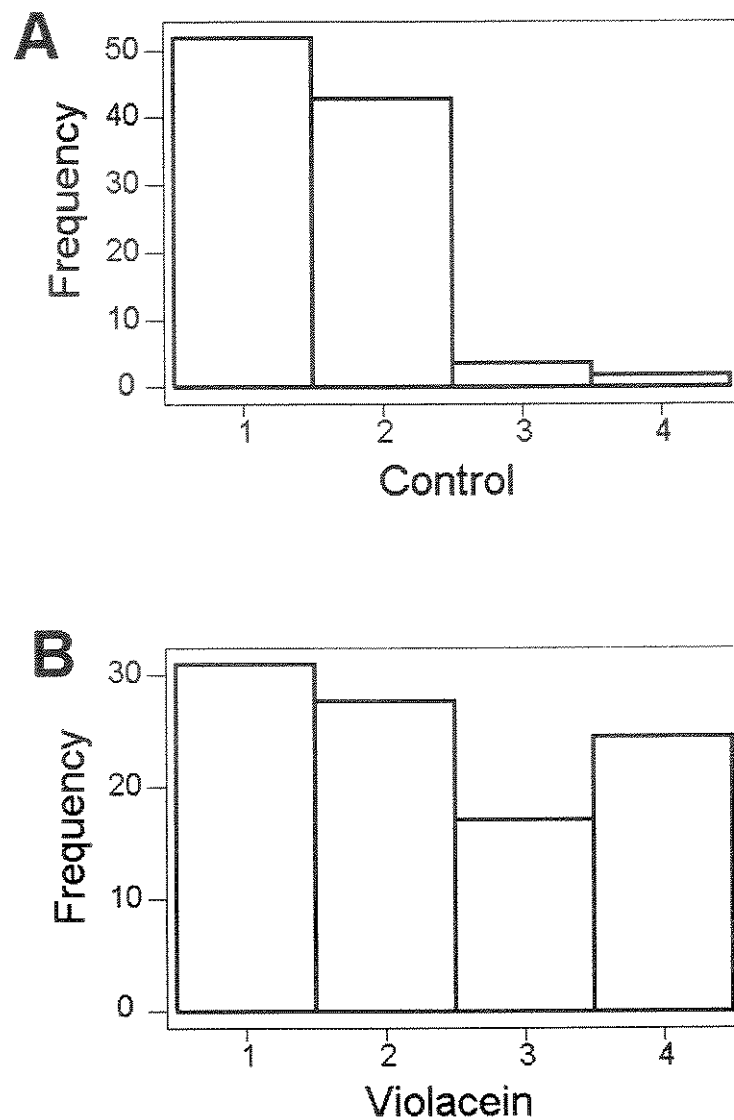
Figure 4: Frequency histogram of V79 cells subjected to Comet test and classified by phenotypes. Control cells (A) showed a low frequency of apoptotic nuclei (types 3 and 4), in contrast to violacein treated cells (B).

Histochemical analysis of the root-extracellular layer in maize and wheat

Pedro H.P.A. Schildknecht[1,*], Marília de M. Castro[2] and Benedicto C. Vidal[1]

[1]Departamento de Biologia Celular; [2]Departamento de Botânica; Instituto de Biologia, Universidade Estadual de Campinas (UNICAMP), Campinas, SP, Brazil.

*Author for correspondence: Departamento de Biologia Celular, Instituto de Biologia, Universidade Estadual de Campinas (UNICAMP). Caixa Postal 6109, 13084-971 Campinas, SP, Brazil. Tel: (55)(19)3788-6124; Fax: (55)(19)3788-6111. E-mail: pedroh@operamail.com

This article contains 31,842 characters

Abstract

The root extracellular layer (REL) is an important structure at the root-soil interface, but its composition is still unknown. In this work, we examined histochemically the compounds present in the REL of *Zea mays* and *Triticum aestivum*, as well as its anisotropic characteristics. Birefringence analysis of the REL showed a highly crystalline array of microfibrils arranged parallel to the root surface. We speculate that the REL is an integral part of the cell wall. If not a part of the cell wall itself, the REL may be firmly anchored to the wall at so many points as to give the appearance of being part of the cell walls. Tests for lignin, lipophilic compounds, pectin, callose and cellulose detected only the two latter compounds. Callose occurred sporadically as interrupted deposits in the REL, and was detected in only a few plants. Cellulose was the main compound of the REL. The cellulose present in the outer surface of the roots may act as a filtering mesh and a barrier to the external environment. The REL may also be involved in protection against physical, biological and chemical agents.

Introduction

The outer boundary of the root consists mainly of cell walls from the epidermis and deposits of root cap secretions, microorganisms, soil and detached cellular debris. The epidermis of young roots occupies an important position at the root-soil interface since it is the primary site of water and ion uptake. Roots from maize seedlings show a firm, thick (approx. 15 µm) layer, known as root extracellular layer (REL), over the columnar epidermal cells (Clarke et al., 1979; Vermeer and McCully, 1982). This layer overlying the epidermis occurs beneath a population of several thousand "border" cells that are detached every day from the root cap (Hawes et al., 2000). Together, these layers form the outer boundary of maize roots. The importance of such an outer barrier in protecting against physical agents such as aluminium has been reported (Miyasaka and Hawes, 2001). Despite the importance of the REL and border cells to the structure of the root boundary, only the latter have been widely studied (Brigham et al. 1995, Hawes et al., 2000; Miyasaka and Hawes 2001). The REL consists of polysaccharides, as indicated by its intense staining in the periodic acid-Schiff (PAS) reaction (Clarke et al., 1979; Vermeer and McCully, 1982), but its nature is distinct from the root cap exudates (Clarke et al., 1979). The components of the REL have not yet been identified.

The root structure of grasses is excellent for studing epidermal cells because these plants show a precise demarcation of the root cap from the rest of the root (Clarke et al., 1979; Feldman, 1994). We have therefore used maize and wheat roots as models to investigate the histochemical and biochemical composition characteristics of the REL.

Materials and Methods

Plant material

Seeds from maize (*Zea mays*) and wheat (*Triticum aestivum*) aluminium-sensitive lines (L477 and Anahuac, respectively) were surface sterilized with 0.5% (w/v) NaOCl, soaked in sterile water and germinated in a vertical cylinder of moist filter paper for 62 hours at 30°C in the dark. After germination, the seedlings were transferred to plastic screens floating on nutrient solution (in µM: $Ca(NO_3)_2$, 500; KNO_3, 500; KH_2PO_4, 2; NH_4NO_3, 250; $MgSO_4$, 200; $Fe(NO_3)_3$, 2; $MnCl_2$, 2; H_3BO_3, 11; $ZnSO_4$, 0.35; $CuSO_4$, 0.2;

$(NH_4)_6Mo_7O_{24}$, 0.03), pH 4.5, on which they were grown for 48 h. The solutions were aerated continuously and replaced every 24 hours to minimize microbial contamination.

Specimen manipulation

After treatment, the apices were sectioned 5 mm from the root tip, fixed for 48 hours in 3.7% buffered paraformaldeyde, pH 7.4, and dehydrated in tertiary butyl alcohol series under vacuum. The specimens were embedded in Paraplast plus wax (Oxford, USA) and 7 μm thick sections were cut on a rotary microtome (Micron, Germany).

Histochemistry

Acid polysaccharides were detected by immersing the root sections in 0.025% Toluidine Blue for 20 minutes in McIlvaine buffer (0.05 M citrate, 0.1 M sodium phosphate, pH 4.0) (Clarke *et al.*, 1979; Krishnamurty, 1999). Insoluble, non-sulphated polysaccharides were detected by the periodic acid-Schiff (PAS) reaction. The sections were oxidized with 0.5% periodic acid for 10 minutes, rinsed in water, air dried and stained with Schiff reagent for 10 minutes in the dark (Krishnamurty, 1999).

Calcium pectate was detected by the tannic-acid/ferric chloride method (Krishnamurty, 1999). The sections were stained in 5% tannic acid for 10 minutes, rinsed in water and developed in 3% ferric chloride for 1 minutes.

$\beta(1\rightarrow3)$ Glucan (callose) was visualized by staining root sections with 0.1% (w/v) Aniline Blue in 1 M Gly/NaOH buffer, pH 9.5, as described by Yamamoto *et al.* (2001). The sections were pre-stained with Toluidine Blue to quench the natural fluorescence.

$\beta(1\rightarrow4)$ Glucan (cellulose) was stained with 1% (w/v) Congo Red in water (Woodcock *et al.*, 1995) for 30 minutes and then rinsed to avoid nonspecific staining. The dichroism from Congo Red-stained sections was observed under polarized light using a light-polarizing Zeiss microscope from which the analyzer had been removed.

The presence of lipophilic compounds (as cutin or waxes) were assessed by staining root sections for 30 minutes with in a saturated solution of Sudan Black B in 70% ethanol, followed by rinsing in ethanol, air drying and mounting in glucose jelly (Krishnamurty, 1999). Lignin was detected by staining with 2% phloroglucinol in 95% ethanol for 5 min. A

drop of 5 M HCl was added to differentiate lignin in purple, and the mixture was covered by a coverslip and immediately observed under light microscopy (Krishnamurty, 1999). Sections were stained with aqueous 0.01% ethidium bromide for 5 s and water-mounted to detect lignin (yellow) after excitation at $\lambda = 365$ nm (Krishnamurty, 1999) and also to enhance the difference between the autofluorescence emitted by the REL and the cell walls.

The autofluorescence of the REL was examined in water-mounted sections after excitation at $\lambda = 365$nm in a Zeiss Axiophot fluorescence microscope.

All preparations (unless stated otherwise) were air dried, cleared in xylene and mounted with Canada balsam (n_D=1.54). All observations were made with a Zeiss Axiophot microscope in the transmitted light or epi-fluorescence modes.

Birefringence analysis

The birefringence of cell walls from the REL was examined in 7 µm thick sections, hydrated for at least 1 h in distilled water. The observations were done using a light polarizing Zeiss microscope, with the cell walls at a 45° angle relative to the axis formed by the crossed polars and a λ of 546 nm. The birefringence was determined by measuring the optical retards using a Brace-Köhler compensator (1/10 λ, λ=546 nm). Each experiment was repeated twice and 50 measurements were obtained from several specimens at each repetition. All data were analyzed by ANOVA, using the Minitab statistical software package (Minitab Inc., State College, USA). The level of significance was set at $p < 0.05$.

Enzyme treatment

Pectin and starch were removed from root sections by incubation in 1% (w/v) pectinase (Fluka, Switzerland) and 1% (w/v) α-amylase (Sigma, USA) in buffered saline, pH 6.8, for 4 hours at 37°C. Cellulose was digested with 1% cellulysin (Calbiochem, USA) in buffered saline for 12-24 hours at 37 °C.

Bacterial culture

Colonies of *Acetobacter xylinum* strain ATCC 23769 were purchased from the Fundação André Tosello (Campinas, Brazil) and grown as described elsewhere (Sakari *et al.*, 1998). *A. xylinum* produces cellulose pellicles in static culture (Sakari *et al.* 1998), which were harvested after 48 hours in our experiments. The pellicles were washed in distilled water and then in 4 M HCl for 12 hours to remove cellular debris followed by washing in ultrapure water for several times to remove the acid. The bacterial cellulose was air dried on a glass slide, hydrated for 15 minutes under a coverslip and observed with epi-fluorescence microscopy. The autofluorescence of wet cellulose pellicles produced by *A. xylinum* was observed after excitation at 365 nm using a fluorescence microscope and compared to the autofluorescence of the REL.

Results

Since the maize and wheat root sections analyzed gave similar results (except where stated), they are described and discussed together whenever possible. The main findings are shown in Table 1.

Under polarized light microscopy the root sections showed a highly birefringent REL that extended from the root cap junction (Fig. 1A, arrow A) to the zone where the elongation zone. The birefringence of the REL was totally extinguished when the layer was placed parallel to the plane of polarized light or to the analyzer (Fig. 1B, arrow A). The REL often appeared to be interrupted or broken, but this could be corrected by slightly turning the microscope stage to adjust the microfibrils of the dark region to a 45° orientation relative to the polars. The same phenomenon occurred in dim regions within highly birefringent portions of the REL (Fig. 1C-D, arrow B), suggesting that not all microfibrils are parallel to each other. Cell walls of the root cap periphery also showed intense birefringence (Fig. 1A). These cells are the same as those that give rise to the border cells (Moore and McClelen, 1983; Hawes *et al.*, 2000), the walls of which were also highly birefringent (Fig. 1C-D, arrow C). In some roots, a secondary REL was observed in close

contact with the border cells (Figs. 1C-D, arrow D). Similar results were observed in wheat (Fig. 1D).

The REL was deeply stained by the PAS reaction, which delineated the deposition of this over the epidermis/protodermis and under the border cells, and also indicated the junction with the root cap as the probable origin of this stained material (Fig. 2A). In some roots, an intense staining also occurred at the border of root cap. The cell walls were PAS positive, but were not as intensely stained as the REL. The PAS-positive cell walls showed strong fluorescence at 485 nm, not seen with the REL (Fig. 2B). Digestion of the root sections with amylase and pectinase prior to the PAS reaction completely abolished the fluorescence of the cell walls at 485 nm (Fig. 2C), although the walls remained PAS positive under conventional microscopy.

The cell walls showed a light red fluorescence at 365 nm after staining with ethidium bromide, whereas no induced fluorescence was observed in the REL (Fig. 2D). Only a bright blue autofluorescence was emitted by the REL, similar to the autofluorescence observed in non-stained sections. Pure cellulose pellicles produced by *Acetobacter xylinum* also showed a bright blue autofluorescence at 365 nm (Fig. 2E), comparable to that emitted by the REL (Fig. 2E). The fluorescence appeared brighter in the cellulose pellicles because of their thickness, which was several times greater than of from the root sections (7 μm).

Acid polysaccharides (pectin) were almost absent from the REL, as seen in root sections stained with Toluidine Blue (Fig. 3A). Almost no Toluidine Blue staining (sometimes only pale green) occurred in the REL, in contrast to the cell walls and nuclei from border and inner cells which were intensely stained. No calcium pectate was detected in the REL by tannic acid/ferric chloride staining (data not shown). Callose [β-(1→3) glucans] was detected by Aniline Blue staining and occurred as interrupted deposits that shared the same region with the REL (Fig. 3B). However, callose was observed in all plants, rather it was observed only in a few specimens. Lipophilic compounds, such as cutin and waxes, were not observed at the REL of root sections stained with Sudan Black (Fig. 3C). Based on Clarke *et al.* (1979), who suggested the presence of phenolic compounds in

the REL, we tested for the presence of lignin, but none was detected after the HCl-phluoroglucinol reaction (data not shown) and staining with ethidium bromide.

In view of the absence of acid polysaccharides, lignins, lipophilic compounds, of the occasional presence of $\beta(1{\rightarrow}3)$ glucans and of the a highly positive PAS reaction, we examined whether the REL was composed mainly of insoluble non-sulphated $\beta(1{\rightarrow}4)$ glucans (cellulose), as suggested by its autofluorescence. Treatment with Congo Red resulted in a deeply stained REL with unequal absorption of polarized light (dichroism) in transversal and longitudinal sections; there was greater light absorption when the REL was placed parallel to the azimuth of polarized light ("positive" dichroism) (Fig. 4). However, some regions of the REL absorbed light when placed at right angles to the plane of polarized light ("negative" dichroism) (Fig. 4). The existence of some clusters of microfibrils that were not oriented in the same direction as their neighbors was already been observed during the analysis of REL birefringence.

The digestion of root sections with cellulase virtually abolished the birefringence of wheat (Fig. 5) and maize roots, except for a few regions within the REL of maize that were faintly birefringent when observed under crossed polars (Fig. 6). Extensive digestion with cellulase (16–24 h) extinguished these remnants of birefringence in maize REL (Fig. 6). The birefringence was completely abolished in all cell walls from maize and in all tissues from wheat roots, including the REL, after 12 h of enzymatic treatment (Fig. 5B).

Discussion

Most of the soluble polysaccharides that could have contributed to the REL were probably removed during the hydroponic growth of the root, leaving behind a thick PAS-positive layer, similar to that observed by Clarke et al. (1979). The origin of the REL appears to be the junction of the root with its cap, being produced by the protodermal cells. It seems improbable that the REL originated from root cap/border cell exudates (mucigel) since this layer was also present in regions not adjacent to the root cap and where border cells were not detected. Moreover, the border cells and root cap mucilage detach from roots grown in hydroponic culture and are dislodged from the root tip periphery as they are produced (Hawes et al., 2000; Miyasaka and Hawes, 2001). The REL may result from

epidermal/protodermal cell wall thickening or from highly oriented microfibrils that are produced and secreted by the epidermis/protodermis. However, our data do not support any of these assumptions. We speculate that the REL is an integral part of the cell wall since it was not removed from the walls even after the procedures for paraffin inclusion (dehydration and clearing in butanol, and paraffin baths at 58 °C). If not a part of the cell wall itself, the REL may be firmly anchored to the wall at so many points as to give the appearance of being part of the cell walls.

The strong birefringence of the REL suggested an oriented microfibrilar and crystalline supramolecular organization in its structure, as did the complete extinction of birefringence when the long axis of the root was placed parallel to one of the polars. However, not all REL microfibrils were oriented in the same direction since some regions showed their highest birefringence when placed at angles slightly below or above the crossed polars than that of their neighbors. These sudden alterations in the orientation of the microfibrils agree with the geometrical model of plant cell walls proposed by Emons and Mulder (1998, 2000) and will be discussed later. The appearance of a double-layered REL in some plants was puzzling. It is still not clear whether this secondary layer was a response to an unknown stimulus in certain plants or if it occurred naturally in all plants but was lost in most roots during processing of the specimens. The double-layered REL was considered not to be an artifact, since it appeared in roots processed at different time using reagents from different vials. Furthermore, Clarke *et al.* (1979) also described a two-layered REL after Alcian Blue and Calcofluor staining. The intermediary space between the two highly birefringent layers was possibly filled by an isotropic compound, such hemicellulose, which is not birefringent (Krishnamurty, 1999). Similarly to the double-layered REL, callose was also observed in only a few specimens. Since we did not verify whether the plants that had a double-layered REL were the same as those with callose deposits, no correlation can be established between these two phenomena.

The PAS reaction stains insoluble and non-sulphated polysaccharides, such as cellulose, starch and pectin (Krishnamurty, 1999), so it was not surprising that all cell walls were deeply labeled by this procedure. The intense staining of the root cap periphery was probably due to the high amounts of mucilage secreted by the external root cap cells as well

as cell wall debris, which appear after the partial hydrolysis of cell walls during mucilage exudation by root cap cells (Moore and McClelen, 1983). This staining could also be due to pectin that was part of the cell walls but part of the mucilage exudation, since the latter would be removed from the root cap during hydroponic growth. The REL also stained intensely in the PAS reaction, suggesting a similar composition to the cell walls. However, this was not confirmed by fluorescence analysis of PAS-stained sections, in which the cell walls showed an intense fluorescence at 485 nm while REL did not. The removal of pectin abolished the fluorescence of the cell walls, which became similar to the REL, indicating that pectin does not occur in the REL structure. These results were confirmed by the tannic acid/ferric chloride reaction and toluidine blue staining which detected calcium pectate and carboxylated/sulphated polysaccharides, respectively, in the cell walls but not in the REL.

Callose was detected by Aniline Blue-induced fluorescence, and appeared as interrupted deposits within the REL. Callose can be induced by physical damage (Brett and Waldron, 1996), such as that which can result from the manipulation of plantules and from constant collision with air bubbles and other roots. This could explain the punctuated deposition of callose along the REL and its absence in most of plants. The presence of callose in the REL was not expected, since callose makes the tissue impermeable to water (Yim and Bradford, 1998) and prevents the exchange of soluble compounds between the root apex and soil. Although callose was not present in most of the plants examined, its contribution to the REL in the few plants in which it was detected could not be ruled out because of the abundance of the interrupted callose deposits in the REL of these plants. Other compounds which do not stain in the PAS reaction, such as lignin and lipids, were also absent from the REL.

Cellulose was detected by Congo Red staining (Pearse, 1985; Woodcock *et al.*, 1995) and coincided exactly with the REL, as determined by the PAS reaction and birefringence analysis. The presence of cellulose was expected based on the blue autofluorescence of the REL, even in ethidium bromide stained sections, which was similar to the blue autofluorescence of the cellulose pellicles produced by *A. xylinum*. The two sulfonate groups of the Congo Red molecule form strong polar interactions with the hydroxyl groups of cellulose. This results in the axial orientation of the chain axis and the

aromatic rings of the Congo Red relative to the glucose rings of cellulose; there is also deposition of the dye along the axis of the cellulose fibril (Pearse, 1985; Woodcock et al., 1995). This enhances the anisotropic characteristics of cellulose, as observed by its dichroism after Congo red staining.

According to the architectural model of the cell walls proposed by Emons and Mulder's (1998; 2000), cellulose microfibrils would always be parallel to the plant surface whilst their orientation to the long axis of the root changes from axial to transversal and back to axial. The REL is composed mainly of cellulose (seen histochemically and by specific enzymatic digestion, as discussed later). Cellulose fibrils stained with Congo Red absorb light very strongly when the azimuth of polarized light is parallel to the fibril axis, since the Congo Red molecules are parallel to the cellulose fibrils and also to the azimuth of light. However, Congo Red will not absorb light when perpendicular to the long axis of the molecule (and thus to the azimuth of polarized light), in a phenomenon known as dichroism. In this case, positive dichroism should occur in Congo Red-stained REL whatever the plane of root sectioning. In microfibrils with an axial orientation in the plane of the root section, the long axis of cellulose and Congo red will be similar to the direction of maximum light absorption; in microfibrils with a non-axial orientation, the plane of the aromatic rings of Congo red will have the maximum absorption. In both cases, greater absorption of light and birefringence will occur if the REL is oriented parallel to the azimuth of polarized light. This hypothesis agrees with our results, and suggests that the cellulose matrix of the REL was synthesized according to the model of Emons and Mulder. Hence, the helicoidal array of cellulose fibrils will always result in positive dichroism after Congo Red staining.

On first analysis, the regions with negative dichroism were apparently unexplainable by the hypothesis above. However, the helicoidal model of Emons and Mulder was proposed for walls that were synthesized individually by each cell, and not for a collective cellulose as the REL. Physical interactions can be expected to occur between cellulose microfibrils at the interface of two sectors of the REL produced separately by each epidermal cell. The meeting of cellulose microfibrils that were synthesized in opposite directions possibly changed the orientation of the microfibrils at cell interface and altered

the dichroism observed in Congo Red-stained sections. The birefringence of the REL also suggested a sudden change in microfibril orientation, since black REL sectors became birefringent if the microscope stage was rotated slightly, in agreement with the results for dichroism.

The complete removal of the REL by cellulase digestion confirmed that cellulose was the main constituent of the REL suprastructure. The wheat REL was more sensitive to enzymatic digestion that of maize, and was less heterogeneous, since it was completely removed from wheat while some sectors remained birefringent in maize after 12 h of digestion (Fig. 6). However, the REL of maize roots was totally removed after 16 h of digestion, thus indicating the presence of cellulose.

The highly crystalline array of cellulose microfibrils present at the outer surface of roots may act as a filtering mesh or a barrier to the external environment. The REL may therefore restrict the access of toxic compounds (e.g.: Al or La) and pathogenic organisms to the interior of the root and hence serve as a passive defense mechanism in plant roots.

Conclusions

The REL from maize and wheat consisted mainly of a highly crystalline array of cellulose microfibrils arranged parallel to the cell surface. Pectin, lignin and lipophilic compounds did not occur in the REL whereas callose occurred occasionally. Cellulose is the major constituent of the REL.

Further studies of the REL should help us to understand its role in plant defense mechanisms against physical, chemical and biological agents.

Acknowledgements

References

Brett,C. and K.Waldron. (1996). Physiology and biochemistry of plant cell walls. London: Chapman & Hall pubs.

Brigham,L.A., H.H.Woo, and M.C.Hawes. (1995). Root border cells as tools in plant cell studies. *Methods Cell Biol.* 49,377-387.

Clarke,K.J., M.E.McCully, and N.K.Miki. (1979). A developmental study of the epidermis of young roots of *Zea mays* L. *Protoplasma* 98,283-309.

Emons,A.M.C. and B.M.Mulder. (1998). The making of the architecture of the plant cell wall: How cells exploit geometry. *Proc. Natl. Acad. Sci. USA* 95,7215-7219.

Emons,A.M.C. and B.M.Mulder. (2000). How the deposition of cellulose microfibrils builds cell wall architecture. *Trends Plant Sci.* 5,35-40.

Feldman,L. (1994). The maize root. In *The maize handbook*. (ed. L.Freeling and V.Walbot), pp. 29-36. New York: Springer-Verlag Pub.

Hawes,M.C., U.Gunawardena, S.Miyasaka, and X.Zhao. (2000). The role of root border cells in plant defense. *Trends Plant Sci.* 5,128-133.

Krishnamurty,K.V. (1999). Methods in cell wall cytochemistry. Washington: CRC press.

Miyasaka,S.C. and M.C.Hawes. (2001). Possible role of root border cells in detection and avoidance of aluminum toxicity. *Plant Physiology* 125,1978-1987.

Moore,R. and E.McClelen. (1983). Ultrastructural aspects of cellular differentiation in the root cap of *Zea mays. Can. J. Bot.* 61,1566-1572.

Pearse,A.G.E. (1985). Histochemistry: Theoretical and applied. Analytical Technology. London: Churchill & Livingstone Ltd.

Sakari,N., H.Asano, M.Ogawa, N.Nishi, and S.Tokura. (1998). A method for direct harvest of bacterial cellulose filaments during continuous cultivation of *Acetobacter xylinum*. *Carbohyd. Pol.* **35**,233-237.

Vermeer,J. and M.E.McCully. (1982). The rhizosphere in *Zea*: new insight into its structure and development. *Planta* **156**,45-61.

Woodcock,S., B.Henrissat, and J.Sugiyama. (1995). Docking of congo red to the surface of crystalline cellulose using molecular mechanics. *Biopolymers* **36**,201-210.

Yamamoto,Y., Y.Kobayashi, and H.Matsumoto. (2001). Lipid peroxidation is an early symptom triggered by aluminum, but not the primary cause of elongation inhibition in Pea roots. *Plant Physiol.* **125**,199-208.

Yim,K. and K.J.Bradford. (1998). Callose deposition is responsible for apoplastic semipermeability of the endosperm envelope of muskmelon seeds. *Plant Physiol.* **118**,83-90.

Figure legends

[**Table 1**: Results of the histochemical and birefringence analyses of REL and cell walls from maize and wheat: since the findings were similar, they are shown together. The intensity of the response was scored from + + (highest) to - - (lowest). The color observed in the structure is showed in parentheses.]

[**Figure 1**: Root sections from maize (A-C) and wheat (D) observed under polarized light. A) Root birefringence when oriented at 45° to the polars. Note the high birefringence at the interface of the root cap (RC) and root cells and over the root protodermis (arrow A) that form the REL. The periphery of the root cap also showed intense birefringence. B) Root birefringence when oriented at 90° to the polarizer (parallel to the analyzer). The REL birefringence was completely extinguished (arrow A). C and D) Root birefringence when oriented at 45° to the polars. Some sectors appeared black (arrow B), but their birefringence was recovered after a slight increase/decrease in their angle of rotation relative to the polars. A close association of the root cap cells with the REL was seen (arrow C). A double-layered REL was detected in maize and wheat (arrow D), although it occurred in only a few of the specimens. Bar = 200 µm (A) and 100 µm (B-D)]

[**Figure 2**: Maize root sections stained with the PAS reaction (A-C) or ethidium bromide (D), and unstained cellulose pellicle from *A. xylinum* (E). A) PAS-stained root seen under visible light showing a deeply stained REL (arrow A) and root cap (RC) periphery. B) Same material as (A) observed at 485 nm. Only the cells of the root interior showed fluorescence; the REL gave no response (arrow A). C) Same material as (B) observed at 485 nm after enzymatic removal of pectin and starch. D) Blue autofluorescence of REL (arrow A) in ethidium bromide stained section (365 nm), showing the position of the REL under the root cap cells (arrow B); lignin, which would be stained yellow, was not detected. E) Autofluorescence of cellulose pellicles from *A. xylinum* at 365 nm. Bar = 200 µm (A-C) and 100 µm (D)]

[**Figure 3**: Maize root sections stained whith Toluidine Blue (A), Aniline Blue (B) and Sudan Black B (C). A) The Toluidine Blue-stained sections showed no staining of the REL

(arrow A). The border cells were deeply stained (arrow B). B) The detection of callose by Aniline Blue staining revealed interrupted deposits of this β-glucan in the REL; this result was seen in only in a few of the maize and wheat roots examined. C) Sudan Black B staining did not detect lipophilic compounds in the REL (arrows). Bar = 100 μm]

[**Figure 4:** Congo Red-stained sections of maize roots observed under polarized light. The light azimuth is given by the double arrows. The extensive staining of the REL by Congo Red suggested an abundance cellulose. The light absorption of the REL was greater when its long axis was placed parallel to the azimuth of polarized light (B, arrow A), and not perpendicular to it (A, arrow A). In contrast, some regions of the REL showed greater light absorption when the long axis of the REL was perpendicular to the azimuth of polarized light (arrow B). Bar = 100 μm]

[**Figure 5:** Wheat root sections observed under polarized light at 45° relative to the crossed polars, before cellulase treatment (A) and after enzymatic removal of cellulose (B). Bar = 100 μm]

[**Figure 6:** Histogram of the mean optical retard values (± S.E.) of the REL from maize and wheat roots before and after cellulose removal by cellulysin. Note the decrease in REL birefringence in maize after 12 h of cellulase treatment and the absence of REL birefringence in wheat after similar treatment (p=0.000 compared to the corresponding control without enzymatic digestion; ANOVA). The birefringence of the maize REL was completely abolished after 16 h of cellulase digestion. The experiment was repeated twice, n=100]

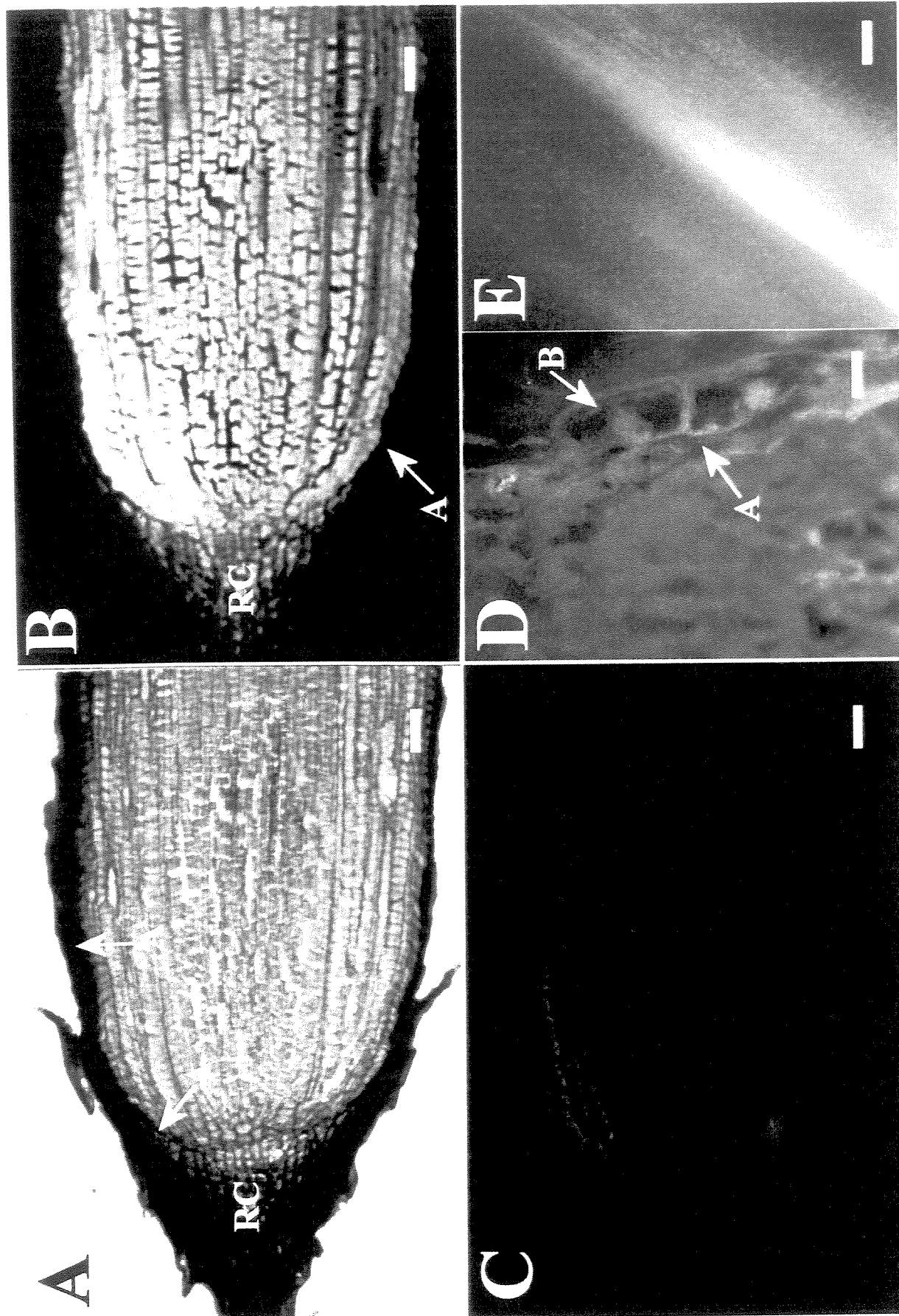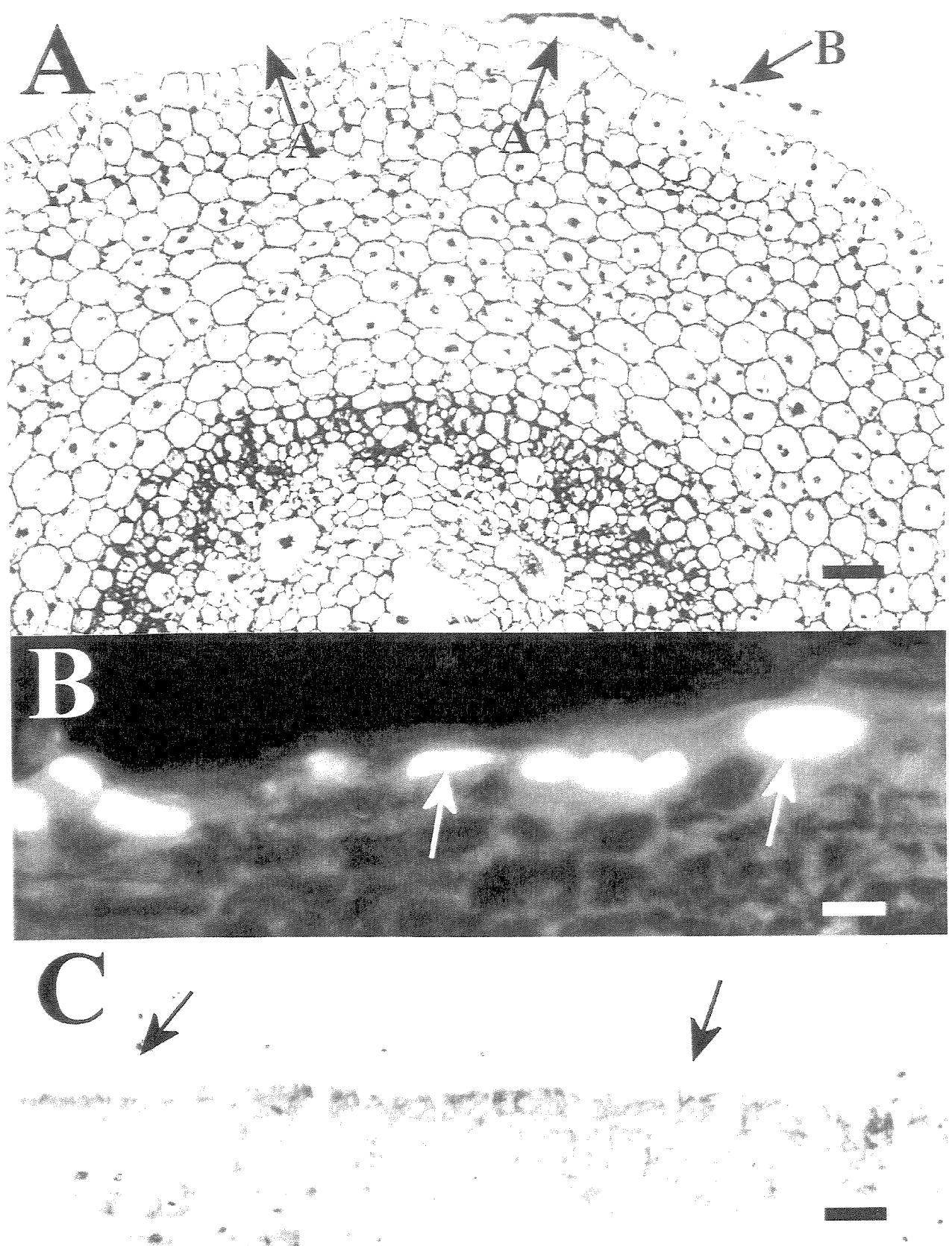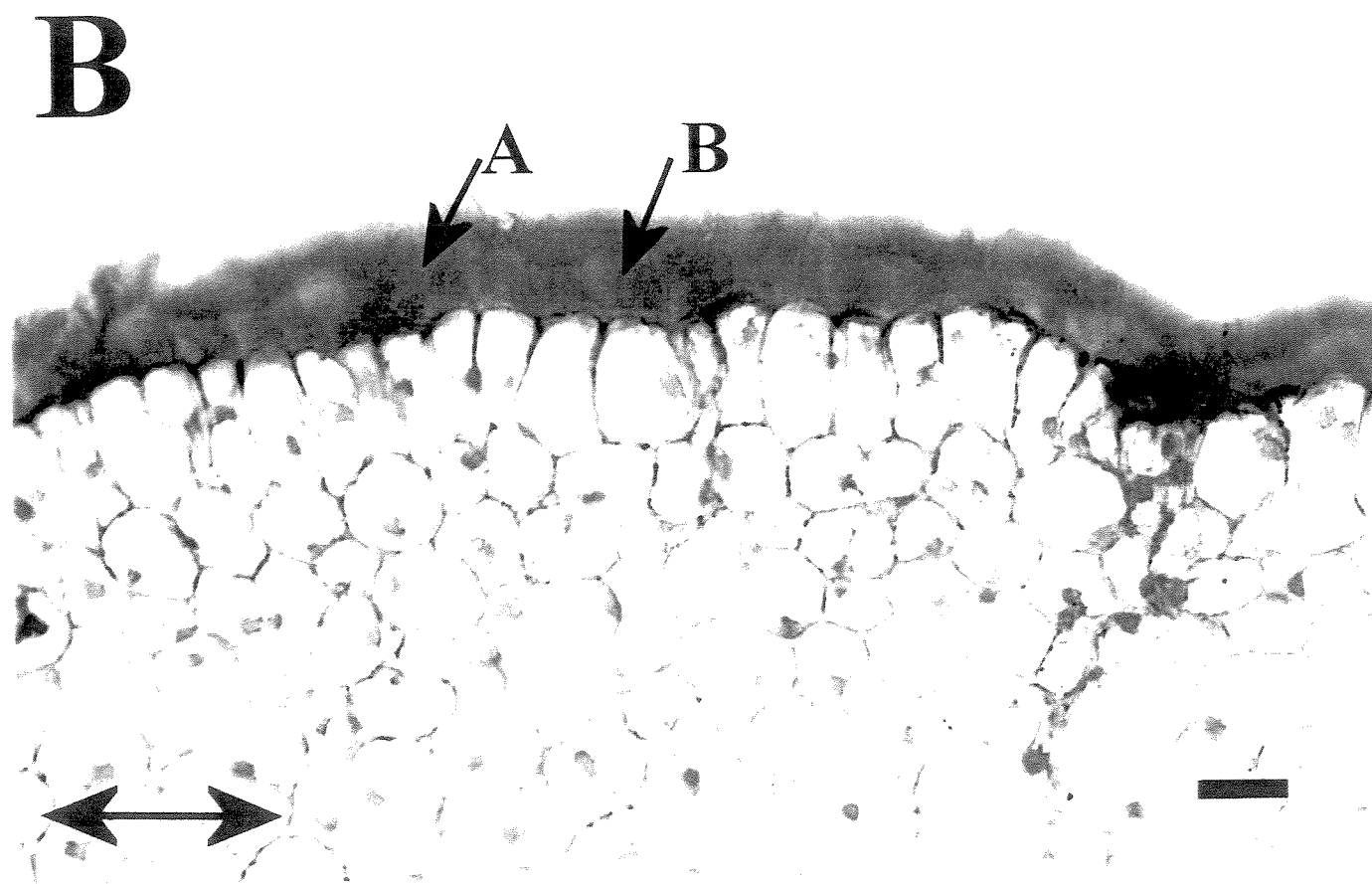| Treatment	Histochemical specificity	Staining		Figures
		REL	Cell walls	
Toluidine Blue	Acid polysaccharides	- (none or faint green)	+ + (purple or purple-blue)	3A
PAS	Polysaccharides	++ (dark purple)	+ (purple)	2A
PAS (485 nm)	N/A	- - (none)	+ + (purple)	2B
PAS (485 nm) / amylase/pectinase	N/A	- - (none)	- - (none)	2C
Aniline Blue / Toluidine Blue (365 nm)	β (1→3) glucans (callose)	+ (interrupted deposits)	- (only a few plugs between some cells)	3B
Congo Red	β (1→4) glucans (cellulose)	+ + (red)	+ + (red)	4A/B
tannic acid/ ferric chloride	Calcium pectate	- - (none)	+ (brown)	Not shown
phloroglucinol/ HCl	Lignin	- - (none)	- - (none)	Not shown
ethidium bromide (365 nm)	DNA, lignin	- - (blue; autofluorescence)	+ + (red-orange)	2D
autofluorescence (365 nm)	N/A	+ + (blue)	+ (blue)	2D/E
Sudan Black B	Lipophilic compounds	- - (none)	- (faint gray)	3C
birefringence	Oriented structures	+ + (strong)	+	1 / 5A
birefringence + cellulase	Non-cellulosic oriented structures	- - (none)	- - (none)	5

Table 1: Sum of the results obtained from *Zea mays* and *Triticum aestivum* analysis
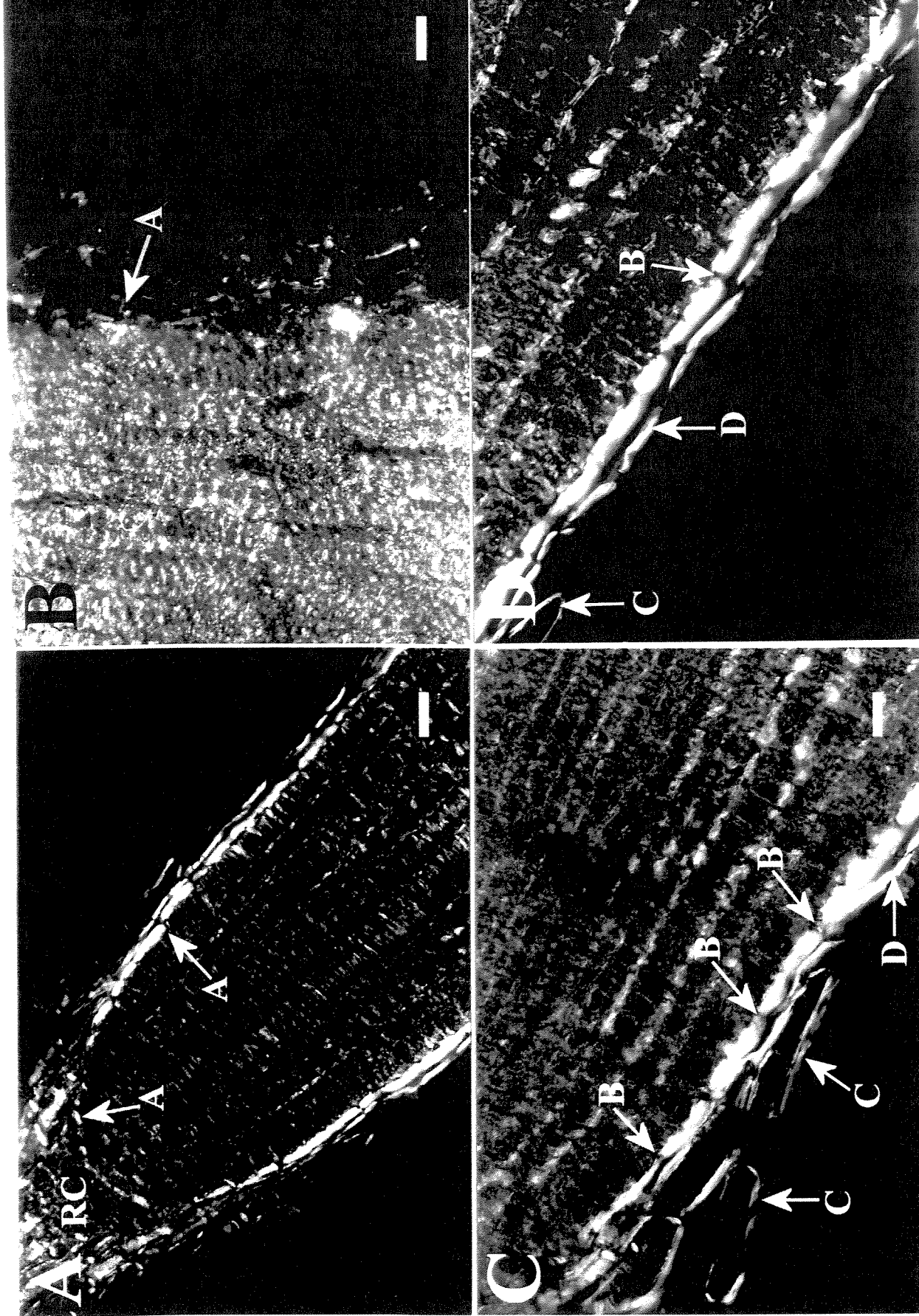
FIG1

FIG.2

FIG.3
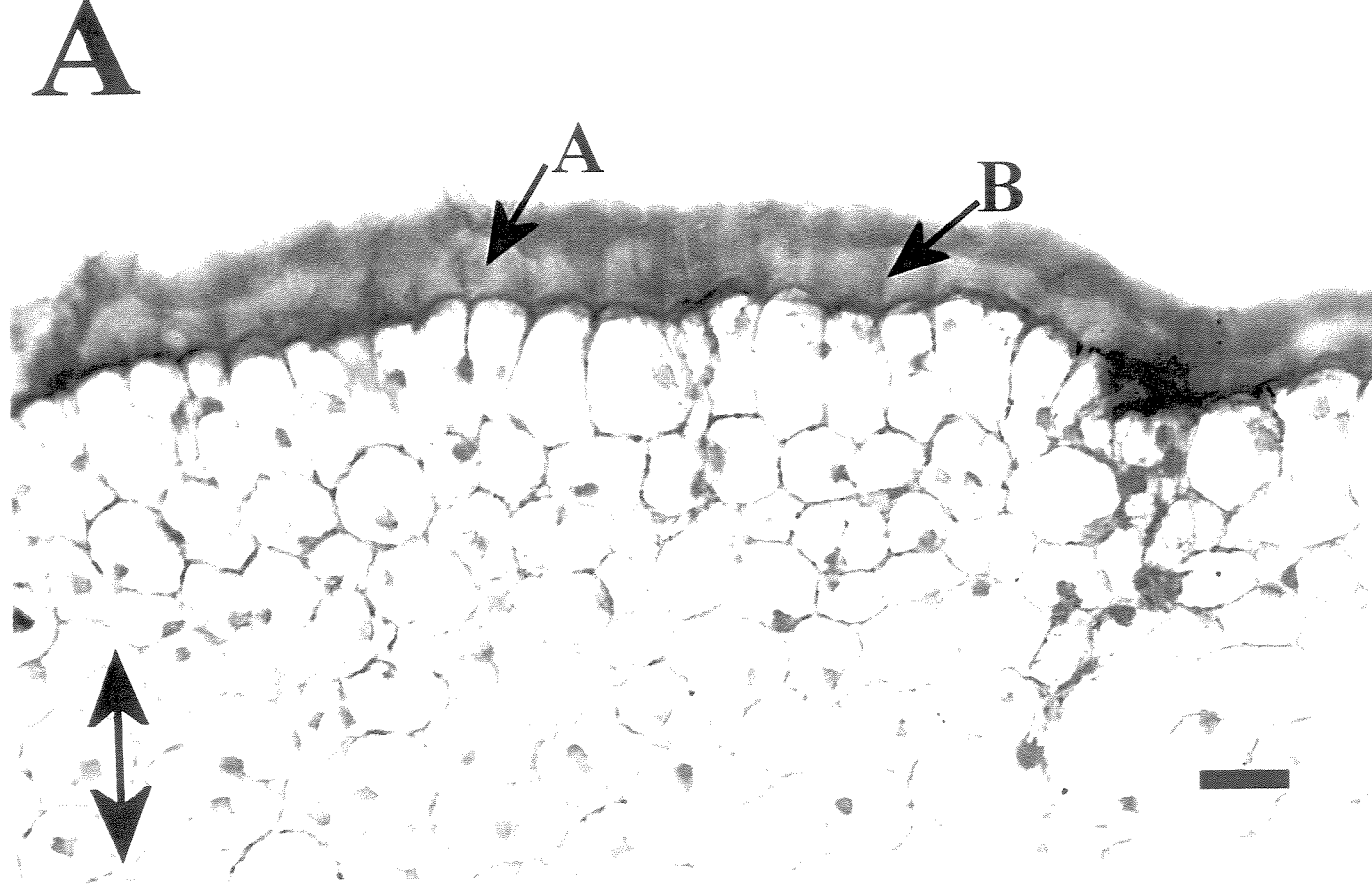
FIG.4

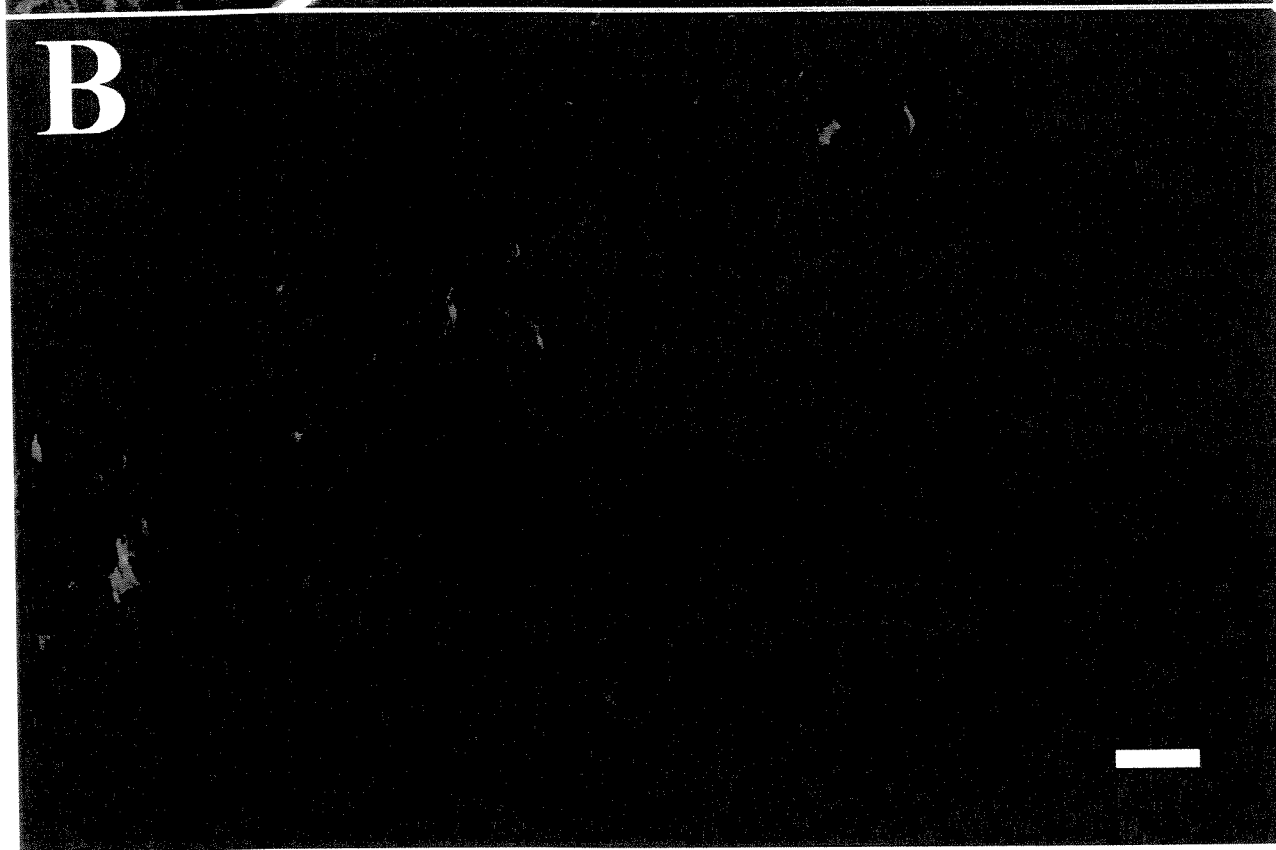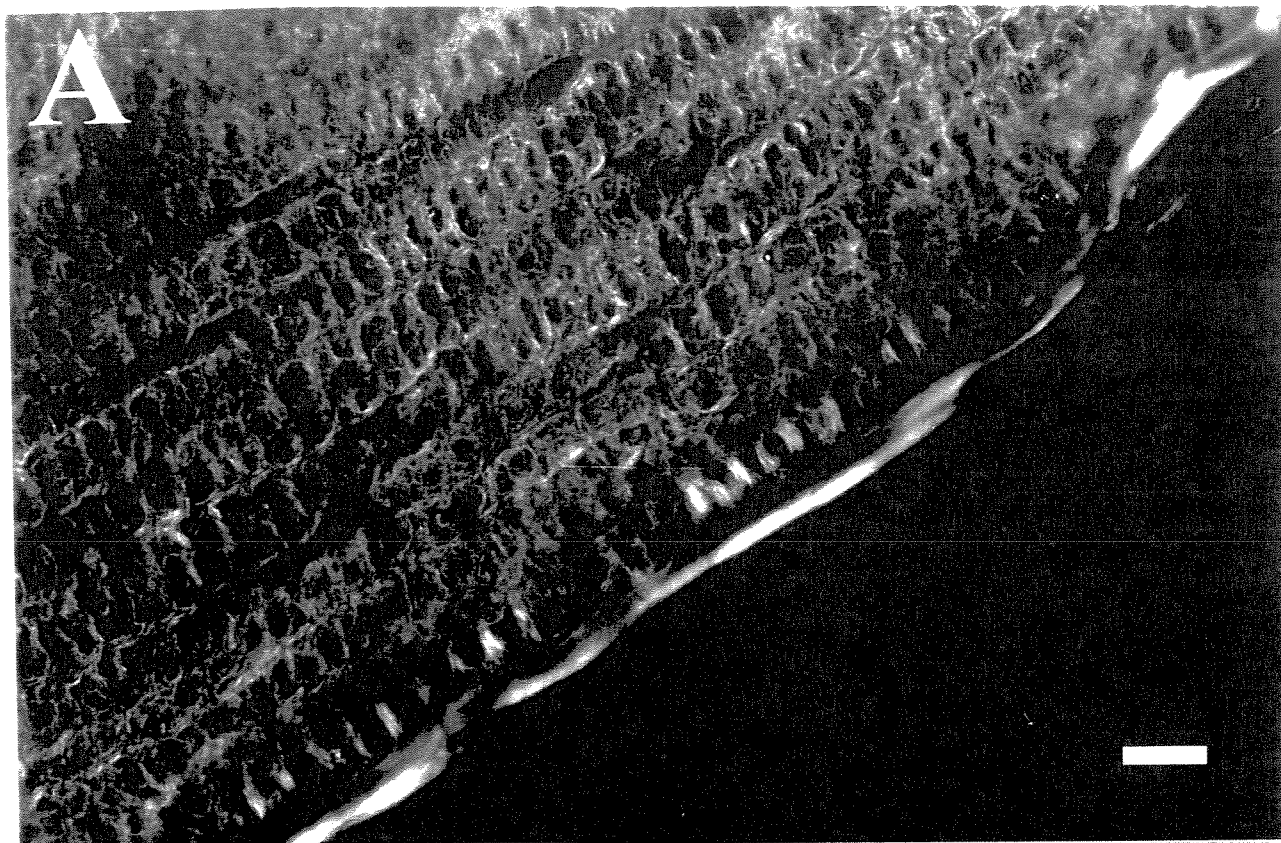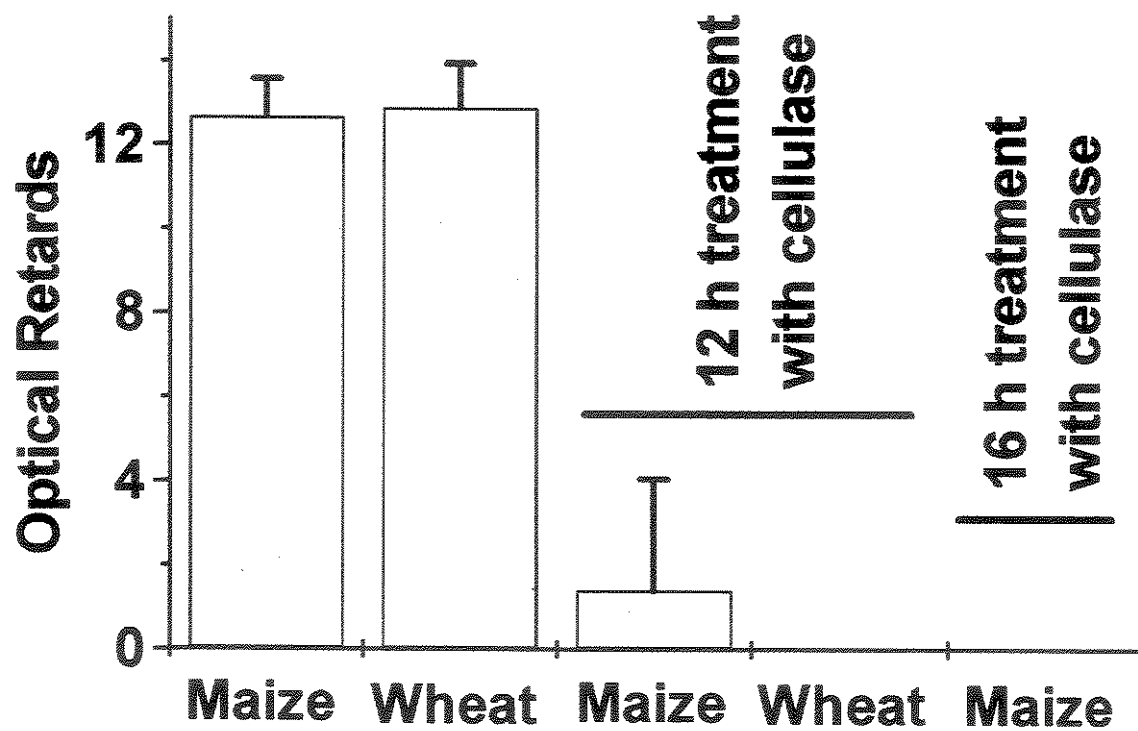FIG.5

FIG.6

CONCLUSÕES

- ✓ O Al^{3+} interage eletrostaticamente com os fosfatos do DNA, alterando sua conformação espacial. A estrutura originada desta interação é dependente das concentrações de Al^{3+} e de DNA presentes no meio onde é dada a reação.
- ✓ As paredes celulares de plantas sensíveis ao Al^{3+} possuem maior disponibilidade de sítios negativamente carregados, onde ocorre a ligação com o Al^{3+} e conseqüente bloqueio destes sítios pelo cátion. O volume de cargas negativas em paredes celulares de plantas tolerantes ao Al^{3+} é significante menor do que o existente em plantas sensíveis ao cátion.
- ✓ O Al^{3+} não inibe a síntese de celulose em bactérias, mas altera o processo de automontagem das fibras aumentando a cristalinidade de sua malha. O mesmo fenômeno ocorre no apoplasto de plantas sensíveis ao Al^{3+}, mas não em plantas tolerantes ao cátion.
- ✓ O apoplasto constitui um mecanismo passivo de tolerância ao Al^{3+}.
- ✓ O Al^{3+} induz a morte de células radiculares em plantas sensíveis, mas não em plantas tolerantes ao cátion, sendo esta a principal causa da inibição permanente do crescimento da raiz de plantas sensíveis ao Al^{3+}. O mecanismo de morte envolvido é similar à apoptose, porém não possui todas suas características.
- ✓ O mecanismo de morte celular induzido pelo Al^{3+} em células animais é dependente da concentração do cátion no meio: apoptose ocorre em baixas concentrações; necrose em altas concentrações de Al^{3+}. O pH do meio de cultivo é um fator determinante na análise da toxidez do cátion.
- ✓ Apoptose é o mecanismo de morte celular induzido por violaceína. A técnica de cometa e a marcação da fosfatidilserina pela anexina V são métodos confiáveis para o estudo da morte celular.
- ✓ O principal componente do revestimento externo das raízes de milho e trigo é a celulose, constituindo a base para a ligação da mucilagem.

PERSPECTIVAS

- ✓ Verificar as alterações no padrão de absorbância do DNA em consequência da interação com o Al^{3+}.
- ✓ Complementar os estudos *in vitro* dos complexos Al-DNA com análises da interação da cromatina com o Al^{3+}, tanto *in vitro* quanto em núcleos isolados.
- ✓ Verificar a participação da parede celular na modulação dos mecanismos ativos de tolerância ao Al^{3+} e seu papel na tensegridade celular.
- ✓ Determinar as vias metabólicas envolvidas na indução de morte celular "tipo-apoptótica" pelo Al^{3+} em plantas e sua relação com o estresse oxidativo.
- ✓ Determinar se a calose possui um papel na tolerância ao Al^{3+} dificultando a entrada do cátion no ápice da planta.
- ✓ Verificar se os cultivares estudados neste trabalho são verdadeiramente tolerantes (convivem com o Al^{3+} intracelular) ou resistentes ao cátion.
- ✓ Complementar os estudos da toxidez do Al^{3+} à células animais com análises em células do sistema nervoso cultivadas em pH < 5.5.
- ✓ Verificar o efeito cumulativo do Al^{3+} em mamíferos.
- ✓ Determinar o mecanismo pelo qual o Al^{3+} atravessa a membrana plasmática, tanto em plantas quanto em animais.

PRODUÇÃO CIENTÍFICA DURANTE A TESE

* 2001: Violacein Induced Apoptosis In V79 Cells As Seen By SCGE And Annexin V Labeling. Schildknecht PHPA, Melo PS, Vidal BC, Haun M, Durán N. Annals of XXX Meeting of the Brazilian Biochemistry Society, B-78.

* 2001: Al3+ Induced Alterations On DNA And Pectin Molecular Order. Schildknecht PHPA, Vidal BC, Pimentel ER. Annals of XXX Meeting of the Brazilian Biochemistry Society, E-69.

* 2000: Aluminium Induces Apoptosis In V-79 Cells. PHPA Schildknecht & BC Vidal. Gen. Mol. Biol. 23 (Supl): 692.

* 2000: Aluminium Triggers Apoptosis And Chromatin Textural Changes In Maize. PHPA Schildknecht & BC Vidal. Gen. Mol. Biol. 23 (Supl): 365.

* 1999: Al3+- Induced Nuclear Chromatin Condensation in Maize (Zea mays L.) Hybrids. PHPA Schildknecht & BC Vidal. Rev. Bras. Fisiol. Veg. 11 (supl):169.

* 1999: Cell Wall Al3+- Induced Variations On Molecular Order, As Seen By Optical Anisotropy Measures. PHPA Schildknecht & BC Vidal. Rev. Bras. Fisiol. Veg. 11 (supl); 169. 1998

* 1998: Al3+-Induced Variations On Nuclear Phenotypes Of Maize (Zea mays L.) Hybrids. PHPA Schildknecht & BC Vidal. Gen. Mol. Biol. 21 (3): 168.

APOIOS RECEBIDOS

* Bolsa FAPESP de Doutorado de Junho de 2000 a Março de 2002.

* Bolsa CAPES de Doutorado de Março de 2000 a Maio de 2000.

* Bolsa FAPESP de Mestrado de Abril de 1998 a fevereiro de 2000.